THE PERFORMANCE OF A ONE AND A HALF STAGE AXIAL TURBINE INCLUDING VARIOUS TIP CLEARANCE EFFECTS

by

George Morphis

Thesis Submitted in partial fulfilment of the academic requirements for the degree of Doctor of Philosophy in the department of Mechanical Engineering.

University of Natal

Durban

1993

ABSTRACT

The necessary clearance at the tip of unshrouded rotors of axial turbines allows fluid to leak from the pressure to the suction side of the blade and produces an important component of loss that is ultimately responsible for approximately 25% of the total turbine rotor losses. Leakage fluid can pass through the tip clearance gap with either high or low loss generation. It has been customary in turbine design to employ high loss designs since it is only by the creation of loss that the gap mass flow rate can be restricted. The present work, however examined the effect of streamlined tips that have low entropy generation within the tip and high leakage flows.

An axial turbine followed by a second stage nozzle (ie one and a half stages) was designed, built and instrumented and used to evaluate performance with particular reference to the understanding of tip clearance effects in a real machine and possible benefits of streamlined low loss rotor tips. A radiused pressure edge was found to improve the performance of a single stage and of a one and a half stage turbine at the selected tip clearances. This was in contrast to previous cascade results where mixing losses reduced the benefits of such tips. Clearance gap flow appears to be similar to other turbine flow where the loss mechanism of separation must be avoided. Loss formation within and downstream of a rotor is more complex than previously realized and does not appear to obey the simple rules used to design for minimum tip clearance loss. For example, approximately 48% of the tip leakage mass flow within a rotor may be a flat wall-jet rather than a vortex.

Second stage nozzle efficiency was significantly higher than first stage nozzle

efficiency, and even increased with tip clearance. This was a surprising result since it means that not only was there a reduction in secondary flow loss but also that rotor leakage and rotor secondary flows did not generate significant downstream mixing loss. The manner in which the second nozzle responds to the complex leakage flows presented to it and how it completes the formation of tip clearance loss for various rotor tip clearances was identified.

The tangentially averaged relative rotor flow in the tip clearance region differed radically from that found in cascades which was seen to be underturned with a high axial velocity. There was evidence rather of overturning presumably caused by secondary flow. Axial velocity followed an almost normal endwall boundary layer pattern with almost no leakage jet effect. Cascade tip clearance models are therefore not accurate in predicting leakage flows of real rotors.

The reduction in second stage nozzle loss was seen to occur near the hub and tip confirming a probable reduction in secondary flow loss. Nozzle exit loss contours showed that the leakage flow suppressed the formation of the classical secondary flow pattern and that a new tip clearance related loss phenomenon existed on the suction surface. The second stage nozzle reduced the hub endwall boundary layer below that of both the first nozzle and that behind the rotor. It also appeared to rectify the secondary and tip clearance flows to the extent that a second stage rotor would experience no greater flow distortion than the first stage rotor would.

Radial flow angles behind the second stage nozzle were found to be much smaller than those measured in a previous study of low aspect ratio, untwisted blades.

PREFACE

The author hereby states that this entire thesis, unless specifically indicated to the contrary in the text, is his own original work, and has not been submitted in part or in whole to any other University. This dissertation describes the work carried out by the author at the Department of Mechanical Engineering, University of Natal from November 1989 to March 1993. This work was part of an ongoing line of research into tip clearance flow understanding and was supervised by Prof. J P Bindon.

ACKNOWLEDGEMENTS

The author wishes to gratefully thank the following people:

The Workshop Staff in the Department of Mechanical Engineering for their assistance in the construction of the one and a half stage turbine and the traverse mechanism.

Ivan Kaiser for his assistance with the automation and control software.

His parents Ourania and Andreas who encouraged and supported him at all times.

CSIR and IZMAR for generously supporting the project.

Finally a special thanks to Prof. J P Bindon who supervised the project and without whom it would not have been possible. His contribution to this work in the form of fresh ideas, discussion and analysing of results was invaluable.

TABLE OF CONTENTS

NOMENCLATURE

Variables

A	Area [m^2]
c_v	Specific heat at constant volume [kJ/kg K]
h	Specific enthalpy [kJ/kg K]
H	Blade length or span [m]
i	Tangential increment, incidence
j	Radial increment
K	Coefficient (calibration)
m	Tangential grid points
$\dot{m}$	Mass flow rate [kg/S]
n	Radial grid points
N	Rotational speed (R.P.M.)
P	Pressure [Pa]
q	Dynamic pressure [Pa]
r	Radius [m]
s	Specific entropy [kJ/kg K]
S	Pitch [degrees]
T	Temperature [K]
u	Specific internal energy [kJ/kg]
U	Blade velocity [m/s]
V	Absolute velocity [m/s]

W	Relative velocity [m/s]
Y	Variable (arbitrary)
α	Absolute angle [degrees] (tangential plane)
β	Relative angle [degrees] (tangential plane)
η	Efficiency
Θ	Tangential angle [degrees]
ρ	Density [kg/m^3]
τ	Torque [Nm]
Ψ	Radial angle [degrees]
ω	Specific work [kJ/kg]

Coefficients

C_m	Mass flow coefficient
$C_{Poref\text{-}Ps}$	Static pressure coefficient
$C_{Poref\text{-}Po}$	Total pressure coefficient
$C_{Poa\text{-}Psb}$	Driving pressure coefficient
$C_{Poa\text{-}Pob}$	Total pressure loss coefficient
C_V	Velocity coefficient
C_W	Work coefficient
ψ	Blade loading coefficient ($2V_x/U$ (tan β_2 -tan β_3))

Subscripts

1	First nozzle inlet
1.5	One and a half Stage
2	Rotor inlet (first nozzle outlet)
3	Rotor outlet (second nozzle inlet)
4	Second nozzle outlet
a	Upstream position
aero	Aerodynamic
b	Downstream position
i	Tangential grid number
is	Isentropic
j	Radial grid number
N1	First nozzle
N2	Second nozzle
o	Total
P	Pressure
r	Radial
R	Rotor
ref	Free stream inlet reference
s	Static
ts	Total to static (single stage)
tt	Total to total (single stage)
x	Axial
θ	Swirl component

CHAPTER 1

INTRODUCTION

Gas turbine engines have become increasingly more important not only for aircraft propulsion, but also for other power applications on land and sea. Understanding the flow structures and improving the efficiency of these machines is important since they combust a large portion of the world's fossil fuels. The shaft power generated by a gas turbine is the difference between the turbine output power and the compressor input power. Small improvements in efficiency of the turbine give a much larger percentage gain in total output power since the turbine produces roughly twice the power of the compressor.

Turbine losses have traditionally been divided into three components, namely profile loss, secondary (or endwall) loss and tip leakage loss. Tip leakage losses exist in both shrouded and unshrouded turbine rotors, but in this thesis only axial, unshrouded turbines are considered. The finite clearance gap that generates the leakage losses, is necessary between the rotor blade tip and the outer casing due to manufacturing tolerances and thermal distortion. Furthermore, this tip clearance changes as the gas turbine warms up from start to full operating conditions. Figure 1.1 shows how tip clearance varies during a typical mission due to different thermal growth rates of the rotor blades and casing.

Tip clearance allows fluid to leak from the pressure side to the suction side of the blade and produces an important component of loss. In linear cascade work it was

shown that tip clearance losses are responsible for approximately 25% of the total rotor losses. Tip clearance loss can be divided into two separate components, namely the internal gap loss and the downstream mixing loss. The internal gap loss (or entropy), which is generated within the leakage flow as it passes through the gap, accounts for some 40% of the tip clearance loss or 10% of the total loss. Mixing loss is created at the interface of the leakage flow and the mainstream flow that have different velocities, in both magnitude and direction.

As in the development of the understanding of basic turbomachinery flow, most of the recent knowledge of tip clearance flows has been obtained in cascade models, both linear and annular. Relative motion between the tip and outer casing has been modelled by rotating the outer casing of an annular cascade and by moving belt walls on linear cascades.

An important part of tip clearance loss control has always been to minimize the gap mass flow. For a fixed area or clearance gap size, the only way to decrease flow rate is by deliberately introducing separations that "block" the flow or by extending the flow path length and boundary layer thickness (i.e. winglets), both of which lead to entropy formation. Previous linear cascade tests showed that the loss generated within the gap could be reduced by 80% by simple streamlined tip gap geometries that avoid separation. Benefits of the lower internal gap loss were, however, reduced by the higher leakage mass flow rate that increased the mixing loss. Even though cascades have proved useful in the qualitative understanding of the leakage flow,

there is nevertheless doubt as to whether the losses, and more particularly the mixing losses, measured in cascades can be accurately translated into a rotor context.

None of this above knowledge has been applied or verified with fully rotating twisted turbine blades. This thesis therefore examines the real performance of a low speed axial turbine and compares it to cascade measurements. In addition, the intention was to deepen the understanding of tip clearance loss mechanisms, and to explore potential benefits of reduced internal gap loss. The thesis measures, at three gap sizes the performance of three 406mm diameter low speed rotors, each being identical except for tip gap geometry. Schematics of the tip gap geometries are shown in Figure 1.2 and are similar to those used in previous cascade experiments. A standard square tip shape was used as a reference since it is commonly found in real engines and since so much of the present understanding relates to it. Two streamlined, low internal gap loss tip shapes were employed. The first low loss tip design (**radiused tip**) had a pressure edge (gap inlet) radiused to suppress the formation of the gap separation bubble, the main cause of the loss in the gap. The second low loss design (**contoured tip**) had a tip contoured to avoid a separation bubble while shedding a radial flow component into the gap in an attempt to reduce gap mass flow.

A method of assessing measured cascade flow field data as though it were a moving rotor was previously used to evaluate the two low internal gap loss designs. Simulated single stage efficiencies were determined and showed that the radiused tip was less efficient than the square tip whereas the contoured tip had the highest

efficiency. It was encouraging to find that not only could a low internal gap loss design outperform the more traditional square tip (with high internal gap loss), but that a further benefit could also be gained. This was that the low loss fluid leaving the rotor may possess kinetic energy not yet dissipated by mixing, that could be utilised by a second stage nozzle downstream of the rotor. Alternatively stated, it means that low loss tip geometries allow fluid to pass through the rotor with low loss but in the wrong direction (i.e. relatively undeflected).

Development of tip leakage flow and the fully mixed out losses downstream of a linear cascade have been measured, but in a multistage turbine neither the leakage flow nor the secondary flows are fully mixed out before entering the next nozzle row. The second stage nozzle will thus play an important part in the ongoing formation and definition of rotor tip clearance loss and rotor secondary flow loss.

There is however also a fundamental interest in the type of flow occurring. If the flow can be redirected and expanded without an undue decrease in nozzle efficiency, it may be found that what was previously considered to be mixing loss has been overestimated. The second stage nozzle has not received much attention from researchers with respect to tip leakage flows. The studies that are available deal with other aspects of multistage turbines. This thesis thus investigated whether a second stage nozzle can benefit from receiving this misdirected leakage flow by examining the flow structure of a full annular nozzle downstream of the low speed, unshrouded axial turbine rotor (i.e. a one and a half stage turbine). The three separate rotors mentioned above were tested in conjunction with the first and second stage nozzles at three different clearances.

The flow into a first stage nozzle is relatively "clean" and therefore more closely resembles the ideal cascade model than do the flows in the other nozzles which are always downstream of a rotor and in which the flow is disturbed near the casing by rotor tip clearance leakage effects. The flow is also periodic, more turbulent due to blade wakes and the endwall boundary layers are more developed and skewed at inlet. The effect of rotor tip clearance on the second nozzle loss formation and the ability of the second nozzle to take badly deflected leakage flow and convert it to useful flow were also examined in this thesis.

Since small changes in efficiency had to be measured, it was important that the instrumentation was both repeatable and accurate, and that the design point of the turbine was kept constant. In addition to the accurate measurement of various pressures, inlet temperature and rotor speed, a high accuracy torque transducer was used to measure the work transfer. Turbine design point and inlet Reynold's Number were held constant to within 0.1% via computer control.

Atmospheric conditions and thus the density and velocity of the inlet flow varied during measurements. It was therefore necessary to define dimensionless coefficients that eliminated the effect of changing inlet conditions. A new efficiency had to be introduced to describe the performance of a one and a half stage turbine in order to compare the various rotors and their effect on the flows. Various methods were defined to determine the quantities.

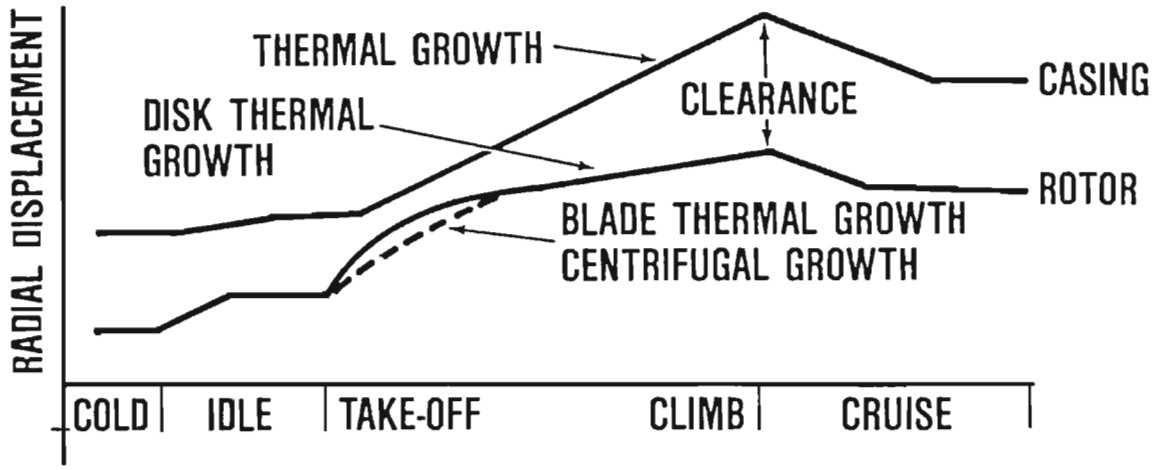

Figure 1.1 Tip clearance variation during engine operation (Booth (1985))

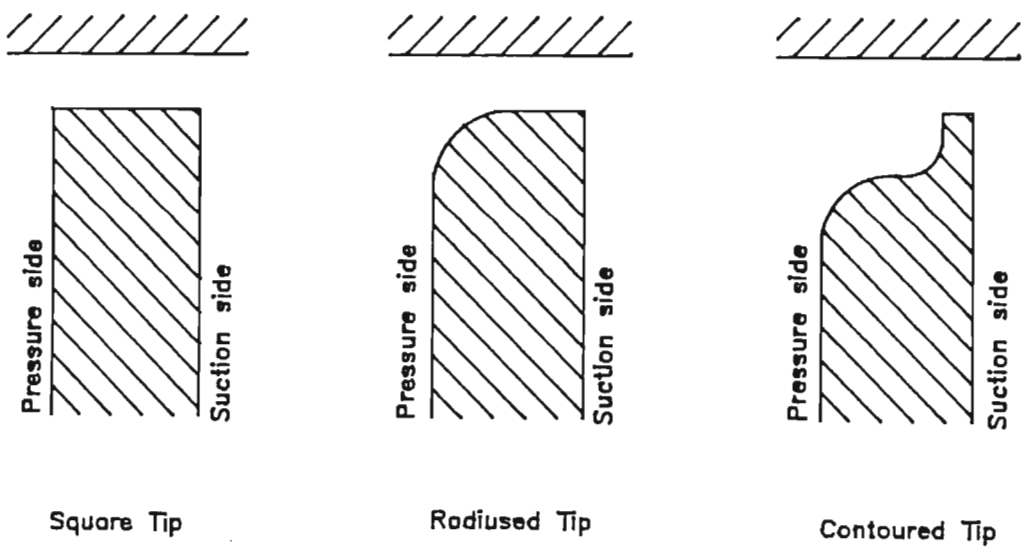

Figure 1.2 Schematic of three blade tip geometries

CHAPTER 2

LITERATURE REVIEW

1 Introduction

This thesis presents a synopsis of the most important and relevant work published on tip clearance effects and losses. The earliest work on tip clearance losses was aimed at simply reducing the size of the clearance gap and thus decreasing the leakage mass flow rate. A minimum clearance that could be used was soon reached due to thermal expansion, creep, manufacturing tolerances and thermal distortion of the outer casing. Simple correlations for estimating tip clearance losses were first developed as far back as the 1950's but these models were simplistic in their approach and made a number of assumptions to aid designers of both compressors and turbines.

Rains (1954) introduced coloured oil droplets into the flow of an axial water pump with blading similar to a compressor, to study the generalised movement of tip leakage fluid. Data gained here was used as a basis from which two loss calculation flow models were developed. The first was an idealised mixing model applying Bernoulli's equation at gap entry and exit, and ignored viscous effects. In a second more correct model, the separation bubble (found at gap entry) with reattachment was included.

Tip clearance losses were investigated and simple rules relating percentage efficiency decrement to percentage tip clearance over blade height were developed. In

Booth (1985) this decrement factor was reported between 1.39 and 1.75 for turbines, and it was noted that higher values had been measured in later work.

In more recent times a great deal of effort has been invested in understanding the basic flow phenomena of tip clearance flows. Due to simplicity and economic reasons, the vast majority of this work was done in stationary linear and annular cascades with tip clearance. Effects of relative motion between the blade tip and outer casing have been modeled using moving walls, however, besides injecting work into the leakage fluid, the effect of centrifugal force, Coriolis force, radial pressure gradients and other effects of rotating machines have been ignored.

The effects of tip clearance on the downstream nozzle or second stage have been largely ignored with the only known detailed study on second nozzle flows having been that of Boletis & Sieverding (1991) for a low aspect ratio, untwisted design. Flows in the second nozzle which is downstream of a rotor are expected to be different to those of the first nozzle and their fundamental nature has not received much attention. Joslyn et al (1983) studied the unsteadiness of the flow at mid-span in a large scale, one and a half stage turbine.

2 Tip clearance flow phenomena

In investigations of compressor and pump tip leakage losses, Rains (1954) described some of the basic phenomena of tip leakage flows. The separation bubble at gap

inlet was illustrated and the leakage jet was found to be inclined at an angle to the free stream direction. Observations showed that the leakage flow rolled up into a strong vortex which was responsible for cavitation in axial flow pumps.

Lakshminarayana (1985) noted, that for a compressor cascade, the leakage vortex was in the opposite direction to the secondary flows, and that the two flows meet to form a core of heavy losses. In one particular case that was examined, the effect of secondary flows was overshadowed by the strength of the leakage flows.

During experiments to investigate the causes of blade tip burn out, Bindon (1986a, 1986b, 1987a, 1987b and 1987c) unravelled some of the basic mechanisms of the flow within the tip clearance gap using a linear cascade with a standard square tip geometry. A static pressure survey was done on the endwall and on the blade tip using a micro pressure tapping technique. As shown in Figure 2.1, it was discovered that as the flow enters the gap, the pressure drops to the lowest value in the form of a narrow trough. This was thought to be due to the flow remaining attached around the corner. The flow then decelerates sharply and separates to form the bubble which causes the static pressure to remain relatively low as the main leakage flow accelerates over the blockage caused by the separation bubble. The static pressure then recovers to approximately the suction surface pressure as the flow reattaches.

Right on the sharp inlet edge of the blade, the chordwise pressure distribution showed the lowest value near mid-chord. It was suggested that the flow that

remained attached around the corner, induced low pressures, high velocities and thus high heat transfer rates which were assumed to be responsible for the heat damage of the tips. The Venturi effect of the separation bubble induced a low pressure zone on the endwall, the minimum being near mid-chord which was where tip burnout occurred. The velocity, total pressure and flow angle were also measured in the tip clearance gap.

Within the upstream half of the separation bubble, the flow was highly attached with strong chordwise velocity components created by the accelerating pressure gradients. The shearing action of the free stream passing above the bubble induced a corkscrew motion in the flow. Zones of true separation were identified near mid-chord where pressure gradients were such as to stagnate the internal flow and force it to mix with the gap inlet leakage flow, to be ejected from the gap as a high loss core of fluid. The leakage flow vortex was clearly seen rotating in the opposite sense to the secondary flow vortex in the suction surface corner, but at small clearances no vortex motion was evident.

In attempting to reduce the low static pressures at gap inlet, and therefore the high velocities and heat transfer rates, the inlet corner of the tip was radiused. Radiusing the tip, eliminated the very low corner pressure and reduced the size of the separation bubble. The effects on loss formation within the gap were not investigated.

Morphis & Bindon (1988) did microscopic static pressure measurements and flow visualisation in the tip clearance region of an annular cascade with a rotating outer casing to simulate the relative motion at the blade tip of an axial rotor. The separation bubble width was found to depend on clearance gap size as shown in Figure 2.2 and the separation bubble reattachment point was identified. The separation bubble width dependence on clearance was also confirmed using surface oil flow visualisation. Effect of pressure corner radius on the separation bubble was investigated for various radii (from .5% chord to 5% chord) since it was believed that the separation bubble played an important role in the formation of loss within the gap. The low pressure generated by the separation bubble was found to decrease as the pressure corner radius increased (Figure 2.3). The separation bubble was shown to disappear when the tip pressure corner was given a radius of 2.5 gap widths. This figure is important in that it was used as a guide for the radiused blade tip in the present work

Bindon (1986b) used smoke flow visualisation at low Reynolds numbers to reveal the flow structure around the tip clearance region. If the gap is considered from leading edge to trailing edge, then the flow that entered the gap near the leading edge or forward part of the blade was seen to exit the gap and roll up into a vortex. Although not noted in the paper, some of the flow visualisation photographs show that the flow exiting the gap over the second part of the blade towards the trailing edge, does not roll up into a vortex within the cascade. This is significant in that it means that part of the leakage flow will enter a subsequent nozzle as high energy fluid that has not generated high entropy by rolling into a vortex.

Sjolander and Amrud (1986) examined the structure of leakage flows using static pressure tappings on a blade of a 250 mm chord linear cascade. In addition to the measurements, surface oil flow and smoke flow visualisation was used. Tip clearance was varied from 0% to 2.86% of chord. After emerging from the gap, the leakage flow was seen to roll up into a vortex whose starting point moved rearward with increasing clearance. A new feature that was noted was that multiple, discrete tip leakage vortices formed as the tip clearance was increased. Integration of the pressure distributions showed that at the larger clearances, the blade loading increased as the tip was approached and only began to decline very near the tip.

3 Tip clearance losses

Bindon (1987a) explored tip clearance losses in a linear cascade for various clearances and compared them to the zero clearance case. It was found that the loss coefficient without tip clearance was radically changed by leakage flow and was five times higher. Despite this high viscous loss generation within the clearance gap, the exit velocities were seen to be high. An unexpected but interesting result was that the loss generated within the gap did not increase with increasing clearance gap size. This was as though the increased leakage quantity at larger gaps was compensated by the reduced viscous losses in the wider gap.

Dishart & Moore (1989) investigated tip leakage flow and its effect on loss production for a single clearance in a large scale linear cascade. Measurements of

the flow exiting the tip gap and at 40% of axial chord downstream of the blade trailing edges were done and the losses determined. It was found that the mixing loss generated up to the downstream location, was equal to the kinetic energy in the leakage flow at gap exit. In other words kinetic energy in the flow leaving the gap, will eventually be converted to loss. However this would only be true if the turbine were single stage since in a multistage turbine the flow would enter the next nozzle before the kinetic energy was dissipated.

In the linear cascade, Bindon (1987a) found that the tip clearance loss has two main components. The first is the internal gap entropy that is generated within the leakage flow as it passes through the gap. The second is the mixing loss as the leakage flow merges with the mainstream within and downstream of the cascade. In a later paper, Bindon (1988) quantified the loss due to internal gap shear flow and assumed that the mixing loss was the additional endwall loss over and above that for zero clearance. It was found that only 13% of the loss was due to secondary or endwall flows, 48% was due to mixing and 39% due to internal gap shear. The separation bubble was strongly associated with the loss generation and a model suggesting the mode of loss formation was proposed as shown in Figure 2.4. Bindon (1987b) showed that a very low pressure is generated at gap entry by the sharp curvature demanded of the leakage flow and by the formation of the separation bubble which creates a Venturi action in the clearance gap. As mentioned in Section 2 the low pressure generated by the separation bubble was observed to decrease as the pressure corner radius was increased. This implied that it may be possible to reduce the entropy generated within the gap and hence reduce the overall loss.

Bindon & Morphis (1992) used a linear cascade to assess the possibility of reducing the overall tip clearance loss by using streamlined blade tip geometries that reduce the internal gap loss. Two blade tip geometries, as shown in Figure 2.5, aimed at reducing or avoiding the separation bubble, were compared to a standard square tip blade. For a tip clearance of 2% of chord, the internal gap loss for a standard square tip blade was estimated at 38% of overall loss generated in the tip region. It was found that radiusing the blade at gap inlet eliminated the separation bubble and reduced the internal gap loss by roughly 80%. An overall advantage was however not realised since the mixing loss increased. In part this could be due to the increased mass flow rate, but also due to complex interactions.

In an attempt to represent actual rotor performance, the linear cascade velocity vectors were converted into rotor vectors to obtain simulated rotor work transfers and performances which depend on the actual deflection and entropy rise of the tip region flow. A contoured tip blade, was found to have a better performance than the square tip blade, whereas the blade radiused on the pressure corner was found to have the lowest performance. Even though the new blade tips were primarily studied to reveal fundamental flow phenomena, the fact that the internal gap loss was reduced and that an improved overall performance was achieved was regarded as encouraging. Despite this, there was some doubt as to whether losses measured in a cascade could be accurately translated into a rotor context to provide a reliable statement regarding all the interrelated effects contributing to actual rotor performance. The only way to obtain certainty as to whether the new streamlined tips work was to test them in a real rotor as is done in this thesis.

Heyes et al (1991) measured the performance of a variety of blade tip geometries in two linear cascades as shown in Figure 2.6. The exit flow field was traversed and the performance of plain square tips, suction side squealers and pressure side squealers were reported. It was shown that the use of suction side squealers could provide a benefit over a standard square or flat tip blade. It was also concluded that the mass flow through the tip gap at a given clearance must be limited rather than the loss generation over the tip. It was further stated that the radius of the corner from which the flow separates to form the 'vena contracta' is vitally important and should be kept to a minimum to achieve the lowest leakage flow.

Kaiser (1992) also examined three blade tip geometries as shown in Figure 2.7 (one of which was similar to Heyes et al (1991)) in an annular cascade with relative motion. He found that the single suction side squealer had the highest leakage mass flow rate and lowest loss through the gap. This is opposite to what was suggested by Heyes et al (1991). The single suction side squealer appears to approximate a blade with a radiused pressure corner. This implies that less loss will be generated in the gap and that a higher leakage mass flow rate will be generated as was also found by Bindon & Morphis (1992). Overall performance of the cascade was however not measured.

Booth et al (1982) simulated several blade tip configurations in three water flow rigs. The tip geometries tested were variants of square tips, squealers, grooves and winglets. The idea behind the winglet design was to provide a large gap inlet

pressure drop by the flow over the sharp edge. Tips with winglets were found to have the lowest leakage mass flow rate.

4 Effect of relative motion

Graham (1986) investigated the effect of tip clearance and relative motion for a linear cascade with water as the flow medium. Increasing the endwall velocity reduced the leakage flow in a complex, non-linear manner. Reducing the clearance gap had a similar effect. It was shown that at the smaller clearances, an increase in endwall velocity completely eliminated the leakage flow. This result was due to the viscous interaction of the boundary layers at small clearances.

The effect of relative motion on the blade tip pressure distribution and on the separation bubble was investigated by Morphis & Bindon (1988). The outer casing of an annular cascade was allowed to rotate at the relative design speed to simulate the conditions at the blade tip of an axial rotor. It was found that relative motion did not have a significant effect on the pressure in the separation bubble or on the separation bubble width. However the pressures reached in the fully attached area behind the separation bubble near mid-chord were significantly higher (about 14%) with rotation. Since leakage flow would increase the viscous shear action within the clearance gap, both the leakage flow quantity and the size of the resulting vortex, could be slightly reduced.

Kaiser (1992) used a traverse mechanism mounted in the hub of the same annular cascade used by Morphis & Bindon (1988) to measure the flow at gap exit. The measurements were done for three blade tip geometries shown in Figure 2.7 with and without relative motion at a single clearance of 2.5% of blade chord. It was found that relative motion did not significantly reduce the leakage mass flow rate except near mid-chord and was also found to reduce the loss generated within the gap by 4%.

Yaras & Sjolander (1991) simulated the relative motion between the tip and endwall in a linear cascade by using a moving belt endwall. Measurements of the gap flow were done for a single clearance of 3.8% of the blade chord. At the test condition it was found that the leakage mass flow rate was reduced by 50%. This is in contrast to the findings of Kaiser (1992) and can possibly be explained by the variations in geometry between the two cascades. The main differences were the length of moving wall in front of the blade leading edges, the tip clearances, and the blade profile. The belt used by Yaras & Sjolander (1991) had 48% of chord length in front of the blades whereas Kaiser (1992) only had 15%. The extra belt in front of the blades would generate a thicker boundary layer of fluid moving in the same direction as the belt, that could cause a reduction of flow through the gap. This however does not explain the overall effect. The large pressure difference between the pressure side and suction side of the blade causes the fluid to leak. At the interface between this leakage fluid and the main stream flow a vortex is generated that consists of low energy fluid (on the suction side of the blade). This vortex acts as a blockage to the main flow and alters the pressure field. It is this pressure field

that determines the mass flow rate through the gap. The relative motion in the two cases above generated completely different pressure fields and thus mass flow rates through the gap.

5 Effect of varying clearance

In a linear compressor cascade with tip clearances varying from 0% to 4% of chord, Storer (1989) found a linear relationship between leakage flow and gap size. It was however, observed that the total cascade pressure loss due to tip clearance was non-linear. This implied that the total pressure loss due to tip leakage cannot be simply attributed to the loss of kinetic energy of the tip leakage flow. Instead it indicated the origin of loss to be the mixing of the leakage flow with the surrounding flowfield.

Yaras et al (1988) measured the flow in the gap of a linear turbine cascade at three clearances from 2% to 3.2% of blade chord. It was found that the discharge coefficient decreased with clearance and that the separation bubble filled a larger fraction of the gap as the clearance was increased.

In a low speed linear cascade with four different clearances, Bindon (1986a) showed that the static pressure on the suction side decreased (i.e. the static pressure diference from pressure to suction side increased) on both the endwall and on the blade tip as the clearance was increased. From this it could be concluded that the leakage flow

has a self enhancing effect since it causes a lower pressure on the suction side which in turn gives a higher driving pressure and thus more leakage. In a high speed (Mach 1.2) cascade with ten different clearances, Mc Donald (1993) found that the static pressure difference on the endwall decreased with clearance. This is opposite to what Bindon (1986a) found but is easier to explain. At the limit, if the tip clearance was increased until the blades vanished, there would be no tangential pressure difference in the flow. Decreasing the tip clearance to zero would increase the pressure difference. Although different blade geometries were used in the two cascades above, the suggestion is that tip clearance flows behave very differently at high flow velocities.

6 Numerical models

Much of the modelling of tip leakage flows has concentrated in calculating the magnitude and distribution of the mass flow rate through the gap. Rains (1954) introduced the basics of the most common approach used for calculating the gap mass flow rate. Rains assumed that the chordwise pressure gradients acting on the gap flow were small compared with those normal to the blade. In other words, the gap flow has a velocity that is induced by the blade pressure difference and is normal to the blade. The magnitude of the gap flow was calculated by applying Bernoulli's equation to the acceleration process. In a second more correct model the gap velocity calculation included loss terms that took into account the separation bubble and friction within the gap. Based on these flow computations, an expression for tip

clearance loss was developed that assumed that the kinetic energy associated with the velocity component normal to the blade chord cannot be recovered. Since the early work of Rains many researchers have sought to improve this model.

Yaras et al (1988) measured the flow in the tip gap of a linear turbine cascade for three clearances and modeled the mass flow rate and velocity distributions in the gap using measured blade pressure distributions. Two models were used here, the first of which used the blade mid-span pressure distribution. A second version modified the mid-span pressure distribution by an amount that was determined by experimental data, to compensate for the different pressure distribution at the tip. Modifying the prediction model with experimental measurements at the tip defeats the object of the numerical prediction.

Moore and Tilton (1987) measured wall static pressures and flow velocities in a linear cascade and used the data to verify a numerical model of the flow (with a separation bubble) in the tip region. A simple two-dimensional potential flow with mixing model, was used for the flow through the tip gap. The model was able to predict the unloading along the pressure surface of the blade and the endwall static pressure distribution of the tip gap.

Heyes et al (1991) used a one dimensional, incompressible flow model similar to that of Moore and Tilton (1987), to predict qualitative effects of the tip clearance geometry on the total pressure losses caused by tip clearance flows. Loss due to leakage flows at cascade exit, was assumed to comprise of the loss generated over

the tip and that due to mixing of the leakage flow with the mainstream. The tip leakage flow was considered to be a jet that enters the blade passage at some angle to the mainstream flow. A good correlation was achieved between their predicted discharge coefficients and measurements taken in linear cascades with a variety of tip shapes (square tip, suction side and pressure side squealers). Discharge coefficient was identified as an important parameter in determining overall cascade losses. Using the model, it was found that an advantage was only gained from a pressure side squealer if the pressure side corner was sharp. On the other hand the suction side squealer showed a benefit over the flat tip even at large values of pressure corner radius. It was thus concluded that small scale details of the geometries were vitally important to the aerodynamic gains to be expected from the addition of squealers.

Heyes & Hodson (1992) used a two-dimensional model to calculate the leakage flow over the blade tips of an axial turbine and compared the results to data obtained from studies of the two linear cascades. The method was shown to predict the leakage flow with accuracy for a range of blade geometries and flow conditions. An improvement in the accuracy of the model was achieved by including the effect of chordwise pressure gradients.

During measurements in a linear cascade, Yaras & Sjolander (1989) found that the leakage vortex had essentially completed its roll-up by the time it reached the trailing edge plane, and that the bound circulation in the tip leakage vortex was substantially less than the bound circulation for the blade. From this, a simple model based on

the diffusion of a line vortex was developed to estimate the lateral diffusion of the leakage vortex, the crossflow velocities through it, and the growth of its diameter with downstream distance. Correlations were presented but not verified for calculating the location of the origin and the eddy viscosity of the vortex.

Basson & Lakshminarayana (1993) used a semi-implicit pressure based computational fluid dynamics scheme that included artificial dissipation, and was applicable to both viscous and inviscid flows, for predicting the flows in turbomachinery blade rows with tip clearance. The numerical model was used to investigate the structure of tip clearance flows and to compare them to experimental data from the linear cascade of Bindon (1987b) and Bindon & Morphis (1992). The model was able to reproduce the tip leakage flows outside of the gap to a high degree of accuracy and the velocity vectors shown in Figure 2.8 were similar to ones measured by Bindon and Morphis (1992) and presented later in this thesis. At a distance of 50% of tip gap from the endwall, the leakage flow vectors can clearly be seen. However at a distance of only 200% of tip gap from the endwall there is no evidence of tip leakage flows. The static pressure distributions of Bindon (1987b) were also compared to the computed pressures and the general shape was similar, the experimental results having slightly lower pressure extremes.

7 Tip clearance work in rotating rigs

The flow into a first stage nozzle is relatively "clean" and therefore more closely resembles the ideal cascade model with inlet vorticity evenly distributed on the two casing walls. The secondary flows in a nozzle and their growth have been extensively studied (Sieverding (1985) & Gregory-Smith et al (1987)). The other nozzles are always downstream of an axial gap and the flow reflects periodic radial and tangential variations in total enthalpy, incidence and vorticity. Distinct aspects of these differing flows have been examined. The skewing of the inlet boundary layer has been studied by Bindon (1979) and Walsh & Gregory-Smith (1987). Boletis & Sieverding (1991), by comparing the real second stage nozzle flow with their previous skewed study (Boletis et al (1983)), showed that the skewed model has almost no validity and some similarity exists only near the inlet and close to the endwall.

Periodic effects on rotor blade flow (for example Blair et al (1989)), is an ongoing and active area of research in heat transfer. Joslyn et al (1983) recorded high response velocity and total pressure measurements downstream of each row of blades in a large scale one and a half stage turbine. The flow unsteadiness downstream of the first nozzle was compared to that of the second nozzle at mid-span. It was concluded that even at mid-span the flow leaving the second nozzle was very unsteady and highly three dimensional. It was also pointed out that current analytical design methods and predictions did not take these effects into account which would have significant effect on loss generation and heat transfer.

Yamamoto et al (1993) made unsteady flow surveys before, within and after the second stage nozzle passage of a one and a half stage axial turbine with untwisted blades by using hot wire anemometry. These measurements gave the velocity distributions at various planes in the second nozzle but total and static pressure fields were not measured thus the efficiencies could not be calculated. The velocity distributions were difficult to interpret but it was concluded that the flows generated in the second nozzle are influenced by the preceding rotor.

Offenburg et al (1987) did a casing treatment study, where the effect of trenching on axial turbine performance was investigated. Twelve trenching configurations were tested and it was found that at nominal tip clearance (1.5% of blade height), an untrenched casing performed best. At a larger clearance of 3% of blade height it was shown that a trench in the casing returned the best performance with the immersed rotor tip preferred to the line-on-line rotor tip.

After cascade tests showed that winglets had the lowest leakage mass flow rate, Booth et al (1982) tested a rotor with winglets at a 3% clearance. The winglet tip rotor showed an efficiency gain of 0.6% (at design) over the square tip blades.

Very few studies relating to tip clearance have been done in multi-stage turbines. Boletis & Sieverding (1991) made a comprehensive comparison of the flows and losses in a first and second stage nozzle, but rotor performance was not measured. Untwisted blades were used, and the amount of losses generated in the two nozzles were found to be the same but the angles were significantly different at the tip of the

two nozzles. Although not specifically noted by Boletis & Sieverding (1991), it may thus be concluded that the misdirected tip leakage flow from the rotor does not cause an increase in loss in the downstream nozzle. If the leakage flow leaving the rotor can be redirected and expanded without an undue decrease in nozzle efficiency, it may be found that what was previously considered to be mixing loss has been overestimated.

Denton (1993) pointed out that the factors influencing loss generation are very complex. Although cascades have been instrumental in furthering the understanding of tip clearance flows and have been useful in separating aspects of the flow, the complex interaction of the flow phenomena and loss mechanisms can only be fully evaluated in a true rotating machine. Very little of the knowledge gained in cascades has been applied or verified with fully rotating turbine blades, thus ignoring the effects of relative motion, scraping vortex, boundary layers, inlet vorticity, downstream mixing, downstream nozzle, centrifugal forces, Coriolis forces and radial pressure gradients.

8 Conclusion and formal proposal of thesis

The vast majority of work on tip clearance flows and losses has been done in cascades, with very little verification of findings in real rotor situations. Even though cascade work has been instrumental in the qualitative understanding of leakage

flow phenomena, rotating rotors have other differences that would influence the quantitative evaluation and overall performance of tip geometries.

Numerical work has been able to model the leakage flow rates through the gap and the losses developed by leakage flows but again mainly for linear cascades. The emphasis of most of the existing work has been to reduce the leakage mass flow rate at the expense of generating losses within the gap. Streamlined tips that avoid excess entropy generation within the gap have not received much attention.

The development of the tip leakage losses once the flow has left the rotor exit plane have been studied in linear cascades and the findings indicate that any kinetic energy that is in the leakage flow will be dissipated as loss. Real turbines are often multi-stage, thus the assumption that leakage flow will mix out does not apply since neither the leakage flow nor the secondary flow will be allowed to develop fully before entering the next nozzle.

Some work has been done on second nozzle flows, but the fundamental nature of the flows and the effects of rotor tip leakage, have not been studied for a second nozzle with real twisted blades.

This thesis therefore proposed to:

1) Verify the validity of cascade models with special reference to loss.

2) Evaluate streamlined tips in a rotating rotor and to find out if low internal gap loss generation is beneficial to overall efficiency.

3) Examine the effect of a downstream nozzle on the rotor tip leakage mixing losses and the nature of mixing within the rotor passage.

4) Explore the response of the second nozzle to leakage flows with high incidence angles.

5) Survey the second nozzle and measure some of the fundamental flow phenomena and compare it to the first nozzle.

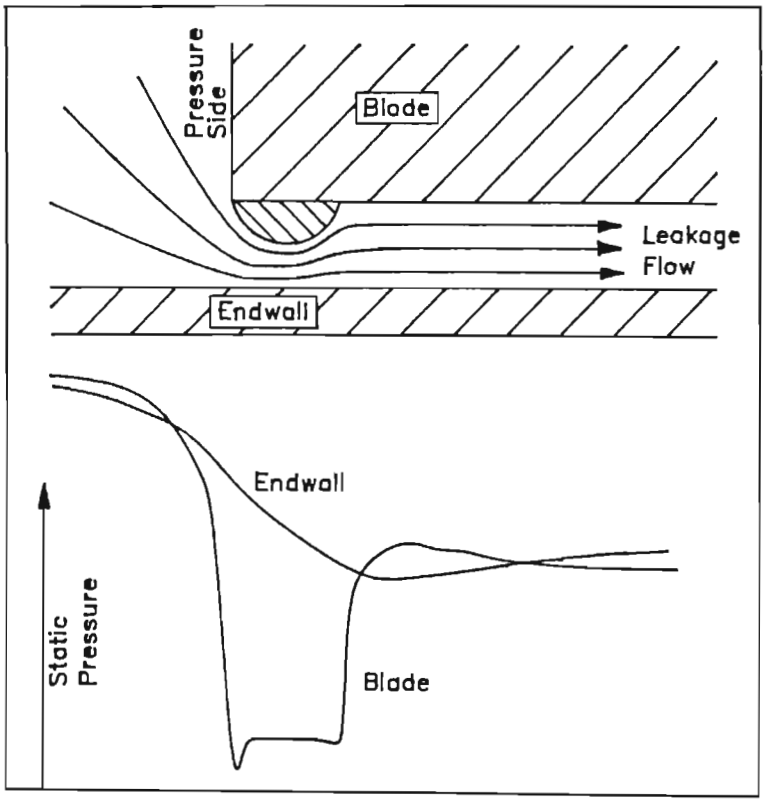

Figure 2.1 Blade tip and endwall static pressure distribution (Bindon 1986a)

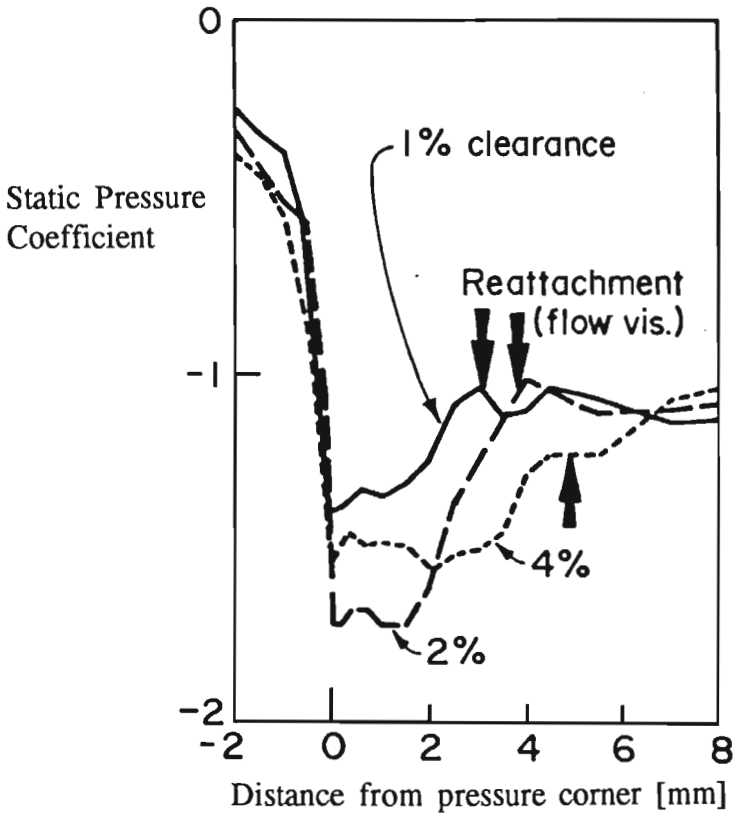

Figure 2.2 Effect of gap size on pressure distribution and separation bubble (Morphis and Bindon 1988)

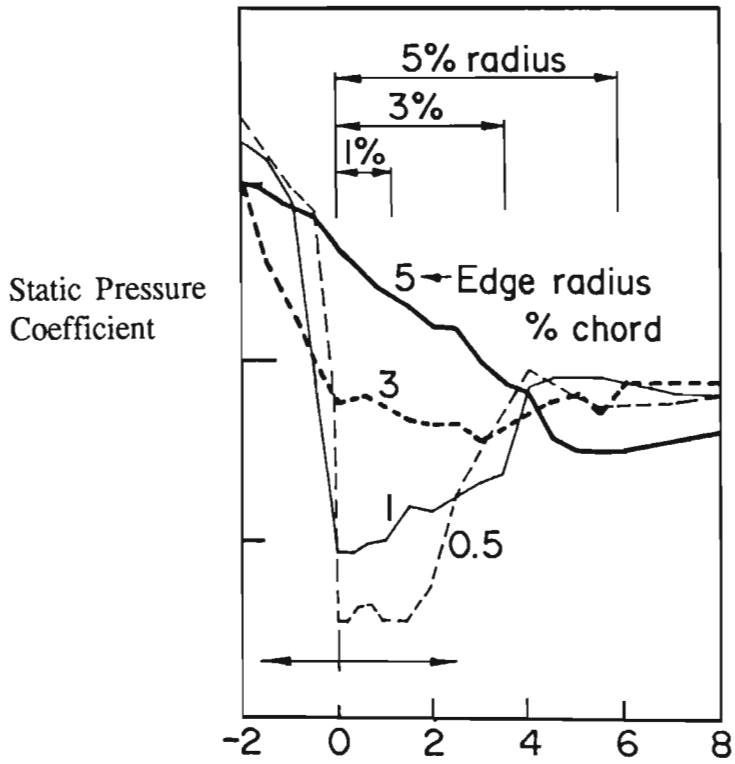

(Morphis and Bindon 1988)

Figure 2.3 Effect of pressure surface edge radius on the separation bubble

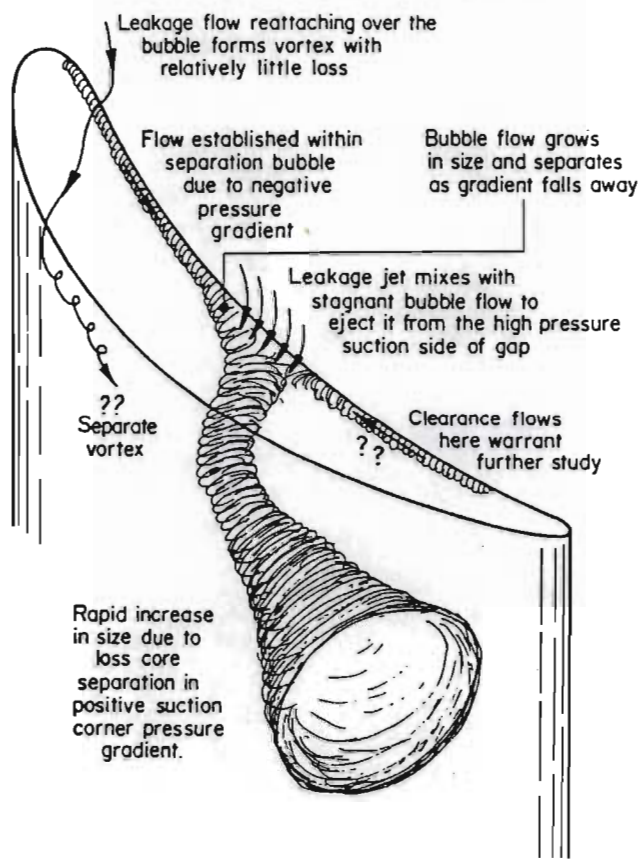

Figure 2.4 Suggested history of tip clearance flows (Bindon 1988)

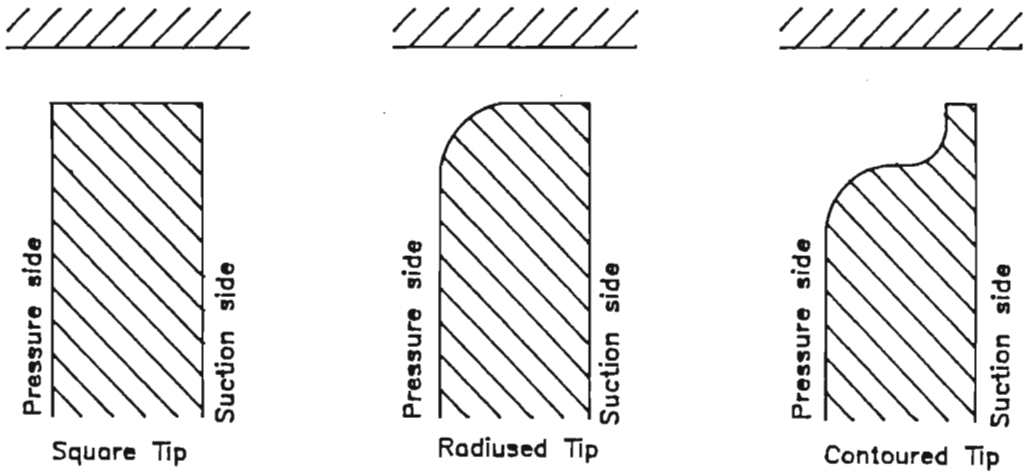

Figure 2.5 Cross sections of blade tip geometries of Bindon & Morphis (1992)

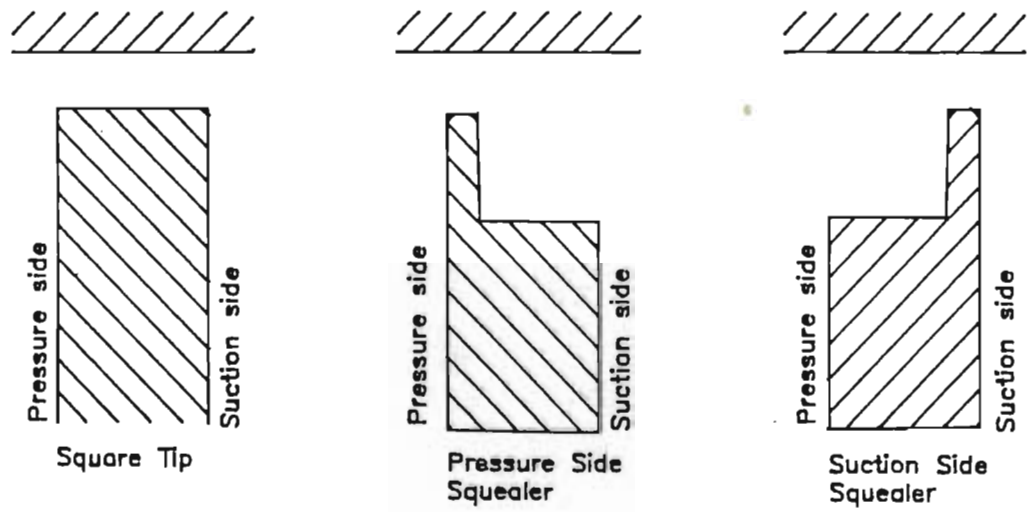

Figure 2.6 Cross sections of the three blade tip geometries used by Heyes (1991)

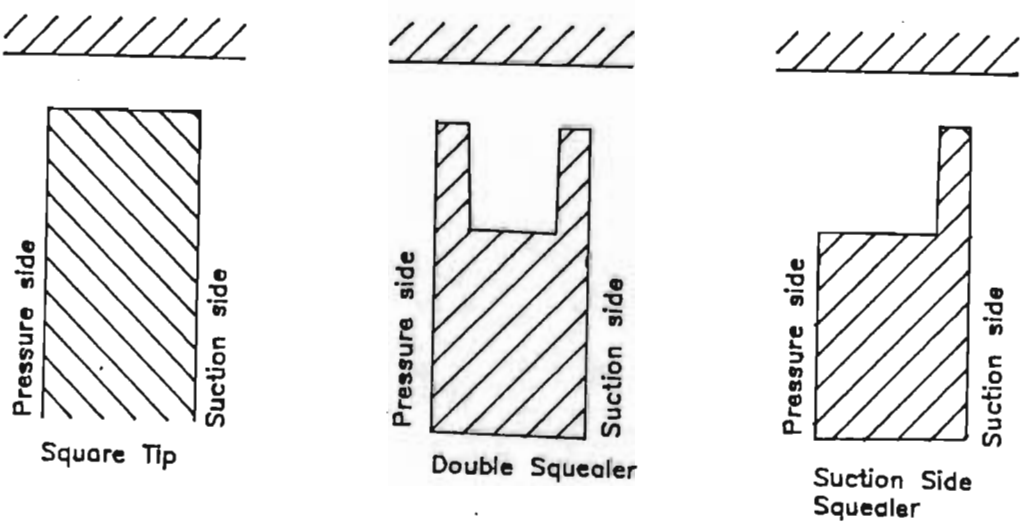

Figure 2.7 Cross sections of blade tip geometries of Kaiser (1992)

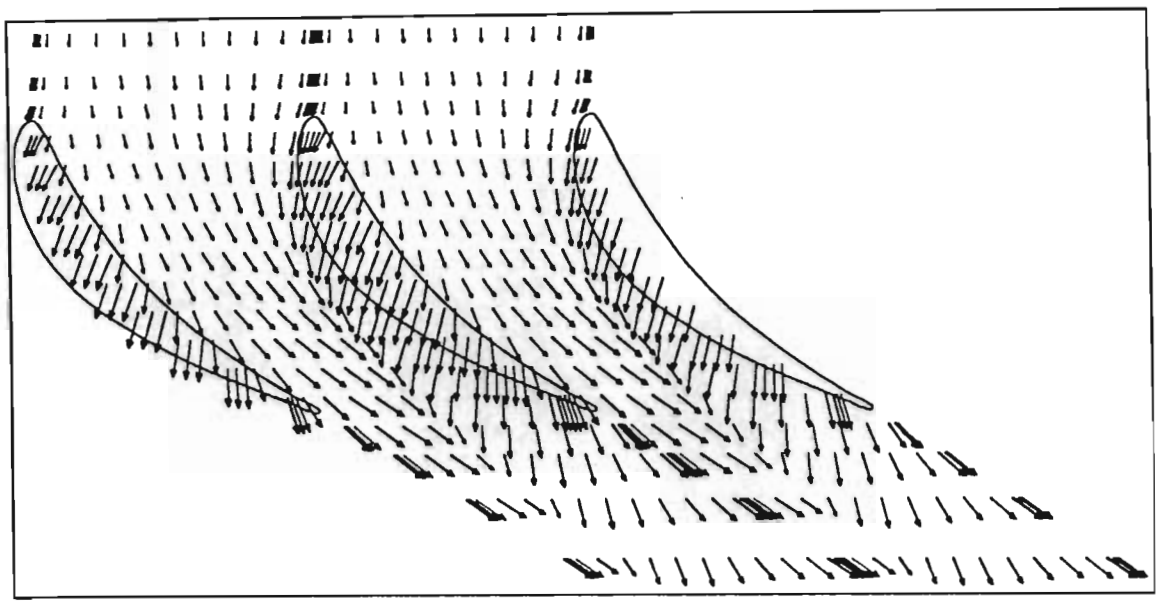

50% of Tip Gap from Endwall

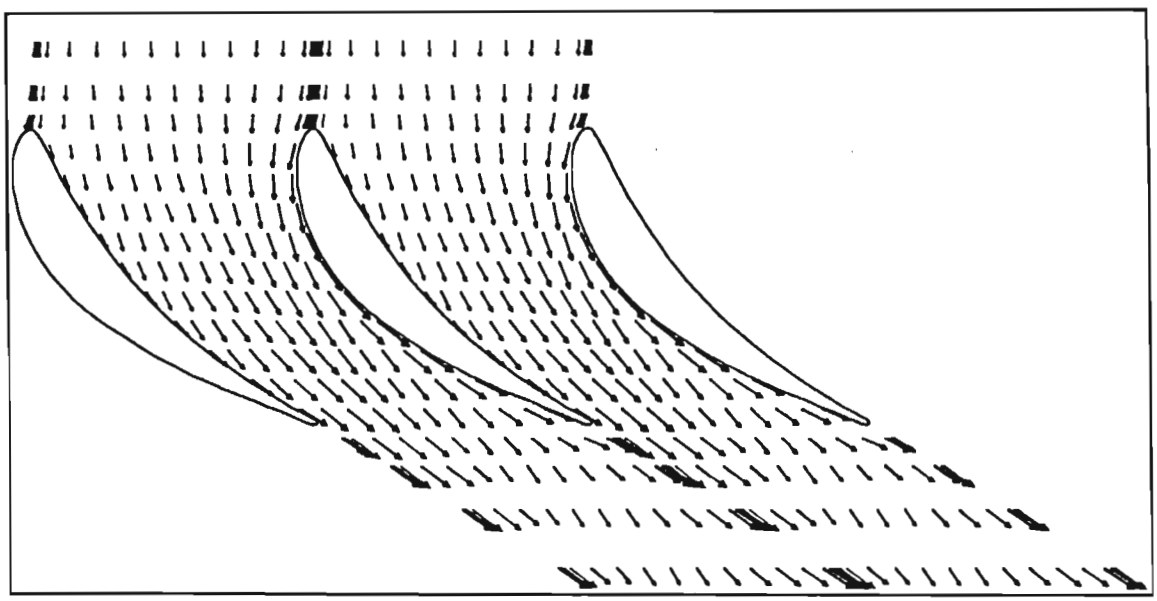

200% of Tip Gap from Endwall

Figure 2.8 Velocity vectors of Basson (1993) at constant spanwise positions projected onto a blade to blade plane.

CHAPTER 3

APPARATUS AND INSTRUMENTATION

1 Introduction

A one and a half stage turbine was designed and built, which included three rotors with different blade tip geometries as well as the first and second stage nozzles. The nominal diameters were 406.5 mm for the outer casing and 284.5 mm for the hub. The performance assessment of the three rotors and of the downstream nozzle, not only required the design and construction of five fully bladed turbine discs, but also required traverse automation to make feasible the numerous measurements that were required. The automatic control of the rig operating point was essential. Since it was necessary to measure small differences in performance, the instrumentation had to be both accurate and repeatable.

The standard rotor tip clearance was 1% of tip chord (.45mm, .75% span, .11% of rotor diameter). The two additional clearances of 2% and 3% chord were achieved by using two larger diameter rotor casings carefully blended back to the standard dimension in front of and behind the rotor to avoid sharp steps.

The outer casing hubs were cast from LM25 aluminium and then heat treated to improve strength and hardness. Rotor and stator hubs were then turned and the chordwise T-shaped slots for blade mounting were milled. A full cross sectional view of the rig is shown in Figure 3.1.

The turbine rig was driven by a downstream centrifugal fan powered by a variable speed hydrostatic pump/motor combination. Turbine power was absorbed and the speed controlled by another hydrostatic pump whose outlet pressure could be adjusted by a throttle valve.

2 Aerodynamic design

Twisted blades were designed with repeating stages (i.e. first stage geometrically identical to second stage) for ease of manufacture (thus only one nozzle row and one rotor row of blades had to be designed). The flow enters the first nozzle in an axial direction thus a restraint was that the absolute rotor outlet velocity had to be axial so that the second stage nozzle is similar to the first.

A free vortex radial variation of the velocity triangles was assumed. Table 3.1 summarises the design data and Figure 3.2 shows the velocity diagrams at hub, mid-span and tip. The blade profiles were designed using a commercial package (Northern Research and Engineering Corporation (1972) (NREC). The original software was re-compiled to run on an IBM-PC compatible computer and a Pre-processor and Post-processor written by Malan (1986) and called PC-NREC was used to facilitate input and output. The NREC program "BLADE" was used to design the blade profiles at the five radial stations using the flow angles calculated above. The program "BLADE" requires the inlet and outlet Mach numbers, inlet and outlet flow angles, and the Mach number distribution. The design process is an

iterative one where the Mach number distribution is entered, then a blade profile is designed and the Mach number distribution is then adjusted accordingly until a suitable blade profile is found. Other parameters used for selecting the blade profile were blade chord, trailing edge thickness and blade area. The guides given in the NREC manual (volume 1) on the Mach number distribution were adhered to. The most important ones were the maximum allowable Mach number as a function of outlet Mach number, and the maximum rate of diffusion on the suction surface. A prime number of blades was chosen for both nozzle and rotor for vibration reasons.

Table 3.1 Summary of turbine data

	Hub		**Mid**		**Tip**
Radius [mm]	142.0	157.25	172.5	187.75	203.0
α_1	0.0	0.0	0.0	0.0	0.0
α_2	66.10	63.86	61.70	59.63	57.64
α_3	0.0	0.0	0.0	0.0	0.0
β_2	42.83	29.49	13.63	-2.93	-17.85
β_3	53.05	55.81	58.23	60.36	62.25
Reaction	0.15	0.31	0.42	0.51	0.58
V_x/U	0.752	0.680	0.617	0.568	0.526
ψ	3.394	2.771	2.292	1.938	1.661

From Table 3.1 it can be seen that the nozzle outlet flow angle only varies by about 10 degrees from hub to tip. This variation was approximately linear and therefore

the hub and tip blade profiles were first designed and then the Mach number distributions were calculated by linear interpolation for the other three intermediate radii. The blade profiles were then computed (using program BLADE). The design nozzle Mach number distributions are shown in Figure 3.3 and blade specifications are listed in Table 3.2. The number of blades selected was 41 giving a nozzle blade chord of 41.8 mm at mid-chord and an aspect ratio 1.46. The blade chords at tip and hub were 46.5 mm and 36.8 mm respectively. Figure 3.4 shows the five superimposed blade profiles at equally spaced radii. The profiles were stacked with their centre of gravity on a common axis. For both the nozzle and the rotor blades a further 24 profiles were calculated by linear interpolation, giving a total of 29 radial profiles for machining the blades.

The rotor blade profiles were first designed at hub, mid-radius and tip, and then the Mach number distributions were linearly interpolated for two more intermediate radii. The number of rotor blades chosen was 43 giving a chord of 46 mm. The blade chord was kept constant from hub to tip. The blade was designed such that the profile cross sectional area decreased from hub to tip for strength considerations. The Mach number distributions and the five stacked rotor blade profiles are shown in Figure 3.5 and Figure 3.6, and the blade specifications are presented in Table 3.2. The blade co-ordinates are given in Appendix 3.1 and stacking was on point (0,0). The axial spacing between blade rows was 20 mm at the hub.

Table 3.2 Nozzle and Rotor blade profile specifications

	Hub		Mid		Tip
Radius [mm]	142.0	157.25	172.5	187.75	203.0
Nozzle chord [mm]	36.8	39.5	41.8	44.8	46.5
Rotor chord [mm]	46.3	46.2	46.0	46.0	46.0
Nozzle thickness max. [%chord]	18.5	19.0	15.8	14.7	14.3
Rotor thickness max. [%chord]	17.3	16.5	15.3	15.3	15.3
Nozzle Blade area [mm^2]	143	154	164	180	195
Rotor Blade area [mm^2]	248	233	201	186	162

	Nozzle	Rotor
Trailing Edge Thickness	1 mm	0.7 mm
Mid Pitch/Chord ratio	0.55	0.63
Number of blades	41	43
T-slot angle [degrees]	42	18

3 Blade moulding

A master rotor (square tip only) and nozzle blade were NC machined in brass including a pedestal that would form the hub endwall and a chordwise T shaped mounting root. After hand polishing, these were used to make multiple moulds for blade production. The moulds for the two additional rotor tip shapes were made by

adapting a square tip mould at the tip only, thus ensuring that variations only occurred at the tip.

It should be noted that the two, low loss blade tips involve radii that are chosen to suppress separation bubbles on the blade tip. These radii were shown to depend on the gap dimension (Morphis & Bindon (1988)). The experimental program could not afford to make the four extra rotors needed for variations in clearance gap and thus only two rotors were made with radii suitable for the 1% clearance considered to be the dimension more closely resembling current engine practice.

The moulds were cast from CIBA GEIGY AEROLDIT CW 216/HY 216 tooling epoxy. A split line was generated with modelling clay and the one side of the mould was cast. After curing the modelling clay was removed and the second side was cast.

The blades were cast from CIBA GEIGY UREOL 6414A/XB3117 Polyurethane resin. This resin was selected for its relatively high tensile strength (45-50 Mpa), high toughness and low shrinkage properties. The stress at the rotor root due to centrifugal forces and bending (caused by the pressure difference across blade) was calculated at roughly 2 Mpa at 3000 rpm and design axial velocity. Despite the blades being moulded in high strength dimensionally stable epoxy, special curing procedures had to be developed in conjunction with the suppliers to ensure the blade length and clearance gap did not change with time.

The moulding of the nozzle blades and the single square tipped rotor was relatively straight forward, since after the blades were cast, cured and mounted in the hub, the assembly was spun in a lathe and turned down to achieve the exact tip clearance desired. However, when attempting to approach the problem of making a rotor with a shaped tip rather than a square tip, not only did a new moulding technique have to be used to create the tip, but a much greater degree of accuracy had to be employed. Any significant removal of material at the tip to achieve the specified tip clearance would have affected the carefully moulded tip shape.

While experimenting with achieving mouldings of a repeatable and accurate length, it was found that the epoxy resins were not meeting their shrinkage specifications. Shrinkage was continuing after the post curing (14 hours at 40 C) specified by the manufacturers to eliminate long term shrinkage. After extensive communications with the suppliers and verification of results by trial mouldings and curing, a new, lengthy post curing method that totally pre-shrank the blades was developed. The new post curing procedure for the UREOL 6414a/xb3117 polyurethane resin which took 17 days is described in Morphis & Bindon (1992).

The shrinkage was determined by inserting the post cured blades back in the moulds and measuring the tip clearance between the blade and mould. A number of blades were measured and it was found that the shrinkage depended on the blade thickness. The shrinkage was 0.15mm at the leading edge and 0.5mm at the trailing edge. The variation from leading edge to trailing edge was approximately linear. New master blades that had been cast and cured were mounted in a rotor hub and the tip

diameters were machined at an angle of 0.74 degrees with an extra 0.1mm to allow for final tip clearance machining on the rotors. The tip diameters of the master blades were 406.2mm at the leading edge and 407mm at the trailing edge to give the correct clearance of 1% chord (0.45mm).

The tips of the master blades were then hand shaped to the radiused tip and the radiused squealer shapes. The radiused tip blade had a constant pressure corner radius from leading edge to trailing edge. The pressure corner shape of the radiused squealer blade had a chordwise variation as shown in Figure 3.10. These blades were then used to produce the moulds. Two sets of moulds were produced for each turbine disc giving a total of ten moulds.

The blades for the two shaped tips were moulded, cured and mounted. The accuracy achieved required very little in the way of final trimming (.1 mm) in a lathe and the effective tip shape was not significantly affected by the amount of material that had to be removed to reach the required tip clearance.

4 Instrumentation

In this research the performances of the first stage nozzle, the second stage nozzle, the single stage and of the one and a half stage, including the different rotor blade tip geometries, was required. The only way to truly evaluate these performances was to define, measure and calculate various efficiencies. Since all turbine efficiency

definitions involve isentropic quantities that are defined by pressure, the complex fluctuating flow field behind a rotor requires a quick response probe and transducer system. A hot wire or a laser cannot be used since they do not measure pressures. A conventional 5 hole probe that records a widely accepted mean of the high frequency pressure field was finally adopted.

The 2 Dimensional flow field in each traverse plane was measured with a 5 hole United Sensor 3.2mm diameter probe (DC-125-12-CD) used in the null yaw mode where the yaw angle was set by the automated traverse system responding to the differential yaw pressures. The pitch angle was found from the probe calibration (which was calibrated from -40 to 40 degrees) and the pitch hole pressures.

The measurements that were required to calculate the coefficients and efficiencies that are presented in Chapter 4, are shown diagrammatically in Figure 3.7 and were as follows:-

Inlet air temperature and absolute pressure.

Reference point (inlet free stream) static and total pressure (position Ref).

Rotor torque and rotational speed.

1-D traverse upstream of the first nozzle (position 1).

2-D traverse downstream of the first nozzle or rotor inlet (position 2).

2-D traverse downstream of rotor or inlet to second nozzle (position 3).

2-D traverse downstream of second nozzle (position 4).

The inlet air temperature was measured with two LM 335 absolute temperature sensors with a 10mV/K output and an accuracy 0.5 K, and the absolute pressure was measured with a Kulite ITQ-1000 (0- 100mv) pressure transducer with a repeatability of 0.25% of full scale. The inlet reference static pressure was measured from 4 holes equally spaced in the circumference of the outer casing and the total pressure was measured with a United Sensor KBC-6 kiel probe. The 1-D and 2-D traverses in front of and behind the blade rows were all done with the 5-hole probe mentioned above. The reference pressures and the pressures from the 5-hole probe were measured using five Fuji differential pressure transducers (3 off 0-250mm & 2 off 0-600mm) connected as in Morphis (1989) to minimise errors and number of transducers. The rotor torque and rotational speed were measured with a Himmelstein MCRTC 2800T(35-1) torque transducer with a speed sensor. The torque transducer was the enhanced accuracy version with a repeatability better than 0.02% of full scale and was matched to a Himmelstein transducer amplifier (Model 6-201).

The analog electrical voltages from the torque, pressure and temperature transducers were recorded by the IBM PC compatible computer via an Eagle Electric PC-30b A/D card with a frequency response of 30 kHz. The frequency output from the Himmelstein speed encoder was first put through a Schmidt trigger amplifier and then read by a Phillips PM2519 multimeter with an IEEE-488 output port. This digital parallel signal was then read by the IBM PC compatible via an IEEE-488 I/O card.

5 Automation of traverse mechanism and rig control

The five hole probe traverse mechanism provided movement in two axes, namely radial and yaw. Tangential movement was achieved with a second traverse mechanism that rotated a section of the outer casing to which the radial/yaw mechanism was mounted. Figure 3.9 shows a schematic of the rig and traverse mechanisms. The three axes were driven by three independent stepper motors with a resolution 200 steps per revolution. Each axis could also be controlled manually for setting up the reference points and dial gauges were attached to each axis so that an absolute reading of the probe position could be obtained. After gearing, the resolutions of the three axes were as follows:

Tangential	264 steps per degree
Radial	200 steps per mm
Yaw	10 000 steps per revolution (360 degrees)

The gearing system for the radial/yaw mechanism had no backlash thus it could be controlled in any direction whereas the tangential axis had about 5 steps of backlash. This backlash was compensated for by the software. Two dimensional traverses were done from 2mm from the hub to 2mm from the outer casing in the radial direction and for one nozzle pitch in the tangential direction. The measurement grid was as shown in Figure 3.9 with 11 tangential and 20 radial stations. This gave grid spacings of .878 degrees in the tangential direction and 3mm in the radial direction, that were approximately the same size as the probe diameter of 3.2 mm. The axial

position of the measurement planes was at a distance of 5mm behind the most downstream part of the trailing edge.

Traversing and null yawing the probe manually to obtain a map of the flow is a very time consuming and laborious task when done manually, thus the rig was fully automated. The automation process was a joint effort between Ivan Kaiser and the author. Ivan Kaiser developed the basic software routines (Kaiser (1992)) and the author produced the hardware. All software was written with Turbo Pascal V6.0 by Borland.

In addition to traversing, null yawing and reading pressures, temperature, torque and rotor speed, two more parameters had to be controlled. These were the axial velocity (and thus Reynolds number) and the V_x/U or design point. Two stepper motors were used to control these parameters. The first stepper motor, was used to adjust the axial velocity via the swash plate of the hydrostatic pump/motor combination. The second stepper motor, was used to adjust the rotor speed and V_x/U ratio via the throttle valve on the outlet of the hydrostatic pump that absorbed the shaft power. A six channel unipolar stepper motor driver that was controlled from the second parallel port on the IBM PC compatible was designed and built to drive the stepper motors.

The throttle valve setting was affected by the viscosity of the hydraulic oil which depended on oil temperature while the axial velocity or Reynold's number was affected by changes in atmospheric conditions such as temperature and pressure.

Thus in order to maintain a constant V_x/U ratio and Reynold's number during operation, the above two parameters were checked at each grid point before and after the measurements and were adjusted if necessary.

Due to the long running times and the complexity of the system the probability of a failure was high and thus it was necessary for the rig to shut down automatically if certain failures occur to protect major components. The major components that needed protection were the hydrostatic pumps and motor, the turbine rotor and the torque transducer. The hydrostatic pumps and motor were protected against over heating (cooling circuit failure) and against lack of lubrication (hydraulic fluid leak). The rotor was protected against accidental over-speed and the torque transducer against overload.

6 Repeatability and optimum V_x/U

The repeatability of the turbine rig and instrumentation is of great importance since small changes in efficiency had to be detected. This was examined by performing full 2D traverses for the same rotor on various days. For a series of 5 runs the efficiencies were found to be repeatable to within .05%. Although encouraging, this result did not however give any indication of the ability of the rig to detect small changes in tip clearance configuration. The second nozzle had a tip clearance of 0.1 mm or .22 %chord necessary for assembly and traversing. An increase in second nozzle efficiency of approximately .3% was measured for all three rotors when this

small clearance was eliminated by inserting 0.1 mm shim between the blades and outer casing. The shim was then removed and the efficiency was once again measured to within .05% of previous runs. The operating point of the rig was set and held to within .1% by computer control of the high pressure oil circuits.

A further check on the reliability of the results was provided by comparing the torque transducer based performance with a purely aerodynamic traverse based performance. The two results reflected identical trends and were different only by a constant that was attributed to disc and bearing friction. The single stage efficiency was measured and plotted for various V_x/U ratios. The point of maximum efficiency on the plot was found to correspond to the design V_x/U.

7 Inlet conditions and turbulence

The radial distributions of total pressure coefficient, velocity coefficient, radial angle and tangential angle at 20 mm from the inlet of the first nozzle are pressented in Figures 3.11, 3.12, 3.13 and 3.14. Since flow velocities were low total temperature was assumed to be constant at inlet.

For completeness, the turbulence level at the turbine inlet was measured. A Disa 55M10 hot wire anemometer system was employed with a 5 micron single wire probe (as used by Adams (1988)). Data Acquisition was done with the PC-30B A/D card and with STATUS-30 data acquisition software supplied with the card. This

software could also execute a Fast Fourier Transform to yield a frequency domain representation. Various sampling frequencies (from 50 Hz to 20 KHz) were used to measure the unsteadiness of the inlet flow. At the operating Reynolds number the turbulence intensity (as defined in Munson et al (1990)) was measured at 3.8%. The turbulence was found to be a broad spectrum noise with no particular peaks.

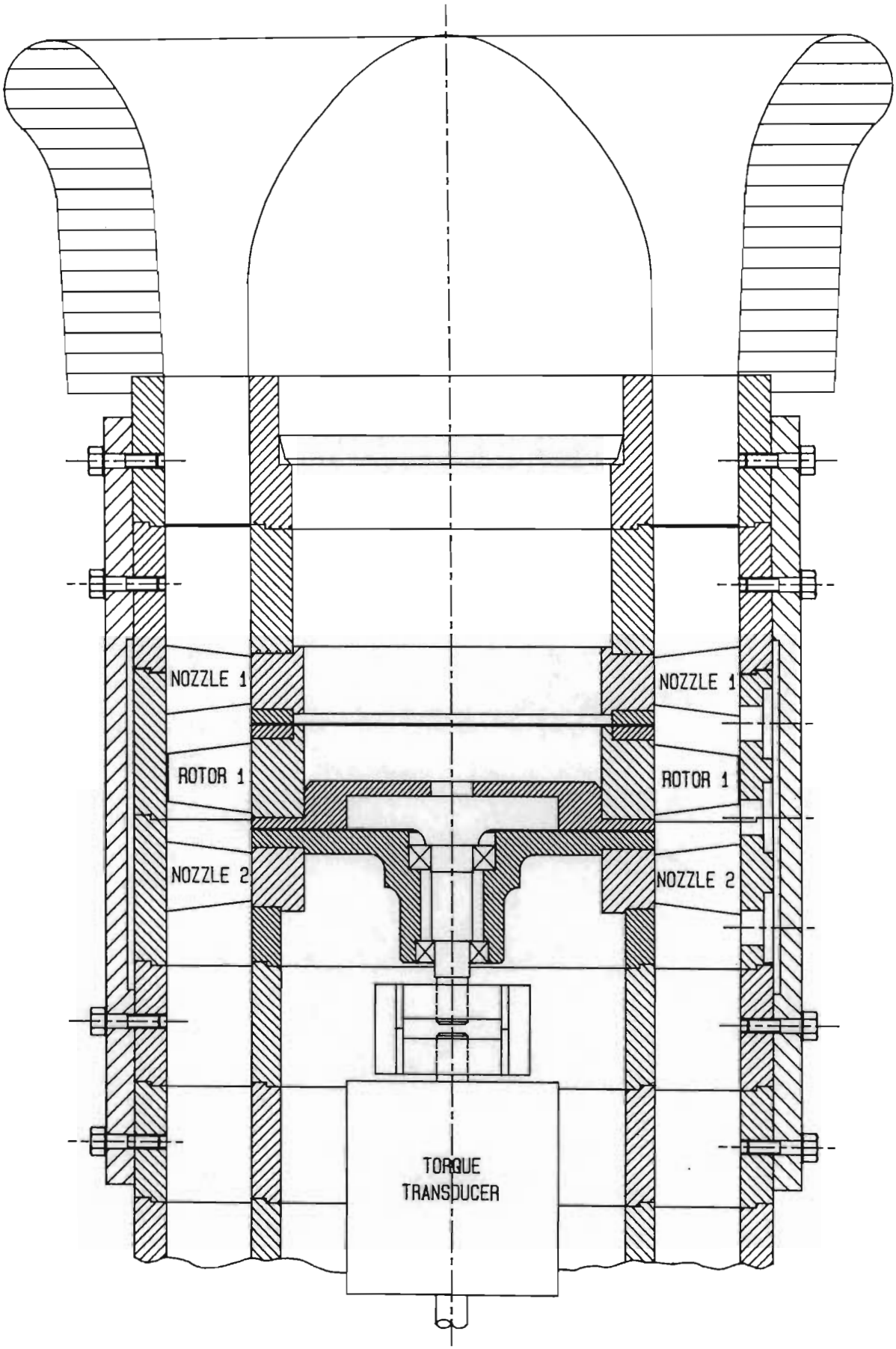

Figure 3.1 Cross sectional view of one and a half stage turbine

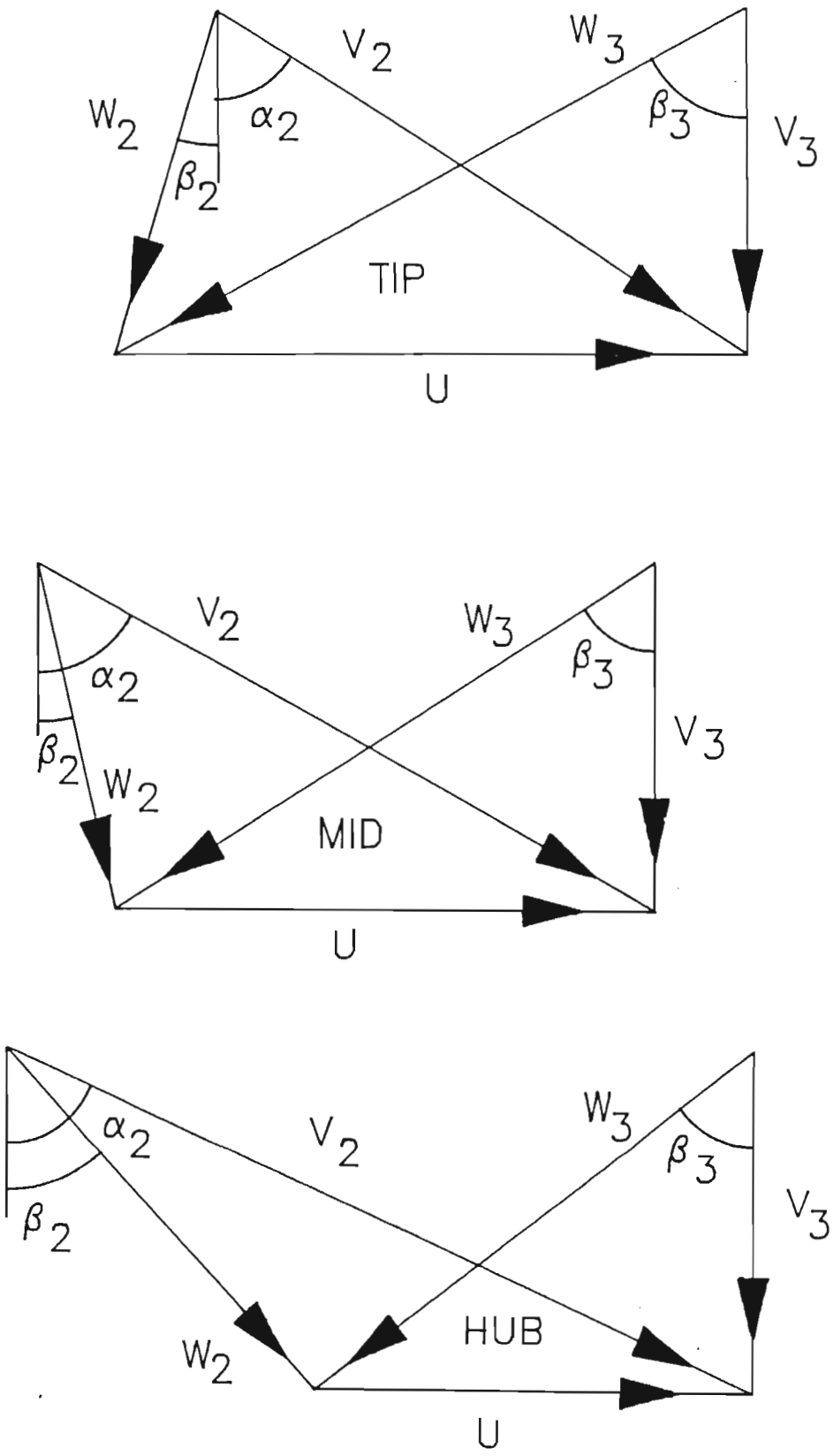

Figure 3.2 Velocity diagrams at hub, mid-radius and tip

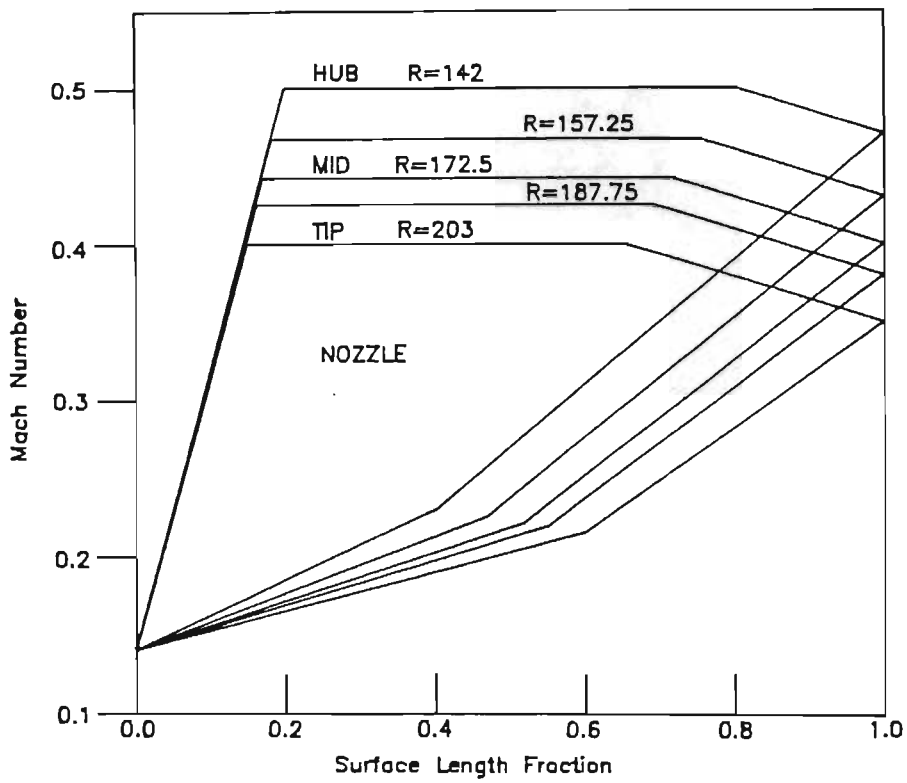

Figure 3.3 Nozzle blade Mach number distributions at 5 radial positions

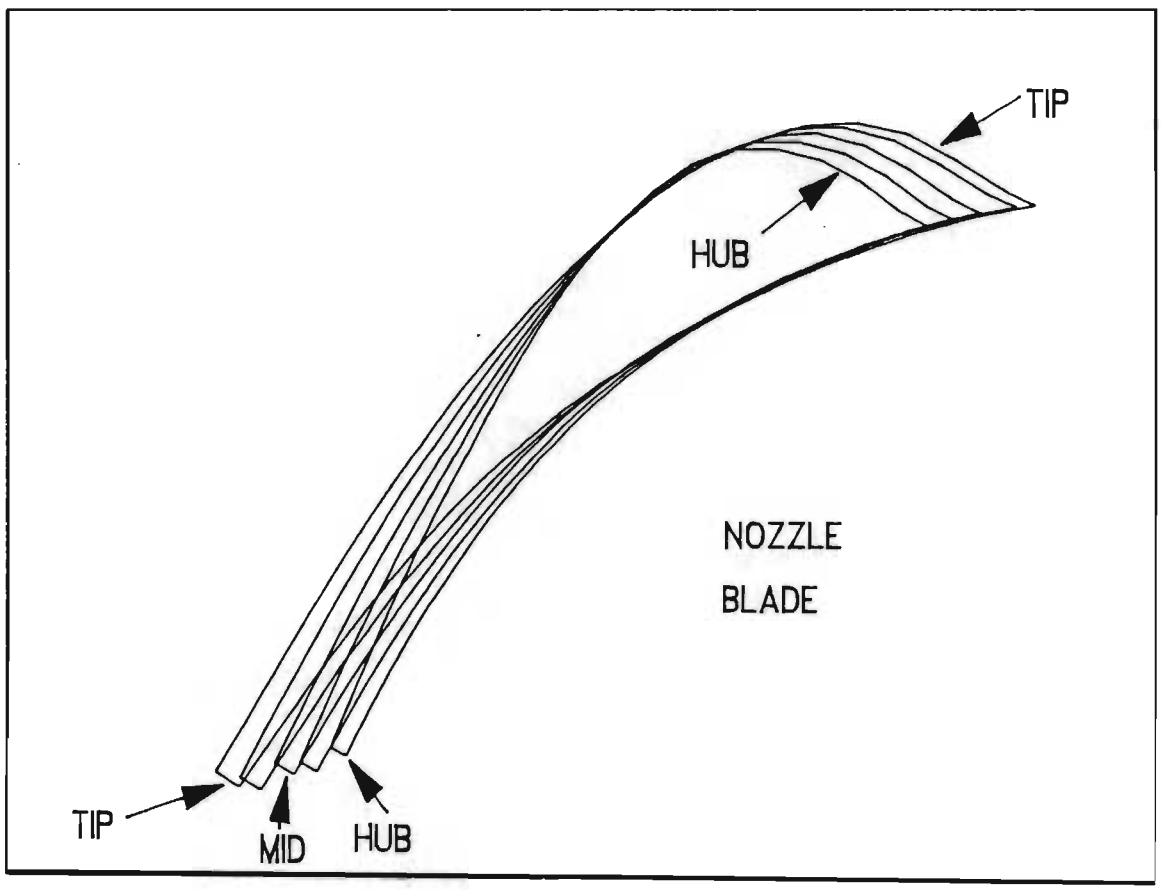

Figure 3.4 Nozzle blade profiles at 5 radial positions

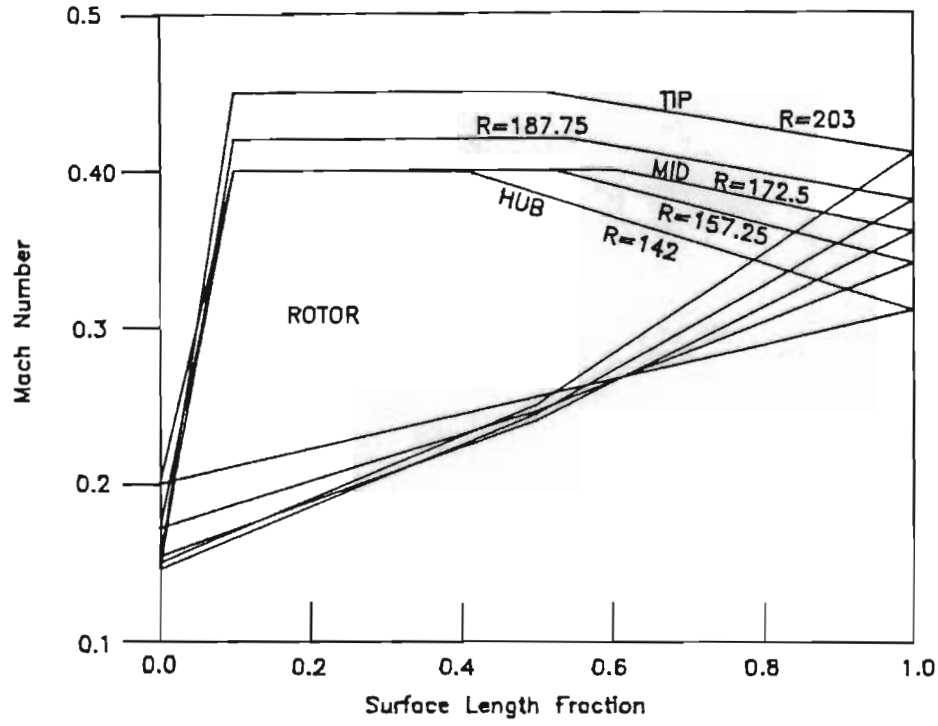

Figure 3.5 Rotor blade Mach number distributions at 5 radial positions

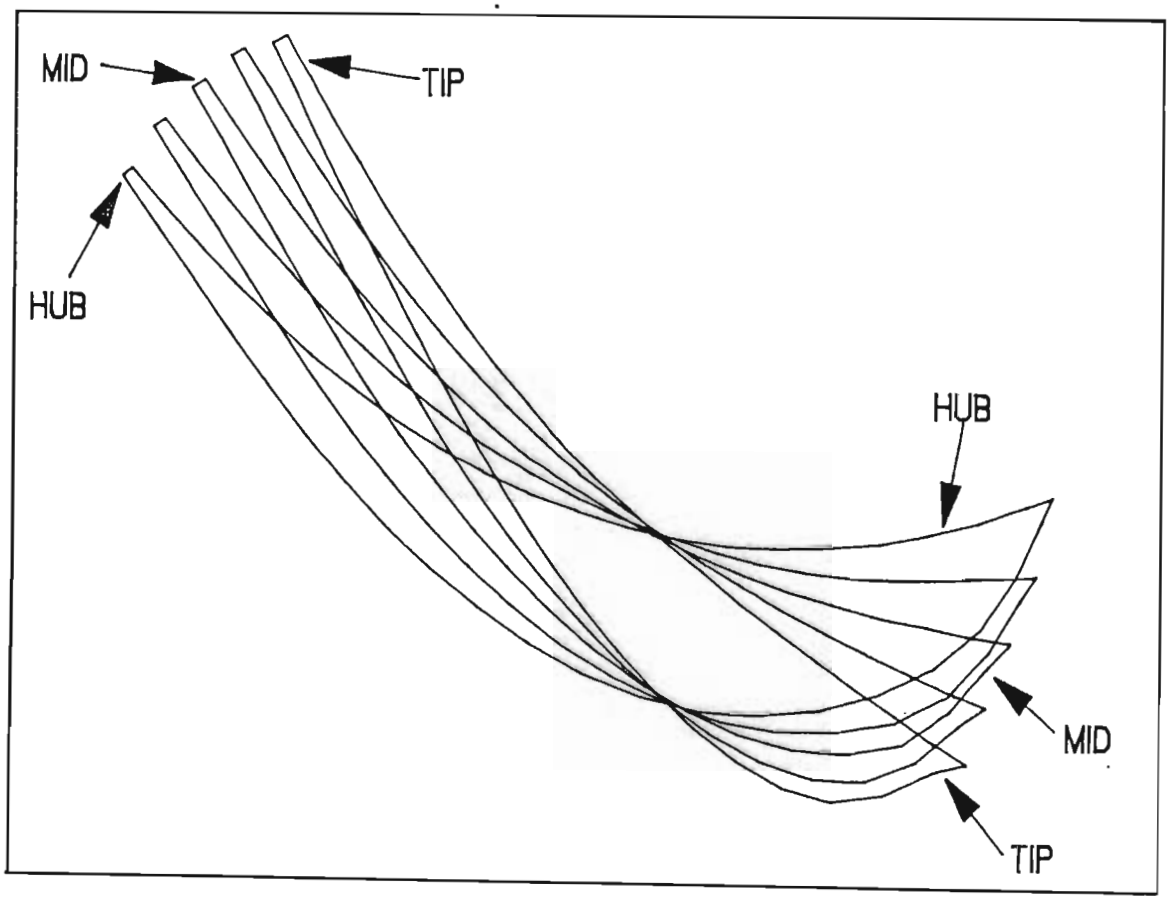

Figure 3.6 Rotor blade profiles at 5 radial positions

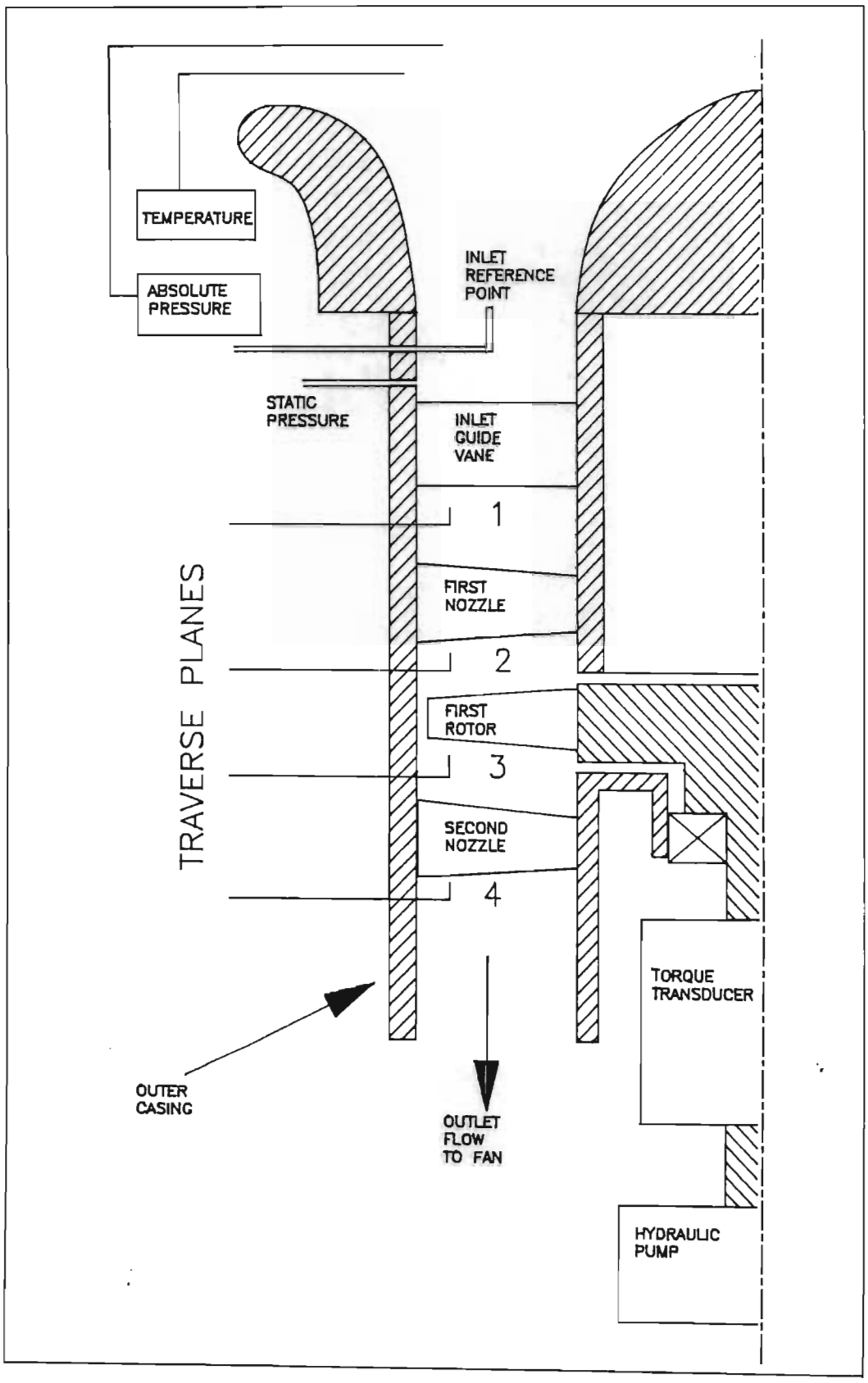

Figure 3.7 Schematic of measurement parameters and positions (not to scale)

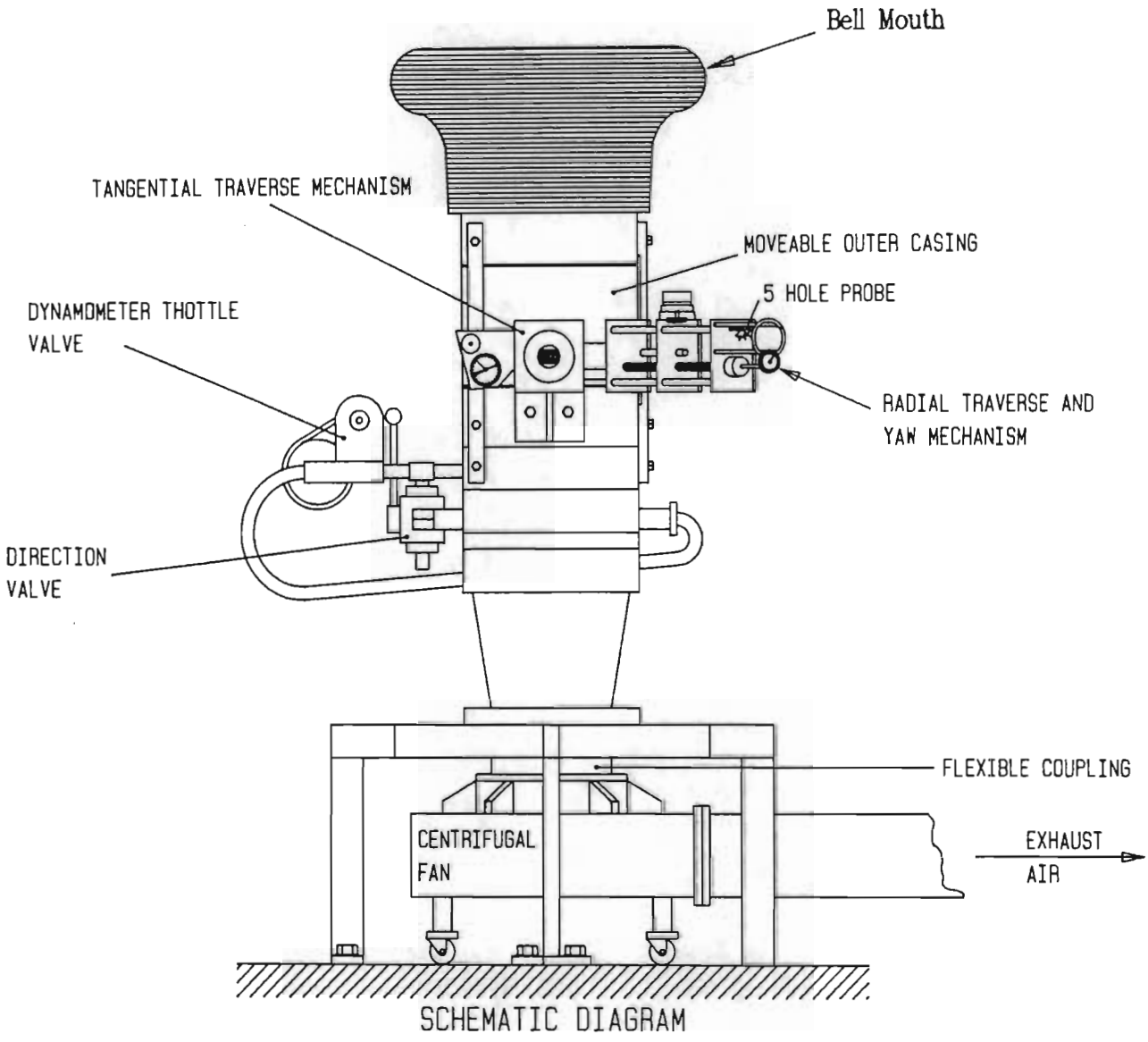

Figure 3.8 Schematic of turbine rig and controls

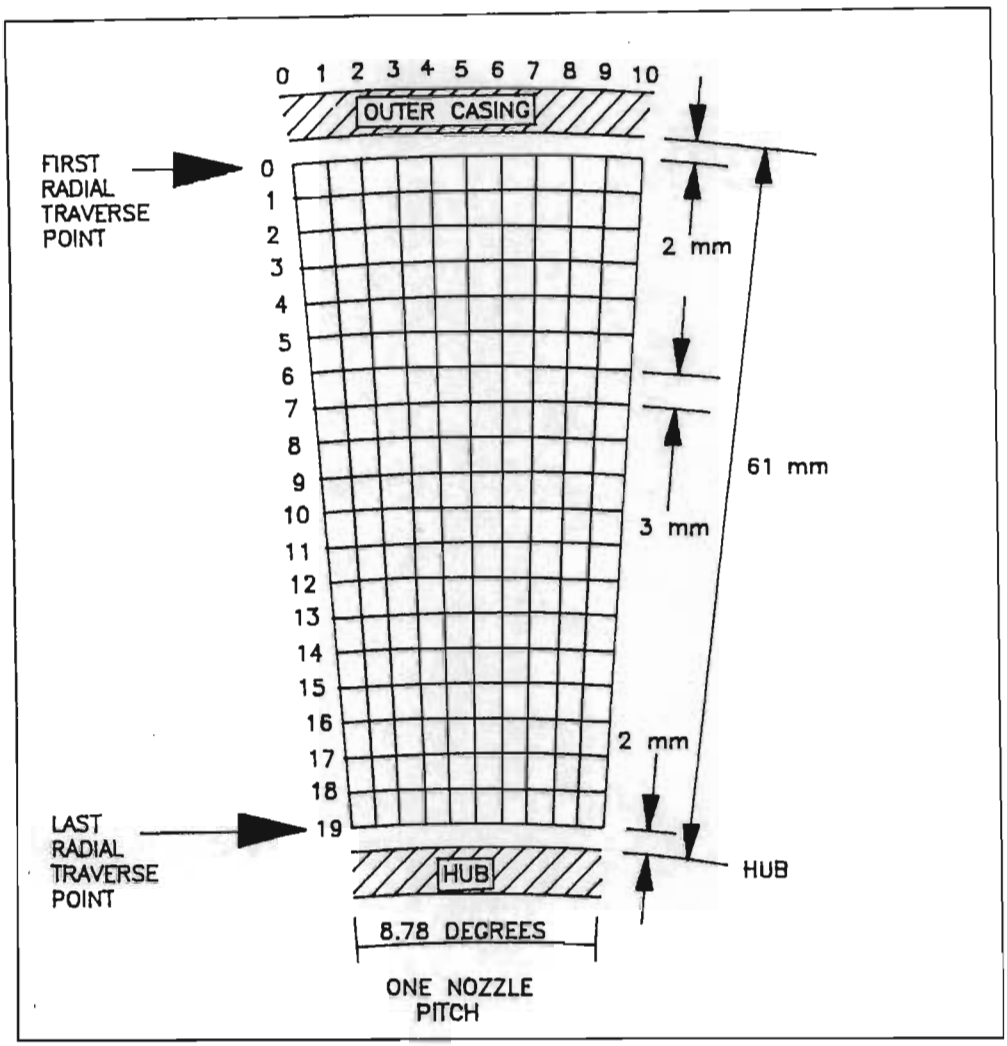

Figure 3.9 Two dimensional polar measurement grid

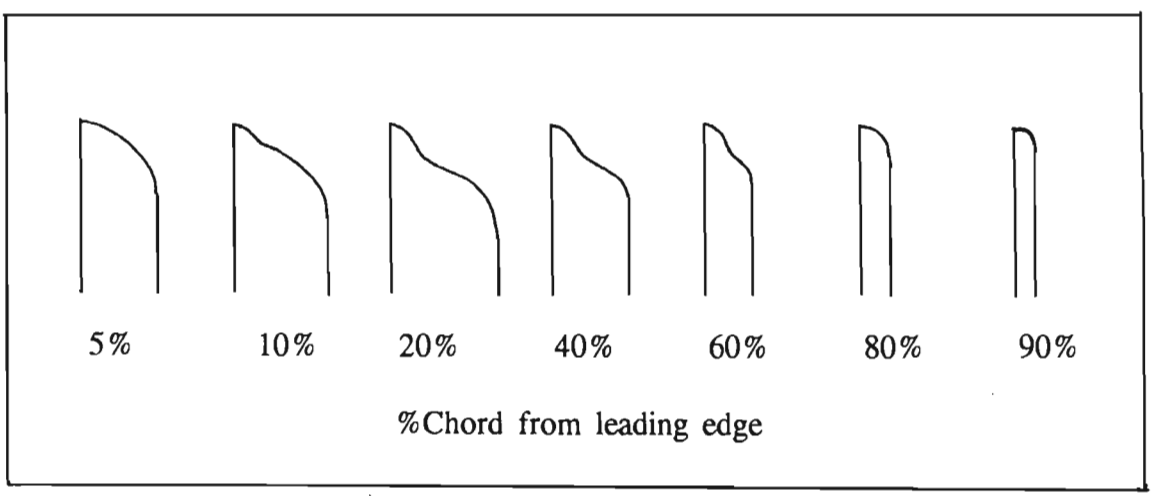

Figure 3.10 Chordwise variation of radiused squealer tip shape

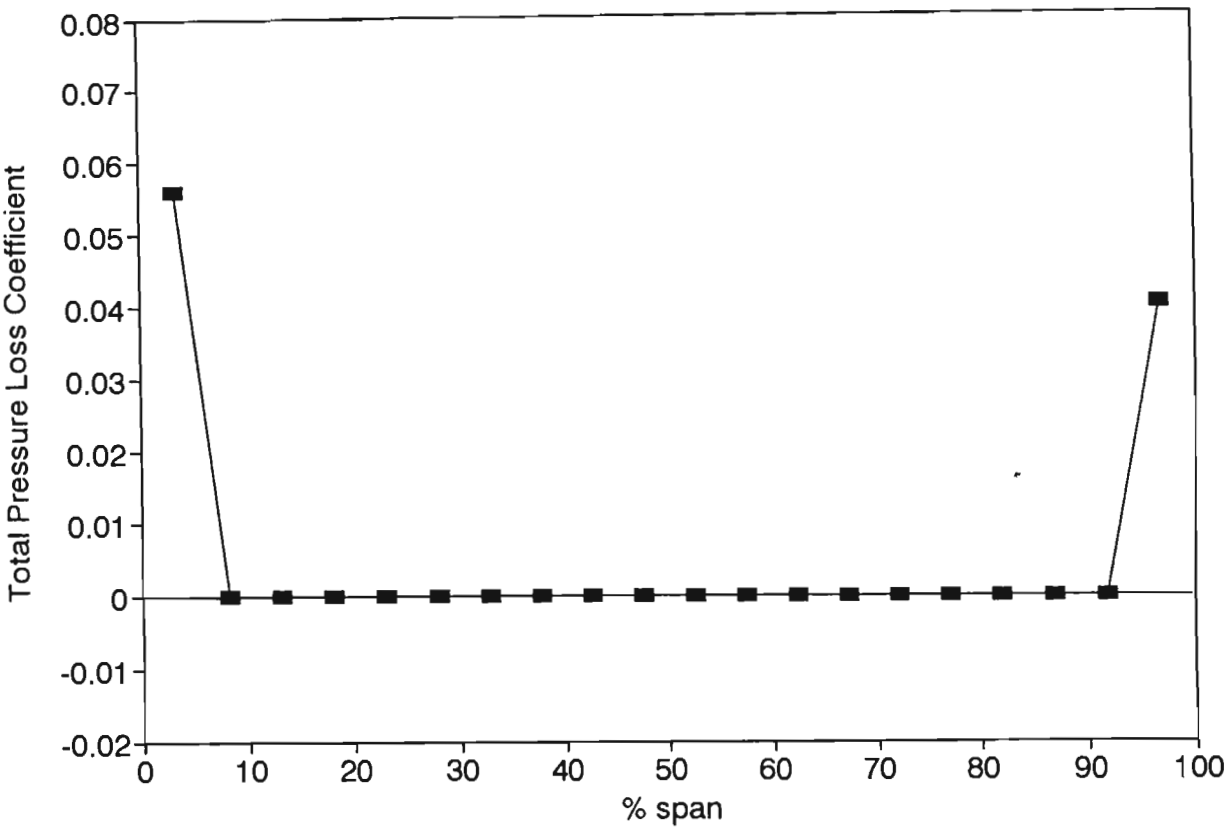

Figure 3.11 Total pressure loss coefficient at first nozzle inlet

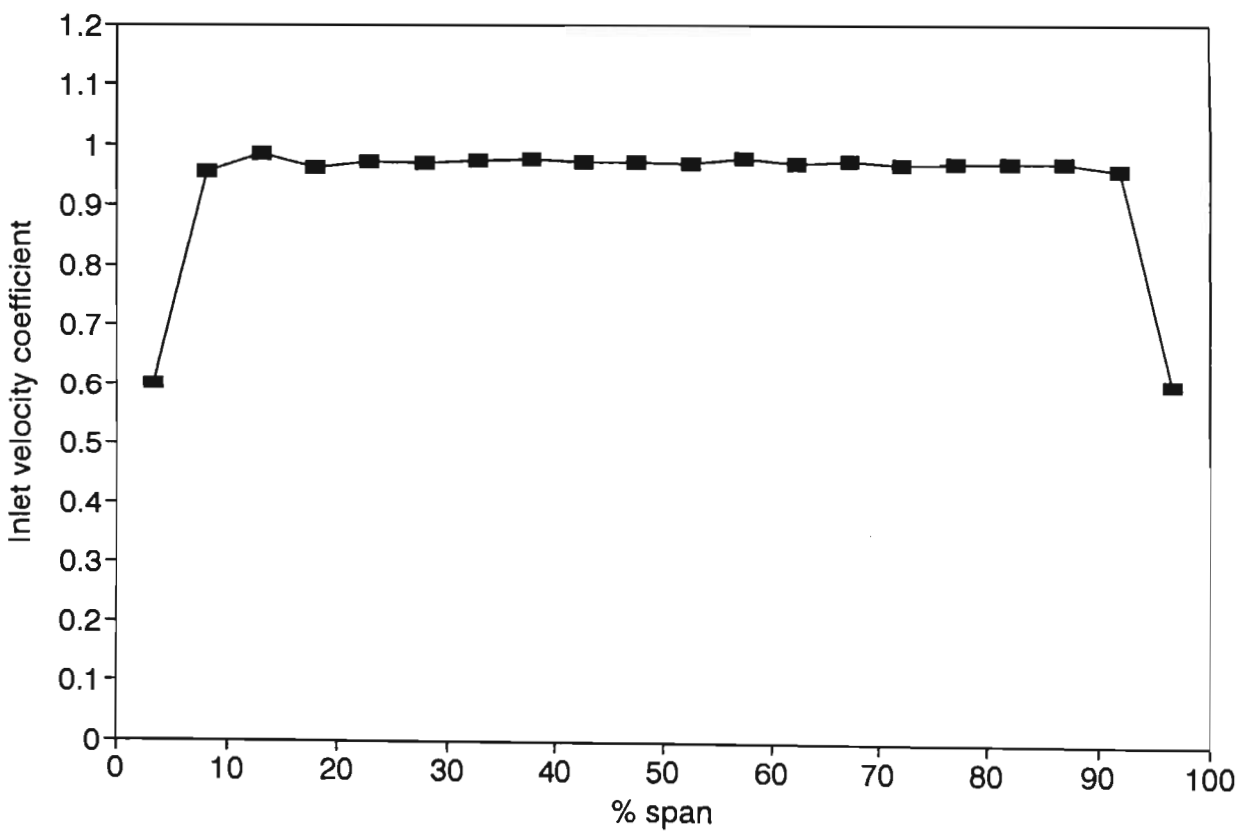

Figure 3.12 Velocity coefficient at first nozzle inlet

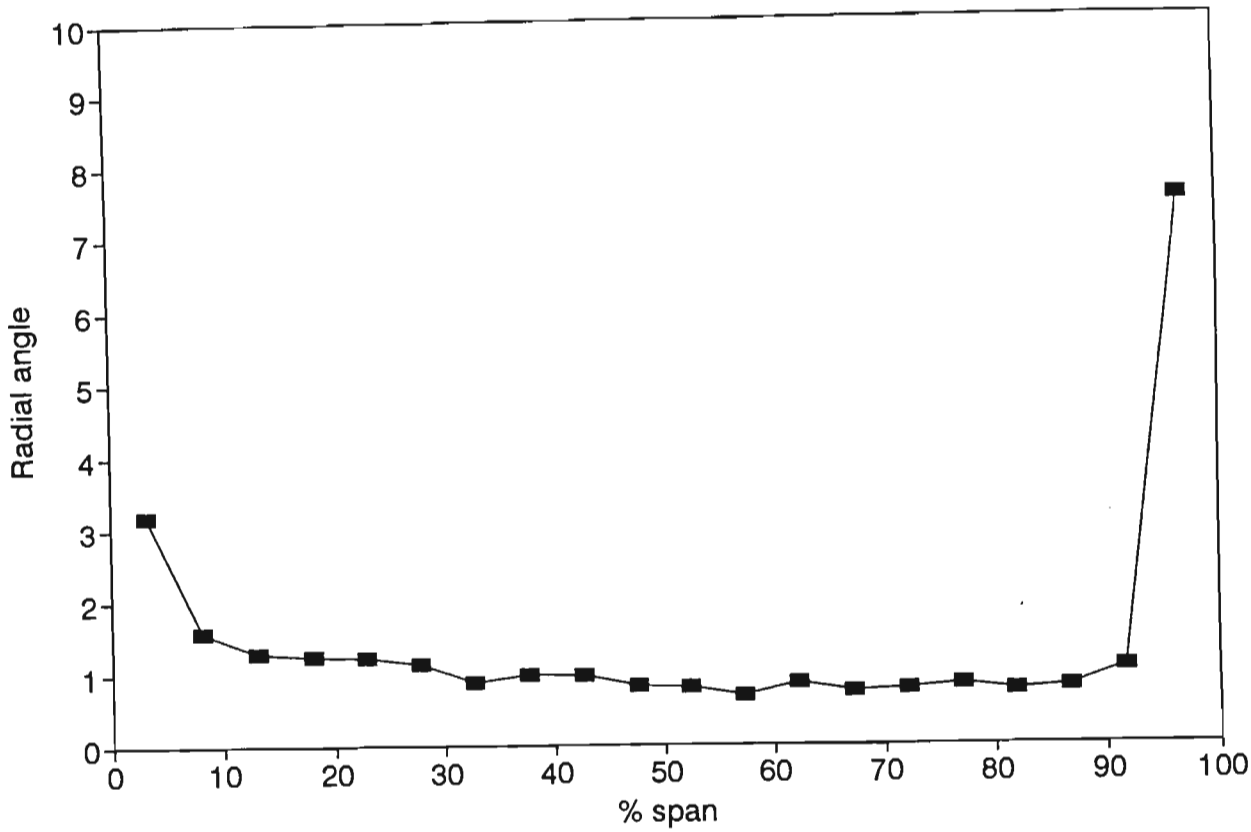

Figure 3.13 Radial angle at first nozzle inlet

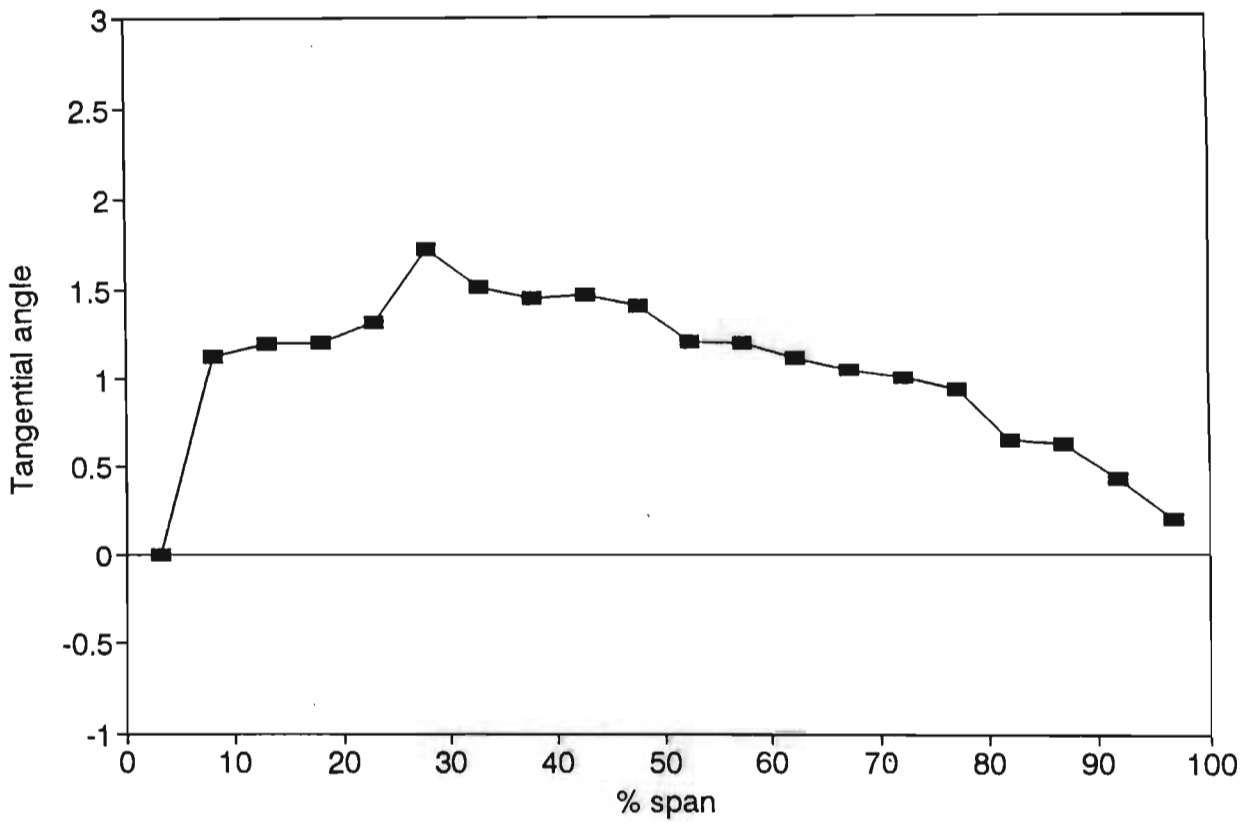

Figure 3.14 Tangential angle at first nozzle inlet

CHAPTER 4

COEFFICIENTS AND EFFICIENCY DEFINITIONS

1 Introduction

The performance assessment of the three rotors and the two nozzles required the definition of various efficiencies. To determine these efficiencies and also to attempt to understand the flow physics, certain dimensionless coefficients had to be defined and calculated. In this chapter, the efficiencies will firstly be defined and then the dimensionless coefficients will be presented.

At each measurement plane the two dimensional grid was made up by discrete measurements at each traverse point. The measurement of the flow for the whole grid took up to eight hours to complete. This meant that inlet conditions to the turbine varied as the atmospheric pressure and temperature changed. The operating V_x/U ratio and Reynold's number were kept constant by the control computer, thus inlet velocity was affected and varied with time. It was thus essential to non-dimensionalise the measured quantities against a reference freestream inlet velocity. The dimensionless coefficients that were generated were thus time independent and direct comparisons could be done between data sets. The flow after the rotor varied as each blade passed the measurement point but was averaged by the five-hole pneumatic probe. The enthalpy-entropy diagram for the complete one and a half stage turbine is shown in Figure 4.1 and was used to define the various efficiencies.

The sign convention used in the definitions and in the presentation of results (Chapters 5 and 6) is shown in Figure 4.2.

2 One and a half stage efficiency

The performance of the various blade tip geometries in a multi-stage environment were evaluated using a one and half stage turbine efficiency defined as follows.

$$\eta_{1.5} = \frac{\overline{\omega} + \overline{\frac{1}{2}V_4^2}}{\overline{h_{o1} - h_{4is}}} \qquad (1)$$

In the numerator of equation (1), the first term represents the specific work extracted by the rotor and the second term embodies the kinetic energy leaving the second stage nozzle. Where ω can be a mechanically averaged quantity based on torque or it can be quantity, like the other terms, that represent an average for the whole flow field. Therefore, for incompressible flow (for more detail see Appendix 4.1) :

$$\eta_{1.5} = \frac{\overline{\rho\omega} + \overline{\frac{1}{2}\rho V_4^2}}{\overline{P_{o1} - P_{s4}}} \qquad (2)$$

The denominator has become the driving pressure across the complete one and a half stage turbine. As mentioned Section 1, the measurements were not all taken in one moment in time and thus turbine inlet condition varied from one measurement to the next and a straight forward mass averaging technique could not be used. Terms in equation (2) were first non-dimensionalised with inlet dynamic pressure as follows.

$$\eta_{1.5} = \frac{\overline{\frac{\rho\omega}{q_{ref}}} + \overline{\frac{\frac{1}{2}\rho V_4^2}{q_{ref}}}}{\overline{\frac{P_{o1} - P_{s4}}{q_{ref}}}} = \frac{\overline{C_\omega} + \overline{C_{V_4}}}{\overline{C_{P_{o1} - P_{s4}}}} \qquad (3)$$

3 Single Stage Turbine Efficiency

Two efficiency definitions are commonly used to evaluate turbine performance, namely total-to-total and total-to-static. The total-to-total efficiency assumes that the kinetic energy in the fluid leaving the rotor can be utilized. That would be as if the rotor was able to 'convert' its exit kinetic energy into a useful effect, for example as in a perfect downstream nozzle or diffuser. The total-to-static efficiency assumes that only the work extracted by the rotor is useful and that all energy in the flow leaving the rotor is lost.

The total-to-total efficiency was defined as follows.

$$\eta_{tt} = \frac{\overline{\omega}}{\overline{h_{o1} - h_{o3is}}}$$

$$= \frac{\overline{\omega}}{\overline{h_{o1} - h_{3is}} - \overline{\frac{1}{2}V_{3is}^2}} \qquad (4)$$

It was assumed that $V_3 = V_{3is}$

As before, for incompressible flow averaged across the flow field and non-dimensionalising with the inlet dynamic pressure, equation (4) becomes.

$$\eta_{tt} = \frac{\dfrac{\overline{\rho\omega}}{q_{ref}}}{\dfrac{\overline{P_{o1} - P_{s3}}}{q_{ref}} - \dfrac{\overline{\frac{1}{2}\rho V_3^2}}{q_{ref}}}$$

$$= \frac{\overline{C_\omega}}{\overline{C_{P_{o1}-P_{s3}}} - \overline{C_{V_3}}} \qquad \textbf{(5)}$$

The total-to-static efficiency was defined as follows.

$$\eta_{ts} = \frac{\overline{\omega}}{\overline{h_{o1} - h_{3is}}} \qquad \textbf{(6)}$$

$$\eta_{ts} = \frac{\dfrac{\overline{\rho\omega}}{q_{ref}}}{\dfrac{\overline{P_{o1} - P_{s3}}}{q_{ref}}}$$

$$= \frac{\overline{C_\omega}}{\overline{C_{P_{o1}-P_{s3}}}} \qquad \textbf{(7)}$$

4 Nozzle efficiency

A first and second nozzle efficiency were defined as follows.

$$\eta_{N1} = \frac{\overline{\frac{1}{2}V_2^2}}{\overline{h_{o1} - h_{2is}}} \qquad (8)$$

and

$$\eta_{N2} = \frac{\overline{\frac{1}{2}V_4^2}}{\overline{h_{o3} - h^*_{4is}}} \qquad (9)$$

(Note: * denotes h at P_4 and s3)

Which, as before, becomes

$$\eta_{N1} = \frac{\overline{\frac{1}{2}\rho V_2^2}}{\overline{P_{o1} - P_{s2}}} = \frac{\overline{C_{V_2}}}{\overline{C_{P_{o1}-P_{s2}}}} \qquad (10)$$

and

$$\eta_{N2} = \frac{\overline{\frac{1}{2}V_4^2}}{\overline{P_{o3} - P_{s4}}} = \frac{\overline{C_{V_4}}}{\overline{C_{P_{o3}-P_{s4}}}} \qquad (11)$$

5 Rotor Efficiency

Here again two efficiency definitions are used that are similar to the single stage total-to-total and total-to-static. The only difference is that the driving pressure is measured across the rotor as opposed to the whole single stage. The total-to-total rotor efficiency was defined as follows.

$$\eta_{R_{tt}} = \frac{\overline{\omega}}{\overline{h_{o2} - h_{o3}}}$$

$$= \frac{\overline{\omega}}{\overline{h_{o2} - h_{3is}} - \overline{\frac{1}{2}V_3^2}} \qquad \textbf{(12)}$$

Which, as before, becomes

$$\eta_{R_{tt}} = \frac{\overline{\frac{\rho\omega}{q_{ref}}}}{\overline{\frac{P_{o2} - P_{s3}}{q_{ref}}} - \overline{\frac{\frac{1}{2}\rho V_3^2}{q_{ref}}}}$$

$$= \frac{\overline{C_\omega}}{\overline{C_{P_{o2}-P_{s3}}} - \overline{C_{V_3}}} \qquad \textbf{(13)}$$

Similarly, the total-to-static rotor efficiency was defined as

$$\eta_{R_{ts}} = \frac{\overline{C_\omega}}{\overline{C_{P_{o2}-P_{s3}}}} \qquad \textbf{(14)}$$

6 Dimensionless Coefficients

In this section the method used to calculate the mass averaged coefficients is presented. The coefficients were firstly calculated at each grid point. These coefficients represent the work extracted, the velocity, the static pressure and the total pressure of the flow at a particular grid point. Together with direction these coefficients describe the flow completely (incompressibly).

$$C_{\omega_{ij}} = \frac{\omega_{ij}}{q_{ref_{ij}}}$$

$$C_{V_{ij}} = \frac{\frac{1}{2}\rho_{ij}V_{ij}^2}{q_{ref_{ij}}}$$

$$C_{P_{o\,ref}-P_s} = \frac{(P_{o\,ref} - P_s)_{ij}}{q_{ref_{ij}}}$$

$$C_{P_{o\,ref}-P_o} = \frac{(P_{o\,ref} - P_s)_{ij}}{q_{ref_{ij}}} \qquad \textbf{(15)}$$

The method used to calculate the velocity coefficient, the static pressure coefficient and the total pressure coefficient from the five hole probe data is presented in Appendix 4.2.

6.1 Mass flow coefficient

In order to mass average the coefficients in the efficiency definitions, it was necessary to define a dimensionless mass flow coefficient that does not vary with time for a particular grid point. The inlet mass flow rate at any instant in time was defined as

$$\dot{m}_{ref_{ij}} = \rho_{ref_{ij}} A_{ij} V_{ref_{ij}} \qquad \textbf{(16)}$$

Notes:
1) $\dot{m}_{ref\ ij}$ corresponds to the time that the (i,j)th grid point was measured
2) The area A_{ij} is measured halfway from the previous point to halfway to the next point in both the radial and tangential dirrections. At the boundaries A_{ij} includes the area up to the solid boundary.
3) The velocity at the solid boundary was assumed to be zero.

The dimensionless mass flow coefficient was defined as

$$C_{\dot{m}_{ij}} = \frac{\dot{m}_{ij}}{\dot{m}_{ref_{ij}}}$$

The mass averaged terms in the efficiency definitions could now be calculated using the time invariant dimensionless coefficients. In other words the data set has been converted to one moment in time.

6.2 Mass averaged work coefficient

As mentioned earlier the work coefficient could be calculated in two ways. The first method was by using the torque and rotor speed measurements as follows

$$\overline{C_\omega} = \frac{\dfrac{2\pi N\tau_{ref}}{60\dot{m}_{ref}}}{(P_o - P_s)_{ref}} \qquad (18)$$

The second way was to consider aerodynamic data only and to calculate a mass averaged coefficient as done with the other coefficients as follows

$$\overline{C_\omega} = \frac{\sum_{i=0}^{m}\sum_{j=0}^{n} C_{\omega_{aero\ ij}} C_{\dot{m}_{ij}}}{\sum_{i=0}^{m}\sum_{j=0}^{n} C_{\dot{m}_{ij}}} \qquad (19)$$

Where the work coefficient at a particular grid point was

$$C_{\omega_{aero\ ij}} = \frac{\dot{m}_{ij}\rho_{ij}U_{ij}\Delta V_{\theta_{ij}}}{\dot{m}_{ref_{ij}}q_{ref_{ij}}}$$

$$= (C_{\dot{m}_{ij}})\ \frac{2\pi\rho_{ij}N_{ij}R_{ij}}{60}\ \frac{(V_{2_{ij}}\sin\theta_{2_{ij}} - V_{3_{ij}}\sin\theta_{3_{ij}})}{(P_o - P_s)_{ref_{ij}}} \qquad (20)$$

6.3 Mass averaged velocity coefficient

The mass averaged velocity coefficient was defined as follows

$$\overline{C_V} = \frac{\sum_{i=0}^{m}\sum_{j=0}^{n} C_{V_{ij}} C_{\dot{m}_{ij}}}{\sum_{i=0}^{m}\sum_{j=0}^{n} C_{\dot{m}_{ij}}} \qquad (21)$$

Where

$$C_{V_{ij}} = \frac{\frac{1}{2}\rho_{ij} V_{ij}^2}{q_{ref_{ij}}} = \frac{(P_o - P_s)_{ij}}{(P_o - P_s)_{ref_{ij}}} \qquad (22)$$

6.4 Mass averaged static pressure coefficient

The mass averaged static pressure coefficient was defined as follows

$$\overline{C_{(P_{o\,ref}-P_s)}} = \frac{\sum_{i=0}^{m}\sum_{j=0}^{n} C_{(P_{o\,ref}-P_s)_{ij}} C_{\dot{m}_{ij}}}{\sum_{i=0}^{m}\sum_{j=0}^{n} C_{\dot{m}_{ij}}} \qquad (23)$$

Where

$$C_{(P_{o\,ref}-P_s)_{ij}} = \frac{(P_{o\,ref} - P_s)_{ij}}{(P_o - P_s)_{ref_{ij}}} \qquad (24)$$

6.5 Mass averaged total pressure coefficient

The mass averaged total pressure coefficient was defined as follows

$$\overline{C_{(P_{o\,ref}-P_o)}} = \frac{\sum_{i=0}^{m}\sum_{j=0}^{n} C_{(P_{o\,ref}-P_o)_{ij}} C_{\dot{m}_{ij}}}{\sum_{i=0}^{m}\sum_{j=0}^{n} C_{\dot{m}_{ij}}} \qquad (25)$$

Where

$$C_{(P_{o\,ref}-P_o)_{ij}} = \frac{(P_{o\,ref} - P_o)_{ij}}{(P_o - P_s)_{ref_{ij}}} \qquad (26)$$

6.6 Mass averaged driving pressure coefficient

The mass averaged driving pressure coefficient was calculated by subtracting the downstream mass averaged static pressure coefficient from the upstream mass averaged total pressure coefficient as follows

$$\overline{C_{(P_{oa}-P_{sb})}} = \overline{C_{(P_{o\,ref}-P_{sb})}} - \overline{C_{(P_{o\,ref}-P_{oa})}} \qquad (27)$$

Similarly the total pressure loss coefficient was calculated

$$\overline{C_{(P_{oa}-P_{ob})}} = \overline{C_{(P_{o\,ref}-P_{ob})}} - \overline{C_{(P_{o\,ref}-P_{oa})}} \qquad (28)$$

7 Tangentially averaged quantities

The above efficiencies and mass averaged coefficients only give an overall picture of a particular traverse plane or across two planes. To study the effects of tip clearance on the rotor and second nozzle, the radial variation of various coefficients and angles were calculated. The coefficients and angles were tangentially averaged for a full nozzle pitch as follows

$$\overline{Y_j} = \frac{\sum_{i=0}^{m} Y_{ij} C_{\dot{m}_{ij}}}{\sum_{i=0}^{m} C_{\dot{m}_{ij}}} \qquad (29)$$

(where Y_{ij} is a particular coefficient or angle at the (i,j)th grid point)

This has the effect of averaging out the tangential variation that is caused by any stationary upstream blade wakes.

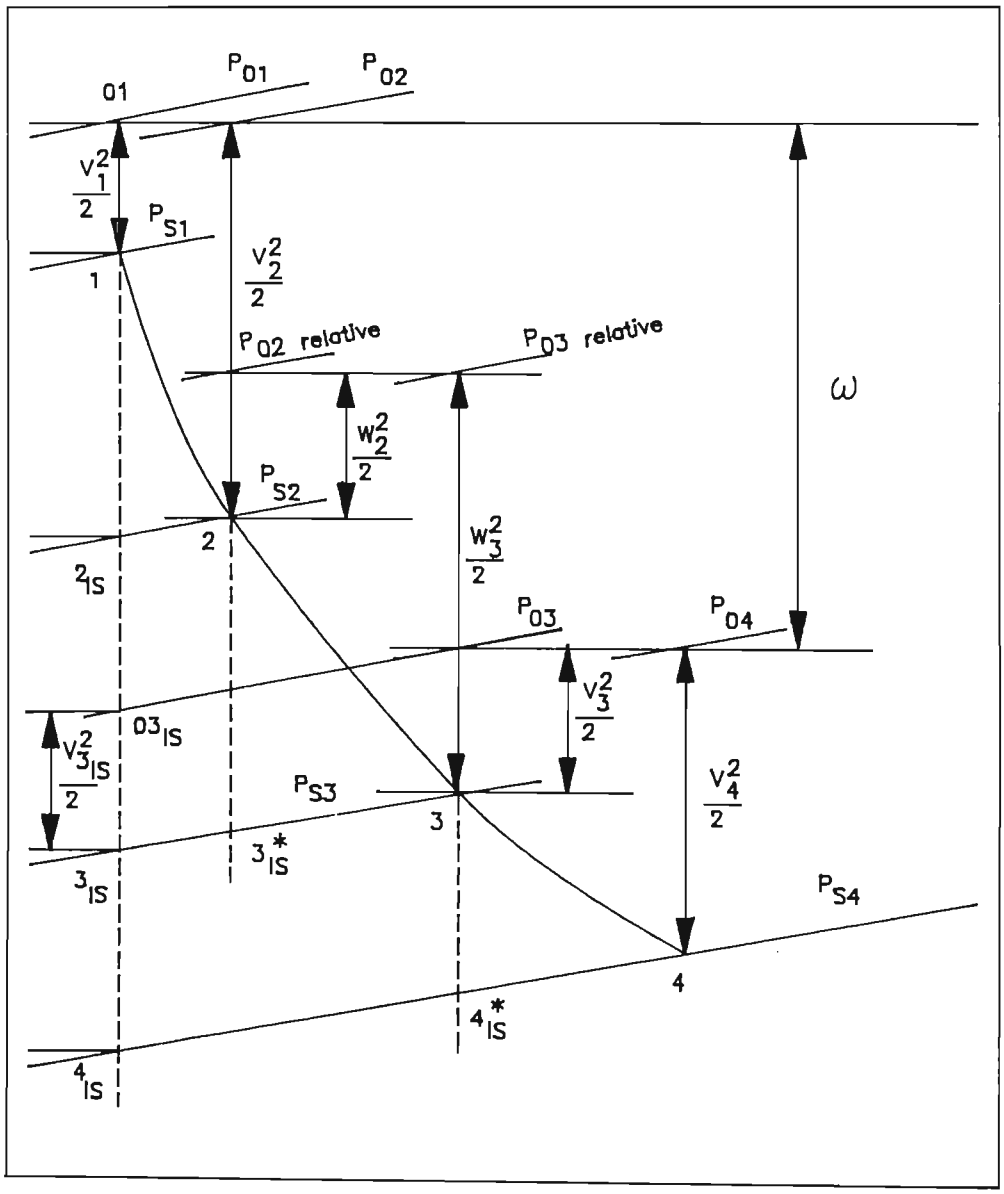

Figure 4.1 Enthalpy - entropy diagram for one and a half stage turbine

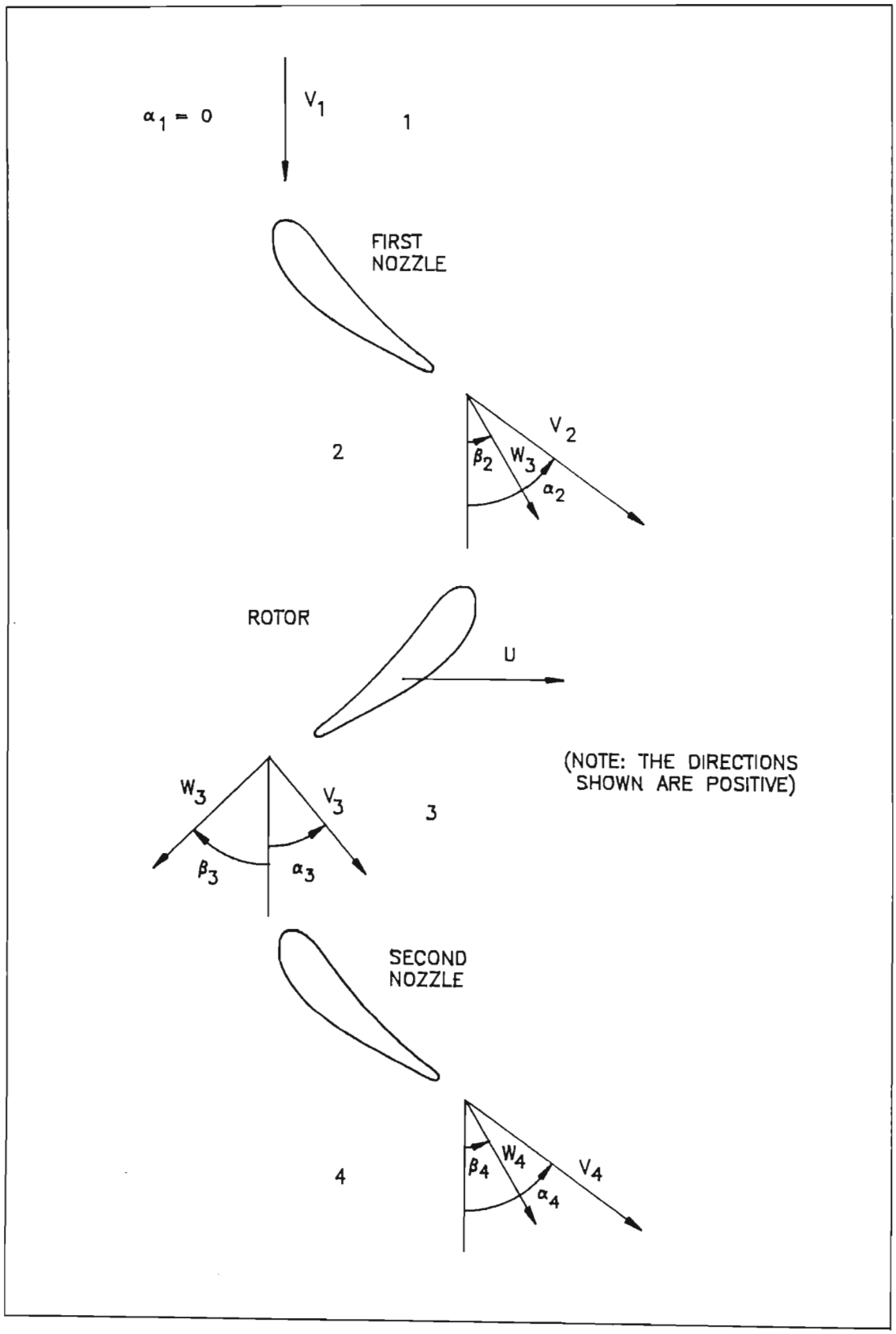

Figure 4.2 Sign convention for absolute and relative angles

CHAPTER 5

PERFORMANCE EVALUATION

1 Introduction

The only true way to evaluate the performance of a blade tip geometry is to measure an efficiency. This chapter describes the performance assessment of the various tip geometries as a single stage and as a one and a half stage turbine. Performance was measured with particular reference to the understanding of tip clearance effects in a real machine and to possible benefits of streamlined low loss rotor tips. This efficiency should take into account the output (work transfer and any kinetic energy in the outlet flow which could still be utilised) and the input which would be driving pressure. Overall performance of the reference square tip and of the two low internal loss shapes (one with a radiused pressure edge and one with the contoured pressure side) are thus presented in the form of the one and a half stage efficiencies and the single stage efficiencies. The efficiency of the rotor alone is also presented.

To investigate the effect of rotor tip clearance on the second nozzle performance, the first nozzle efficiency was compared to that of the second nozzle. The incidence of the leakage flows on to the second nozzle was also investigated. All efficiencies are presented for the three rotor clearances (1%, 2% and 3% of chord). Details of the flow in both the single stage and the second nozzle are examined in Chapter 6. All

measurements were done at design V_x/U ratio and at a Reynold's number of 340 000 (based on chord and the nozzle exit free stream velocity).

2 Effect of tip shape and clearance on single stage efficiency

The single stage total-to-total and total-to-static efficiencies are presented in Figure 5.1 and Figure 5.2 respectively. The most important result seen was that the tip with the radiused pressure edge had the highest performance at all clearances. An improvement over the square tip blade of 0.2% for total-to-total efficiency and 0.5% for total-to-static efficiency was measured at the 1% clearance. This means that the reduction in internal gap loss generated by the radiused tip benefits the performance of even a single stage turbine.

This result has widespread implications regarding the understanding and control of tip clearance loss. It appears that internal gap loss (i.e. the entropy generated within the tip clearance gap) dominates while mixing loss takes place within the rotor to a lesser degree than measured in cascades. The fundamental differences between a linear cascade and a real rotor (such as relative motion and radial pressure gradients) effect the formation of tip leakage loss.

Tip clearance loss does not therefore appear to be simply linked to gap mass flow as has been believed for so long and that, as Denton (1993) points out, is much more complex and depends on entropy generation. Tip leakage flow is not merely flow

that "does no work" and a much better conceptual model is needed to manage tip clearance loss. The flow through the clearance gap must be treated like any other flow within blades and the entropy production minimized rather than maximized as becomes the case when separations are deliberately introduced into the leakage path in order to "block" the flow.

If the tip leakage flow provided no work output and suffered no entropy increase or mixing, it would leave the rotor undeflected and would thus not decrease the total-to-total efficiency of the rotor since its work potential would become fully available at outlet. Alternatively stated, loss free, undeflected tip clearance flow reduces the work output but also reduces the driving pressure ratio (i.e. the isentropic work) and thus the total-to-total efficiency is not affected.

The superiority of the radiused tip was maintained from the smallest to largest tip clearance even though the radius chosen for the pressure edge was sized to prevent separation only at 1% chord. As shown by Morphis & Bindon (1988), a radius of 2.5 times the gap width is needed and thus a completely new rotor would be required at each clearance. If the correct radius were used, a slight improvement in performance at the larger clearances may result.

Regarding the contoured blade tip, except at the largest clearance, the performance was better than (total-to-static) or equal to (total-to-total) the square tip and below that of the radiused tip. At the 3% clearance, the contoured tip blade had the lowest efficiency for both total-to-total and total-to-static efficiencies.

This blade therefore confirms the finding that it is necessary to streamline the tip clearance flow. Previous linear cascade tests (Morphis & Bindon (1992)) showed the contoured tip shape to have the highest performance. It was found that the contoured tip had the same internal gap loss as the radiused tip which was approximately 20% of the square tip. The contoured tip did however have 11% lower gap mass flow that appeared to reduce the mixing loss by 25% giving it the best overall performance.

The partial success of the contoured tip blade in the present work with the real rotor could be for two reasons. The first reason was that the contour geometry was only correct for the 1% clearance. The second was that since mixing losses for the real rotor can be expected to be lower, the reduced efficiency could be due to the gross modification of the tip profile necessary to create the large radii required for the contouring. Increase in profile loss thus offsets some of the gains from internal gap loss and mixing loss. It is interesting to note that the contoured tip blade and the suction squealer blade of Kaiser (1992) are rough approximations of a radiused pressure corner blade (see Figure 5.3) and both had a higher leakage flow rate and lower internal gap loss than the standard square tip blade.

As mentioned in the literature review, Booth (1985) reported a percentage efficiency decrement based on percentage clearance over blade height in the range of 1.4 to 1.8. If instead, this is based on percentage clearance over chord and calculated for the present turbine then the factor ranges from 1 to 1.3. The present measurements

showed a variation of efficiency of roughly 1% for each 1% of chord clearance which corresponds to the range reported by Booth.

The radial variation of efficiency of the single stage will be helpful in understanding the part played by tip clearance as well as in understanding why one streamlined rotor tip was found to improve the performance. The "stream-surface" radial efficiency variation, where the inlet flow at one radius is related to the outlet flow at the same radius, was calculated from flow field measurements. Figure 5.4 presents the total-to-static efficiency for different tip clearances of the square tip rotor. The other two rotors showed the same trends and are thus not presented. A sharp drop off in performance can be seen in the tip clearance region for the larger clearances.

In Figure 5.5, the radial distribution of total-to-static efficiency is presented for the three different rotor tip shapes at the 1% clearance. Here again the main effect on performance is seen in the tip clearance region of the rotor blades. The gain in performance of the tip with a radiused pressure edge over the reference square tip is seen up to about 40% span from the tip.

In an attempt to explain the superior performance of the two streamlined blade tips, it was necessary to understand why the mixing losses do not appear to take place within the rotor as previously found in cascades. When the cascade exit plane flow fields of Morphis (1989) and Morphis & Bindon (1992) are re-examined, (one

example, for the square tip, is re-plotted here in Figure 5.6) some aspects not previously noticed can be reported.

Firstly, there is no evidence of the classical secondary flow vortex that acts in the opposite direction to the leakage vortex and only leakage induced rotation can be seen. It would appear that the leakage vortex is not only much stronger but also that the inlet boundary layer is swept towards the pressure side by the leakage jet on the one side and by the flow entering the gap on the other side. Thus there is far less low-momentum fluid on the endwall to respond with cross flow to the tangential pressure gradient.

The second aspect, is that an envelope of flow can be identified next to the endwall that has no radial component and which intuitively appears to be leakage flow directly from the gap. This envelope (shown in Figure 5.6) contains about 48% of the leakage mass flow rate and is a badly deflected jet that has not wrapped up into a vortex by the exit plane. This leakage jet contains kinetic energy that could potentially be useful to the next nozzle.

When viewed in the blade-to-blade plane as in Figure 5.7 at 50% gap width from the endwall, the leakage wall jet can be distinctly seen with a clearly demarcated directional change at the edge of the jet. This edge demarcation is even more distinct in the recent tip clearance computation (Basson & Lakshminarayana (1993)) of the same cascade and even the predicted leakage jet directions are similar to a remarkable degree (Figure 5.8). Figure 5.9 shows a graphical representation of the

leakage flow. The leakage flow over the first 63% of chord has obviously lifted up and wrapped into the vortex while the flow over the trailing 37% of the gap is seen to flow directly to the outlet of the cascade without lifting. From the mass flow rate distribution at the gap exit of the linear cascade, calculated and presented in Figure 5.10, it can clearly be seen that the latter part of the blade has the highest leakage mass flow rate. The last 37% of clearance gap carries 49% of the leakage mass flow and this tallies almost exactly with the flow identified by the envelope shown in Figure 5.6 that is thought to correspond to the unlifted leakage jet. A further envelope immediately above, of mass flow equivalent to 30% of the leakage flow has a high kinetic energy component and also has the potential of being utilised by the second stage.

The general belief up to now has been that all the leakage flow became a vortex that dissipated all the kinetic energy of the leakage flow and thus it was believed that reducing the mass flow rate through the gap was more important than reducing entropy generation within the gap. The above observations are important in explaining why the low internal gap loss designs are more efficient as opposed to the low leakage flow (high internal gap loss) designs. It can clearly be seen from Figure 5.6 that at rotor exit, a mass flow equivalent to 78%of the leakage mass flow rate has a high kinetic energy and is thus not mixed out and therefore holds the potential for utilisation by the next stage. Mixing losses are mainly generated by the leakage vortex and the shear at the interface between the leakage jet and the main flow. The losses generated at the interface between the two flows are not dominantly mass flow related, thus energy in the unmixed leakage flow that leaves the rotor will

not appear as a rotor debit and the rotor efficiency will be more dependent on internal gap loss than previously thought.

3 The performance of the second stage nozzle

The efficiencies of the first and second stage nozzles for the three tip shapes and for the three tip clearances are given in Figure 5.11. The first stage nozzle efficiency was measured for three different rotor tip configurations and was not unexpectedly found to be independent of the downstream tip geometry. The second stage nozzle efficiency was seen to be significantly higher than the first stage nozzle in all situations. This was in contrast to Boletis & Sieverding (1991) who found the two loss coefficients of the first and second nozzle to be almost identical.

Furthermore, the second stage nozzle showed an efficiency improvement as the tip clearance increased between 1% and 2%, so much so that the subsequent decrease in efficiency at the 3% clearance has only brought the performances back to the levels of the 1% clearance.

It appears, therefore, that not only are there no additional losses generated due to negative incidence onto the blades near the tip and unmixed rotor leakage and secondary rotor flows, but that there are strong mechanisms which reduce loss. At small tip clearances, these mechanisms appear to be enhanced by leakage flows. Since it is unlikely that the profile loss is affected, the most probable reason is a

change in the secondary flow losses. These depend on the blade loading and the inlet vorticity the latter being radically different from that normally associated with the development of endwall loss in cascades. The inlet vorticity is not evenly spread across the inner and outer casings but the majority of it is concentrated in wakes, vortices and leakage jets some distance from the endwalls. The vorticity in the thin boundary layers on the endwalls are fed to the stator as skewed (overturned) and therefore highly energetic flows. The blade loading, and hence the driving force of the secondary flow, is also probably lower because both the rotor leakage flow and the rotor secondary flow at the hub will appear as a negative stator incidence which in turn unloads the blades compared to the first stage where the flow is completely turned.

The different shaped rotor blade tips produced different degrees of improvement in the second nozzle. From 1% to 2% clearance, the radiused blade was the best, but at 3% it was well below the other two tip shapes. However, it is important to realise that flows of this complexity are not easily explained by simple rules and experience gained in simple stationary cascades.

4 The rotor performance

The total-to-total and the total-to-static performances described in section 5.2 above, are stage efficiencies and therefore include both the first nozzle and the rotor. For completeness, the total-to-total and the total-to-static efficiencies for the rotor alone

are presented in Figure 5.12 and Figure 5.13. The results show exactly the same trends as the single stage efficiencies with the radiused tip blade performing best. This was expected since the efficiency of the first nozzle remained unchanged for the different downstream rotor tip geometries.

5 The overall performance of the one and a half stage turbine

Unlike the rotor and single stage performance which are described by two quantities that have somewhat different meanings, a single unique one and a half stage efficiency has been defined which reflects the losses in all three blade rows without any points of argument as to whether certain effects are included or excluded. As described in Chapter 4, this one and a half stage efficiency is a measure of the work extracted by the rotor plus the kinetic energy leaving the second nozzle, divided by the driving pressure of the complete one and a half stages. This one and a half stage efficiency is plotted in Figure 5.14, again for all clearances and blade tip shapes.

At the smallest clearance, the radiused tip was again distinctly superior but this dropped well below the standard square tip blade at large clearances. Since the rotor alone did not show this, the reason was the poor performance of the second stage nozzle at this clearance.

Although the rotor and single stage efficiencies indicated that the contoured tip outperformed the standard square tip blade at the smaller clearances, the one and a

half stage efficiency showed it to be the poorest performer at all clearances. Using a similar argument as that explaining its poor performance for the rotor alone, it is probable again that the loss of blade shape with this tip is simply too radical and increased profile loss is responsible. It is finally worth noting here, the fact that this tip shape had seemed to be the best in linear cascade tests, even when the cascade data was specially adapted to reflect rotor processes. It thus points out the complexity of the flows and the difficulties of some simple models used to make decisions in turbine design.

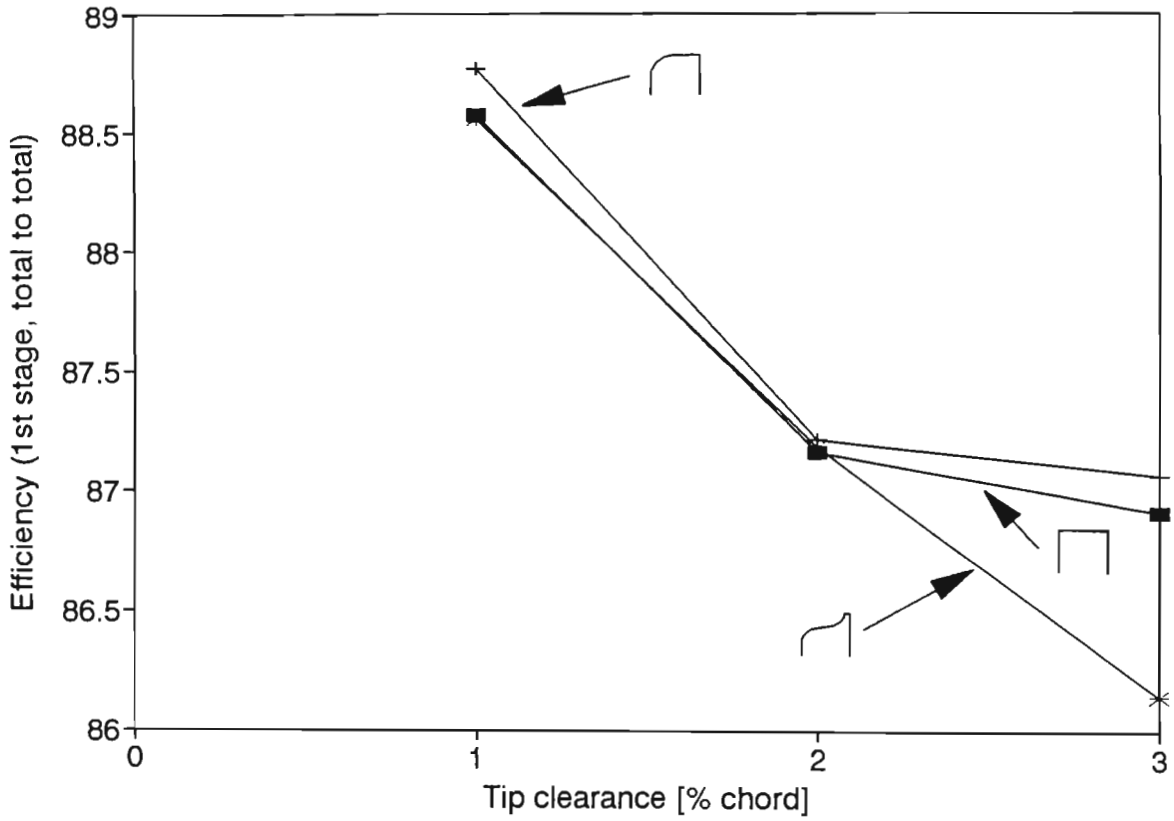

Figure 5.1 Single stage total to total efficiency for 3 tips and varying clearance

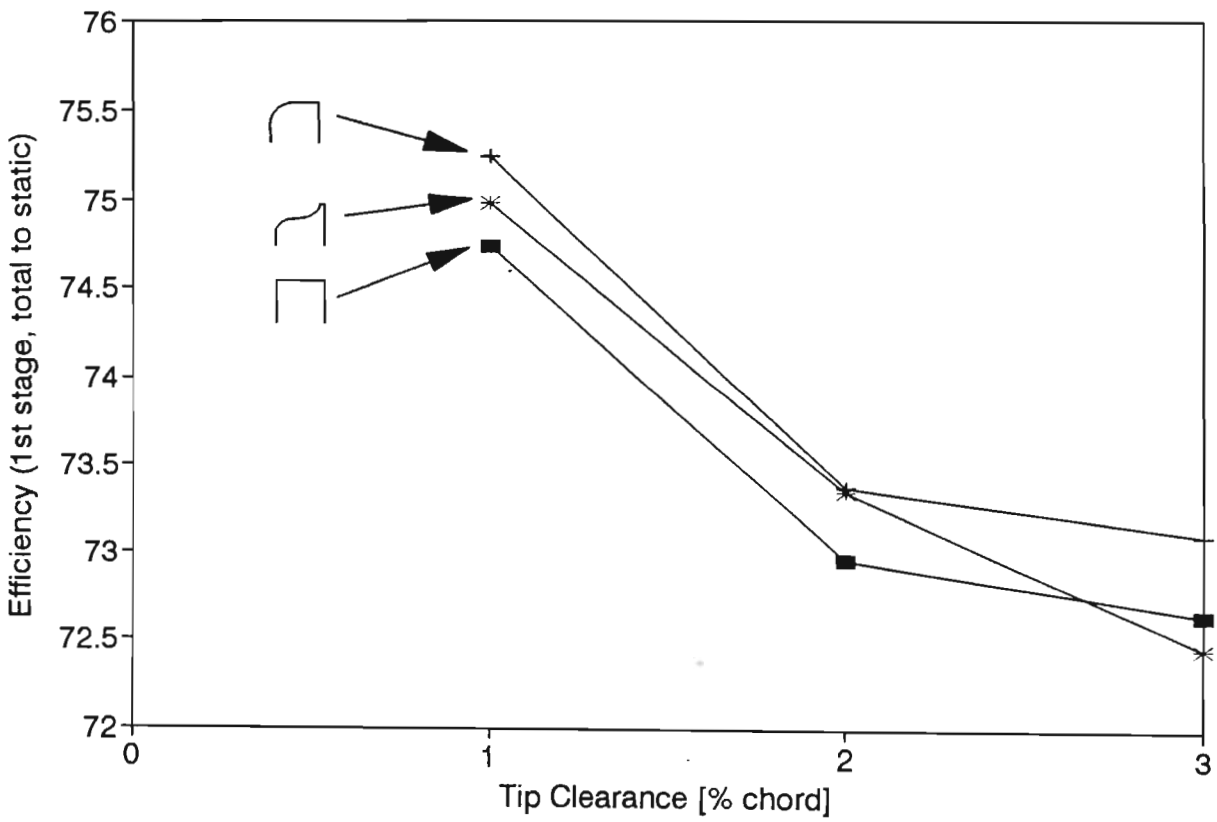

Figure 5.2 Single stage total to static efficiency for 3 tips and varying clearance

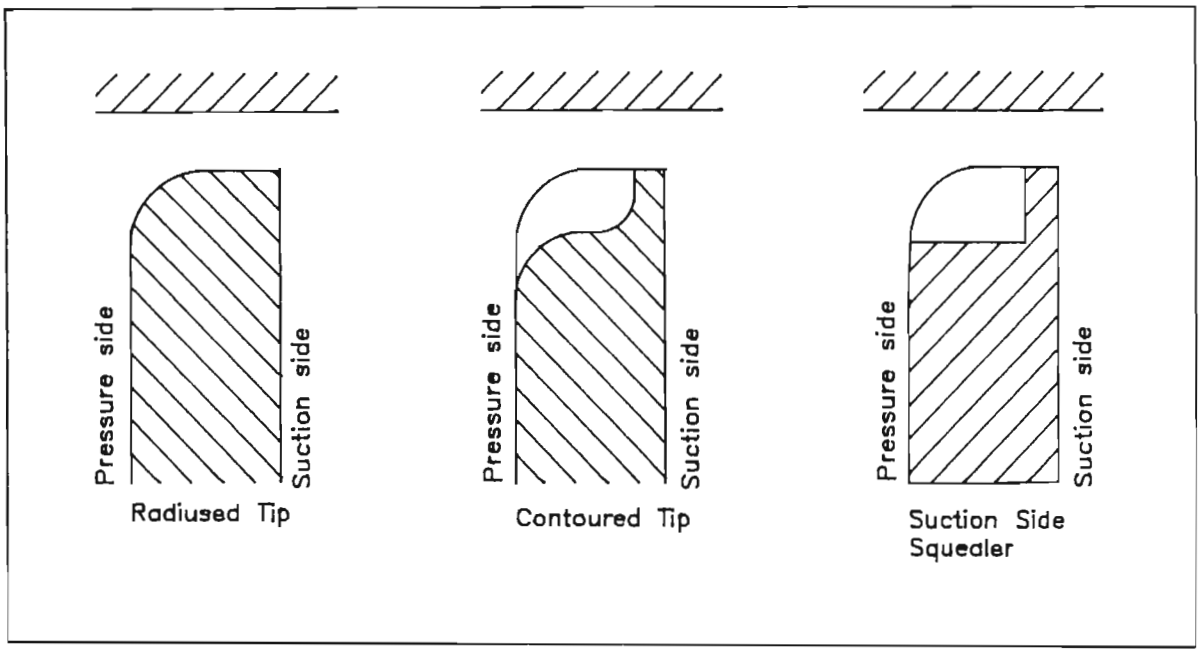

Figure 5.3 Comparison of contoured and squealer tips to the radiused tip.

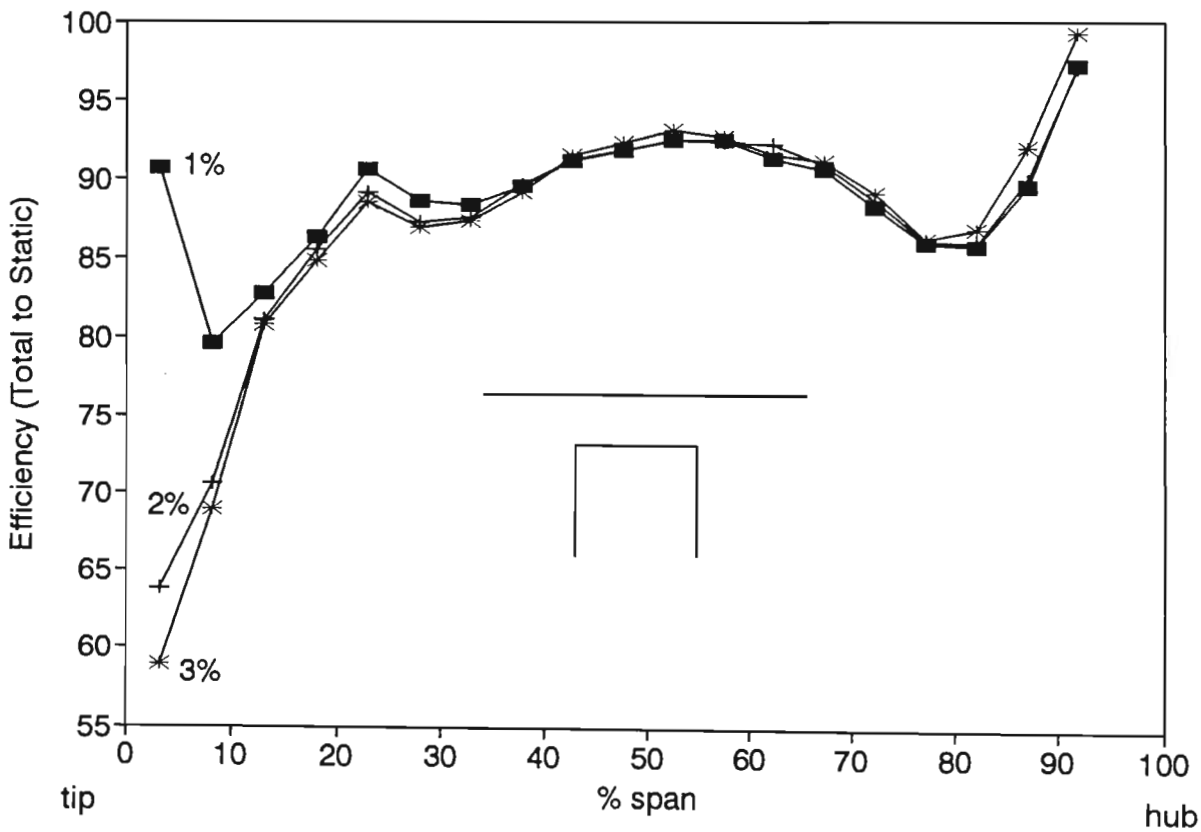

Figure 5.4 Radial variation of single stage total-to-static efficiency for the square tip rotor at three tip clearances.

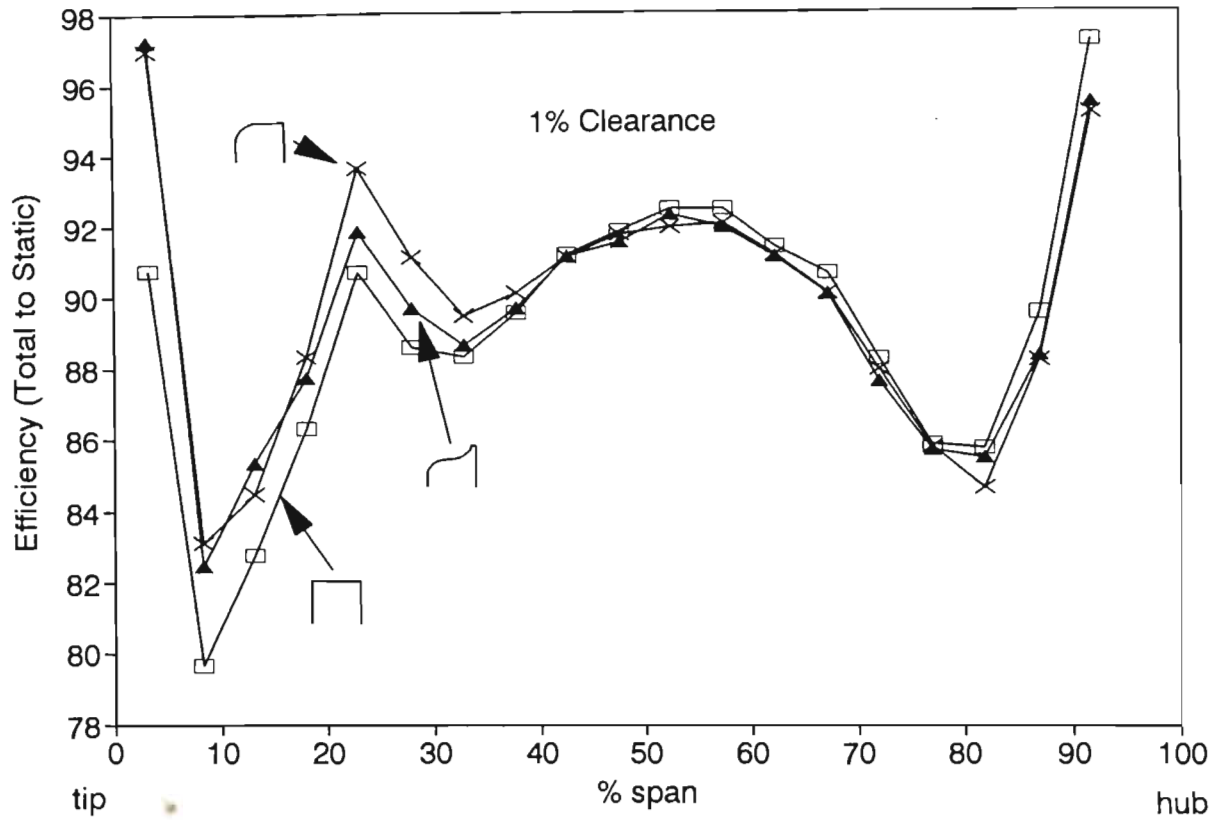

Figure 5.5 Radial variation of single stage total-to-static efficiency for the three blade tip geometries at a tip clearance of 1% of chord.

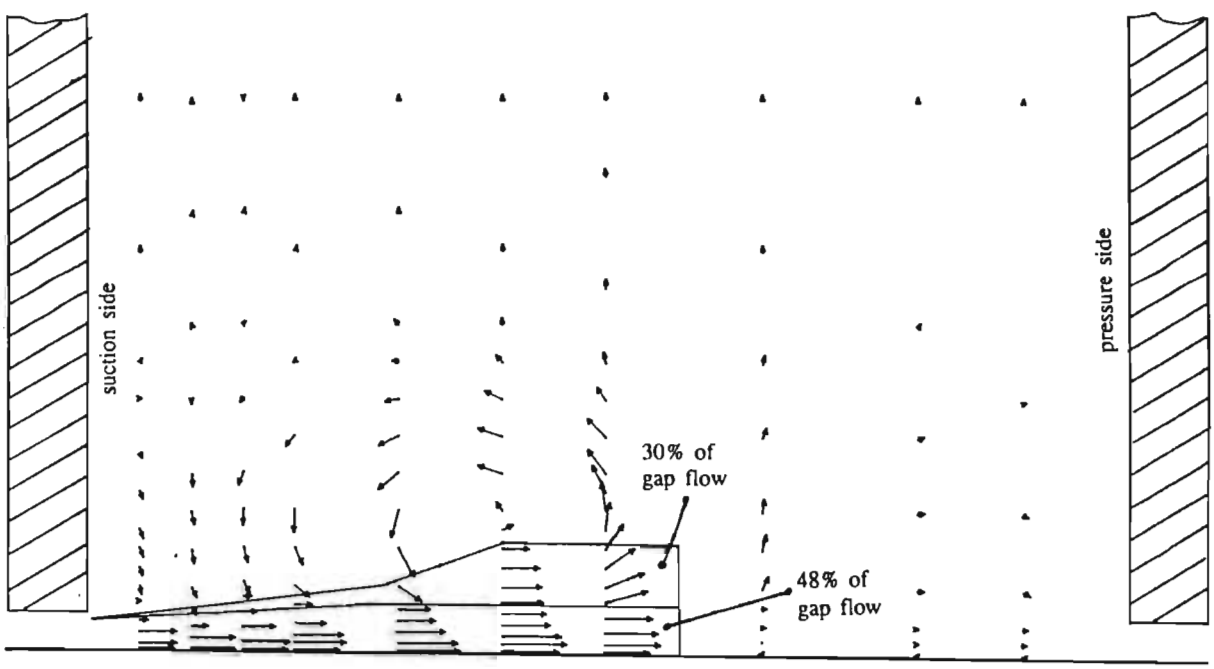

Figure 5.6 Velocity vectors normal to free stream flow at cascade exit plane (Morphis (1989)) identifying possible leakage flow envelopes.

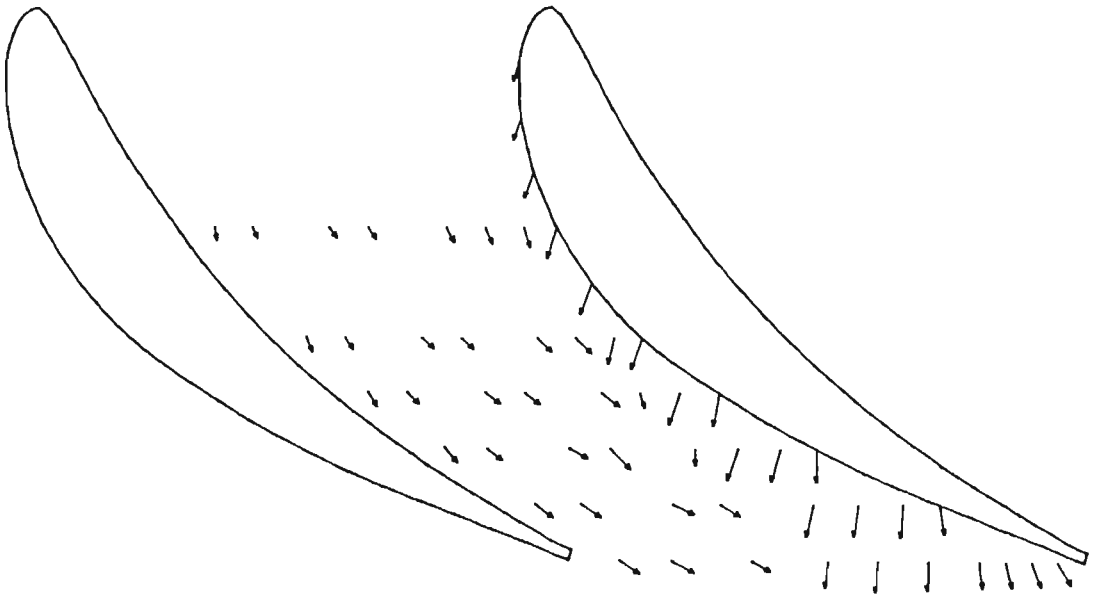

Figure 5.7 Linear cascade velocity vectors projected onto a blade to blade plane at a distance of 50% of tip gap from the endwall.

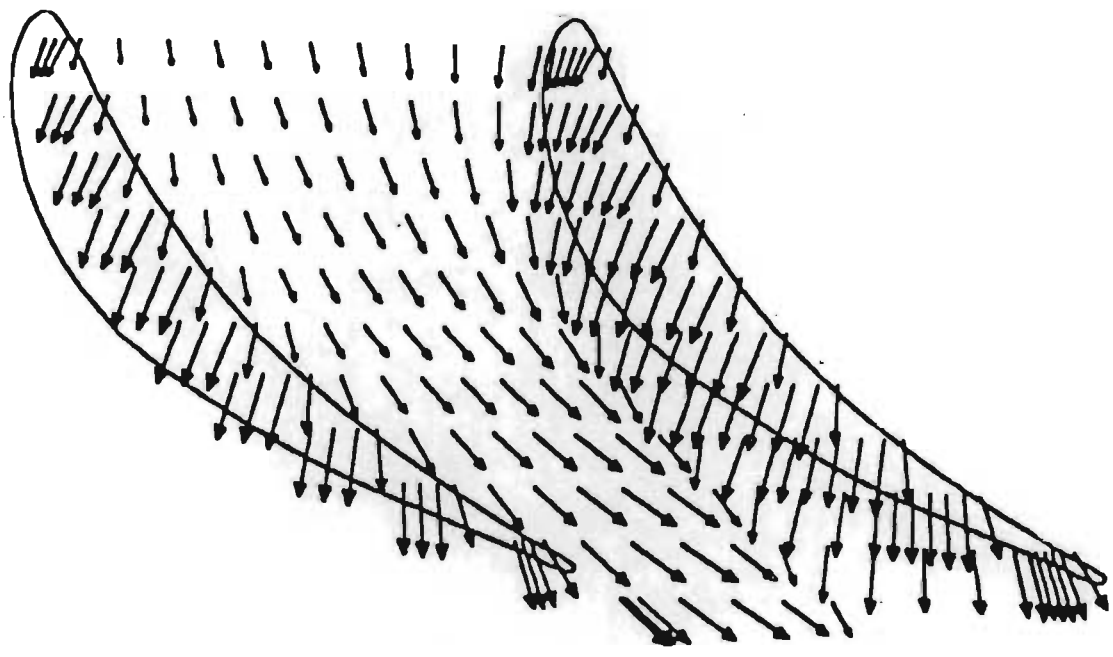

Figure 5.8 Computed velocity vectors projected onto a blade to blade plane at a distance of 50% of tip gap from the endwall (Basson & Lakshminarayana (1993)).

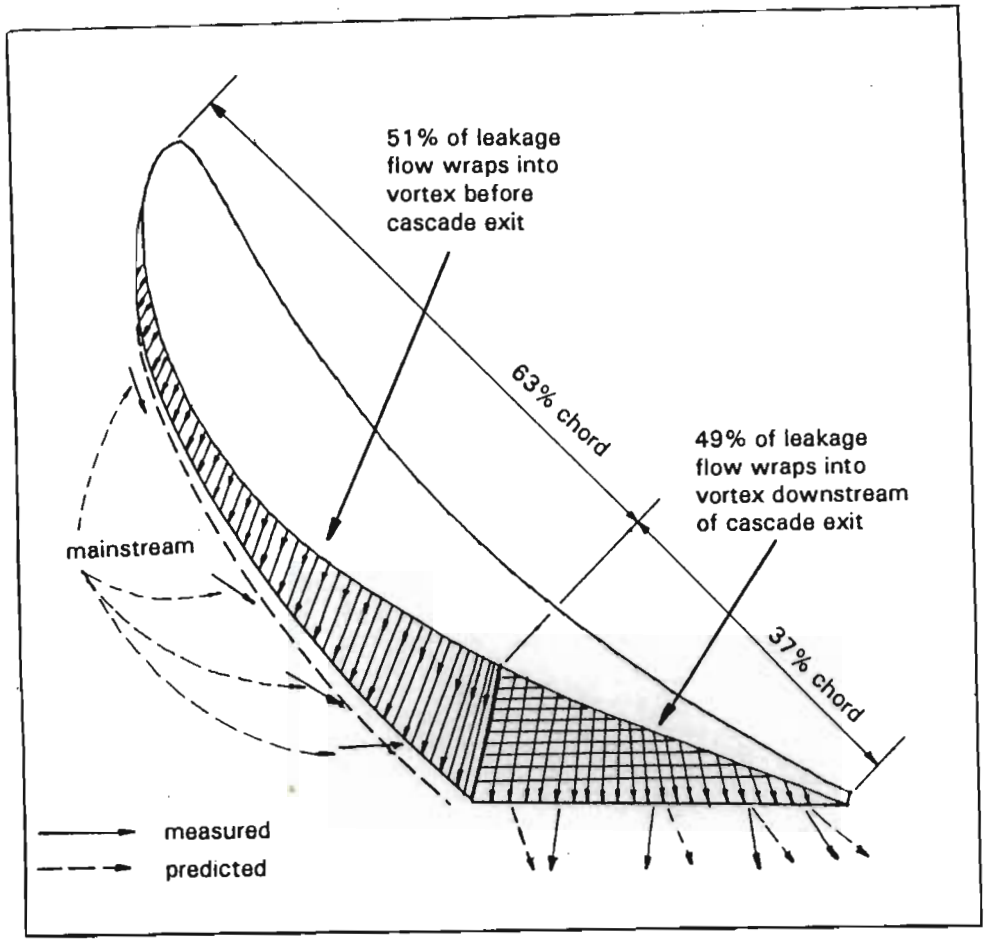

Figure 5.9 Schematic of tip leakage flow showing portion of flow that does not wrap into a vortex before leaving the exit plane.

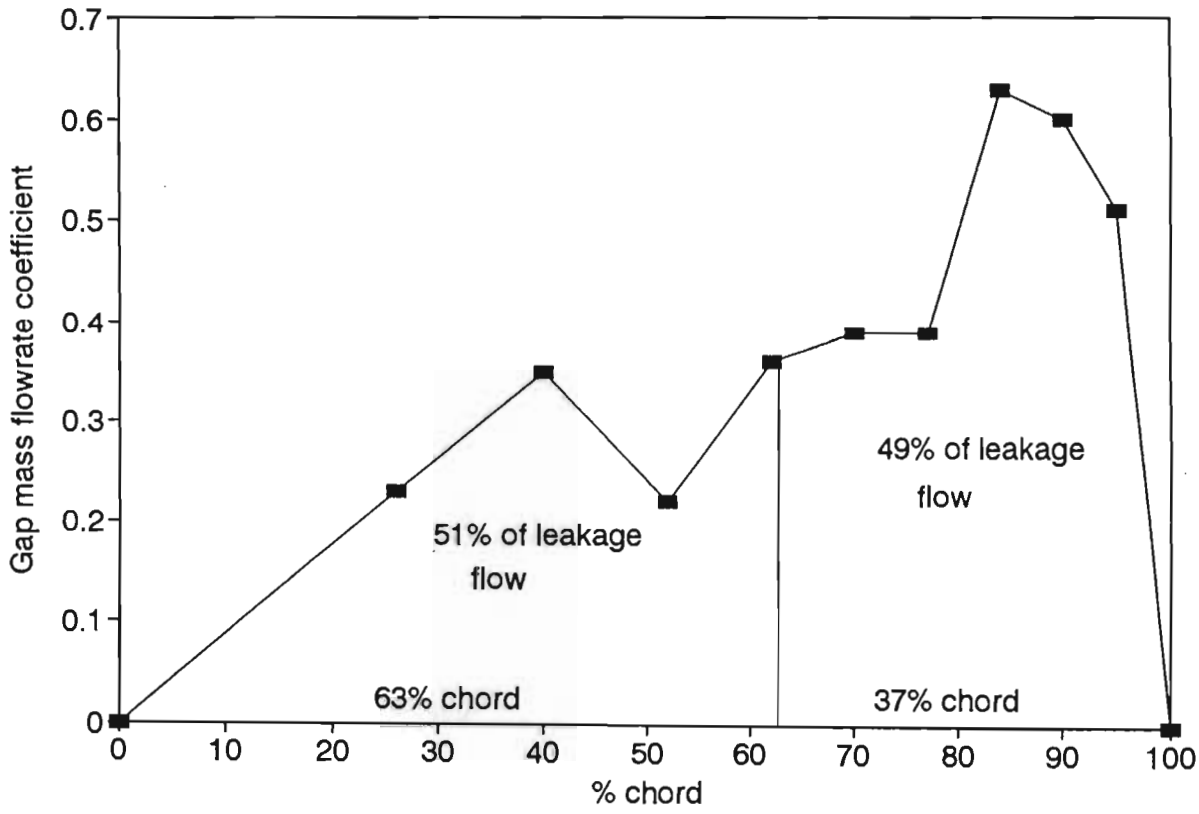

Figure 5.10 Leakage mass flow rate distribution at gap exit of linear cascade

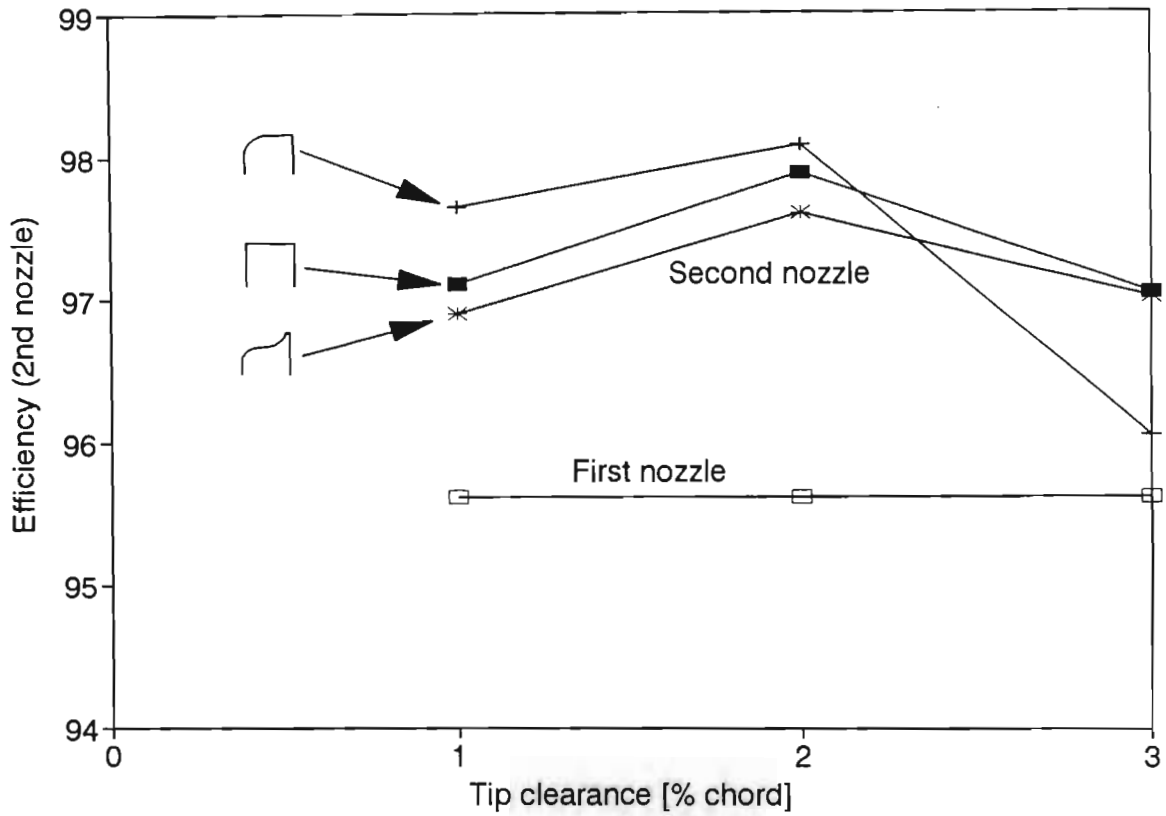

Figure 5.11 First and second stage nozzle efficiency for 3 rotor tip shapes and varying rotor tip clearance.

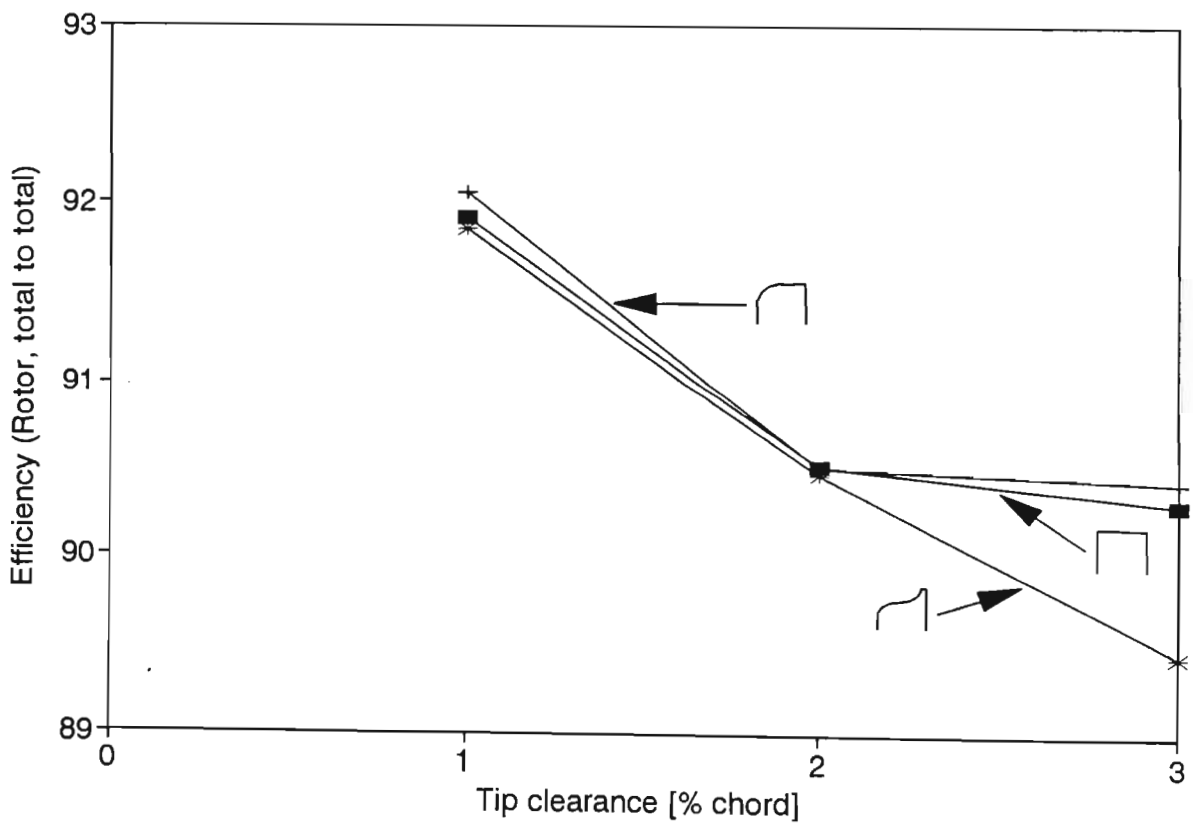

Figure 5.12 Rotor total to total efficiency for 3 rotor tip shapes and varying tip clearance.

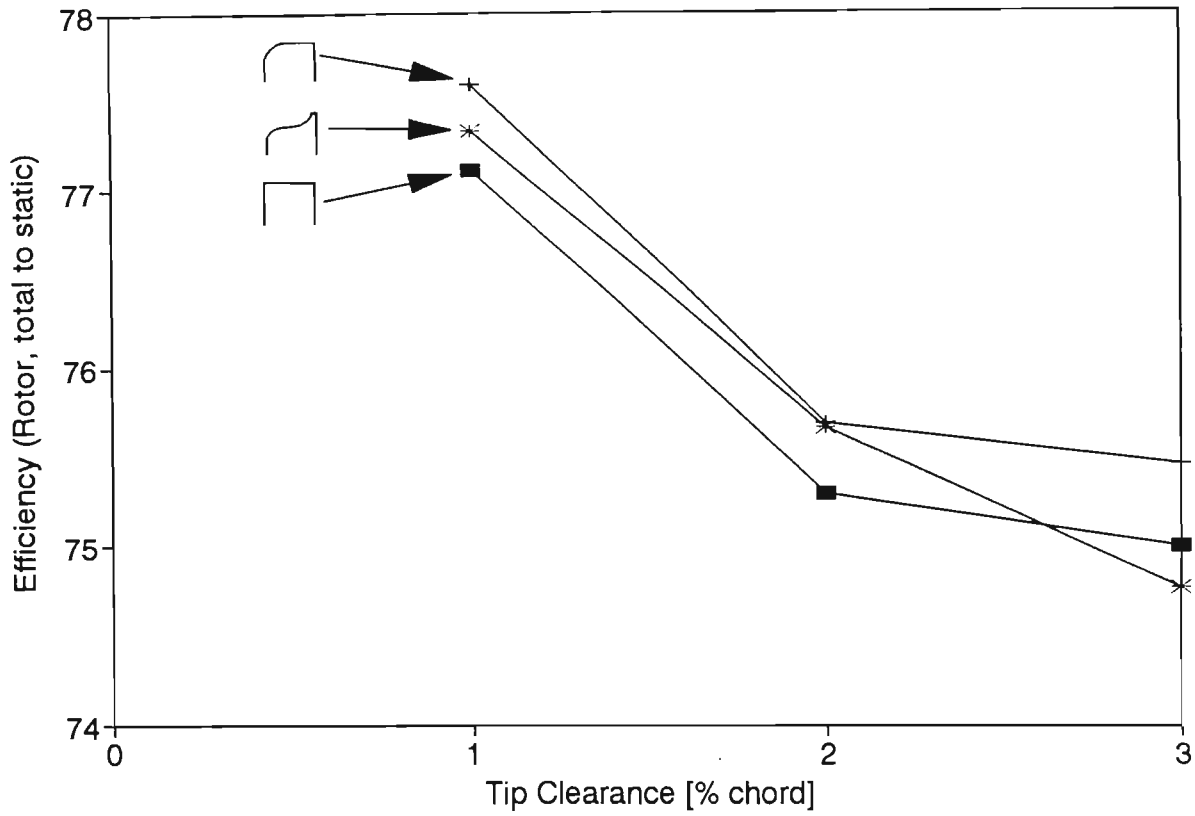

Figure 5.13 Rotor total to static efficiency for 3 rotor tip shapes and varying tip clearance.

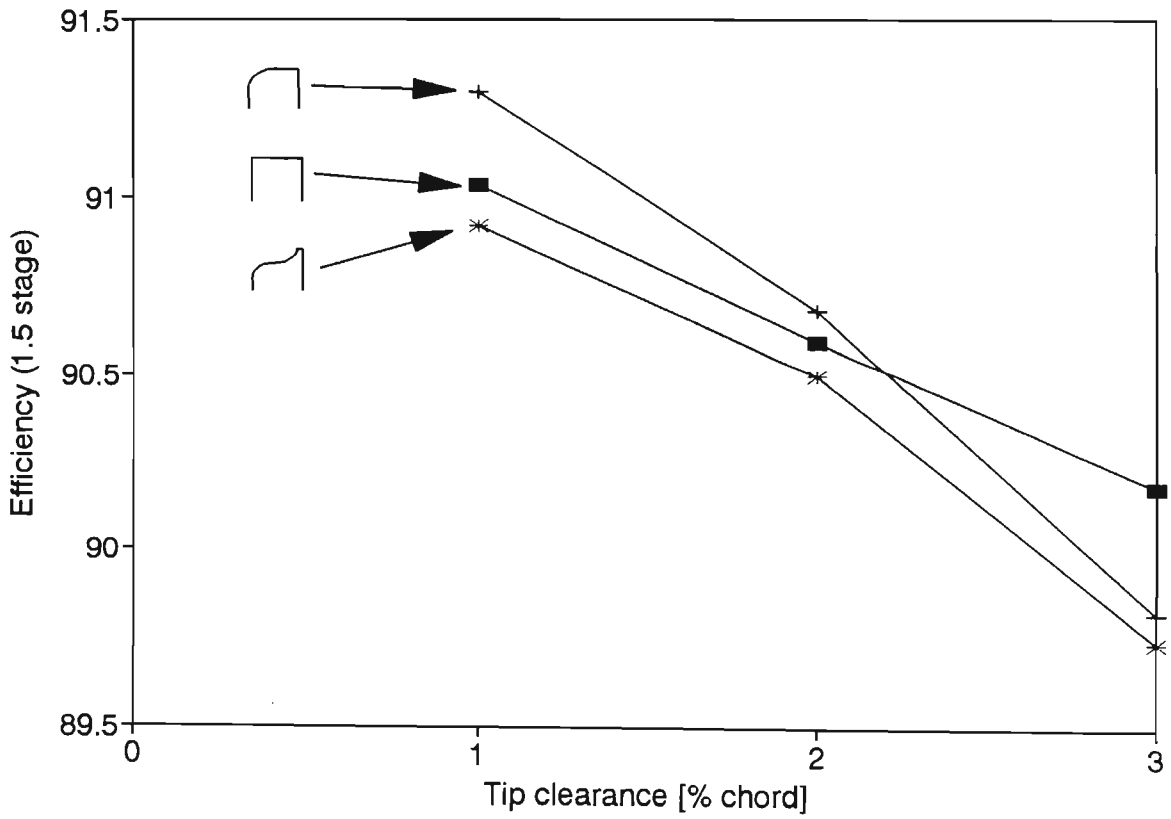

Figure 5.14 One and a half stage efficiency for 3 rotor tip shapes and varying tip clearance.

CHAPTER 6

FLOW FIELDS AND SECOND NOZZLE EFFECTS ON LOSS DEVELOPMENT

1 Introduction

In the previous chapter, the complete performance of the one and a half stage turbine and its various components were presented. In this chapter the flow field of the one and a half stage turbine is examined for three rotor tip geometries and three rotor tip clearances. The second nozzle was of great interest in this research as very little was known about its ability to handle inlet flow vectors caused by the tip clearance leakage. Measurements of the first and second nozzles are compared to identify the manner in which the second nozzle responds to the complex tip clearance dependent flow presented to it. Since time-frozen data of the flow leaving the rotor was not available, linear cascade data was also used to examine the type of flow that the second nozzle has to ingest. Examination of the second nozzle also reveals the development of the leakage losses in the presence of a second nozzle.

The tangentially averaged flow relative to the rotor blade in the tip clearance region was compared to flow measured in a linear cascade. This was done to investigate the validity of using linear cascade data for assessing tip clearance loss development. The reason why the second nozzle showed a reduction in loss over the first nozzle

was investigated. Loss contours are also presented for the second nozzle to illustrate the leakage loss formation and the existence of any classical secondary flow patterns.

2 Rotor determined second stage nozzle inlet conditions

For the first stage nozzle, both the inlet and outlet flows are steady state, however the second nozzle is downstream of the rotor and thus receives flow that not only varies as each blade passes but also depends on tip clearance geometry. The ability of the rotor to deflect the flow will therefore largely determine the inlet to the second nozzle. Flow leaving a rotor is periodic and will fluctuate with each blade passing with respect to flow angle and total pressure (incompressible case) because of varying degrees of loss and work extraction. The second nozzle therefore acts as a flow straightener that takes the fluctuating flow from the rotor and "chops" it up, thus vortices in the flow leaving the rotor wake will not necessarily enter the second nozzle passages as complete formations.

Since the present measurements behind the rotor were pneumatically time averaged by the probe, it was helpful to review the cascade results of Morphis (1989). These were measured at a tip clearance of 2% chord and the periodic flow variations that a typical second stage stator experiences can be constructed. Figures 6.1 and 6.2 present the measured cascade exit flow field results transformed to simulate flow leaving a rotor by including a hypothetical blade speed. These graphs are plotted for various distances from the endwall and are expressed as a percentage of chord since

the span of the blade is difficult to define in a linear cascade. Figure 6.1 shows the incidence angle onto the second stage nozzle. Remote from the endwall (a distance of 54% of chord from the endwall), the incidence changes from mildly negative near the blade surfaces to slightly positive at mid-pitch. Near the tip (at a distance of 1.1% chord) where the leakage jet exists as a strong, poorly deflected jet over half the blade pitch, the incidence has almost a mid-span value near the pressure side and then drops sharply to around -52 degrees and stays low for the remainder of the blade pitch.

In Figure 6.2 the velocity coefficient is presented for the same traverses as Figure 6.1. Here again at 54.4% of chord from the endwall, the velocity coefficient does not vary much from the design value of 1. At 1.1% of chord where the very high negative incidence was seen in Figure 6.1, the leakage flow appears as an extremely high velocity zone where the velocity coefficient peaks at 3.5 (i.e. an inlet velocity 1.9 times the mid-span value since velocity coefficient is proportional to velocity squared).

At increasing distances from the endwall, the incidence angle changes through zero before becoming positive by as much as 50 deg on the other side of the leakage vortex. The velocity coefficient at this point shows that the nozzle will receive a velocity half the freestream value.

When the above blade to blade simulated rotor flow (linear cascade) is tangentially averaged, it can be compared with the present measurements taken at the inlet to the

nozzle where the probe responds with a close approximation to the mean of the periodic flow presented to it by the rotor. This is done in Figure 6.3 as nozzle inlet angle rather than incidence. Both curves are seen to have similar, high positive flow angles (negative incidence) near the wall. At a distance of 16.9% of chord (which is equivalent to 12.7% of span) from the tip and where Figure 6.1 shows the positive incidence associated with the leakage vortex, the velocity is so low that the mass based average does not even show a dip and the angle curve does not even fluctuate at that point.

By design, the first stage inlet angle was zero, however the second nozzle was seen to have an inlet angle of near 10 degrees at mid-span that increases sharply to 25 degrees near the tip at a clearance gap of 2% chord. This 10 degree angle deviation at mid-span seems large but it should be noted that a small deviation from design of rotor relative outlet angle translates to a much larger absolute angle deviation. The real rotor also shows an increase of flow angle near the hub which is caused by the rotor hub secondary flow.

Figures 6.4, 6.5 and 6.6 show the tangentially averaged angle at second nozzle inlet for the three tip clearances and for the three different blade tip configurations. For each blade tip geometry the angle near the tip increases with tip clearance due to the increase of leakage flow. This trend is the same for all three blade tip geometries and is shown more clearly in Figure 6.7. In this figure the maximum magnitude of the leakage jet angle in the absolute frame of reference is plotted against tip clearance for the three tip clearance geometries. The increase in angle with clearance

is monotonic but becomes smaller at the larger clearances. Considering the effect of tip geometry, the square tip was found to have the lowest increase in angle near the tip, and the contoured tip blade had the highest. As shown in Figure 6.8, the increase in absolute angle near the tip for both the streamlined tips was probably caused by the leakage flow being less deflected by the rotor. If the leakage flow from the streamlined tips simply had a higher velocity then the absolute angle would have been smaller.

Since the second nozzle inlet angle was created by the rotor, it was helpful to examine the same flow in the relative frame of reference. Figure 6.9 (for the square tip blade) shows the rather surprising fact that near the hub, secondary flow creates a large amount of overturning. Even more surprising is the overturning at the tip with the 1% clearance where leakage flow was expected to be poorly deflected. Even at the larger 2% clearance there is almost no under-turning and only about 2 degrees of under-turning at the 3% clearance. Both the radiused (Figure 6.10) and contoured (Figure 6.11) tips only showed some degree of under-turning at the 3% of chord clearance.

Figure 6.12 compares the rotor relative outlet angle of the real rotor to that of the linear cascade simulated rotor. At the tip region, the linear cascade results showed the exact opposite of what was found with the real rotor. The linear cascade mean exit flow angle decreased sharply near the wall due to the contribution of the undeflected leakage jet. Since the absolute angles at rotor outlet for the linear

cascade and the real rotor agreed and the relative angles did not, the explanation of this unexpected result must lie in the velocity distribution of the flow.

Figures 6.13, 6.14 and 6.15 show the tangentially averaged velocity coefficient at rotor outlet for the three blade tip geometries. Here again it was surprising to find that at the tip region the velocity is reduced for the 1% clearance and stays approximately the same for the 2% clearances for all three blade tip geometries. At the 3% clearance the velocity in the tip region stays the same for the square tip blade and only increases for the radiused and contoured tips.

In order to clarify the effect that the rotor has on the outlet velocity, the tangentially averaged axial velocity distributions for the three rotors are presented in Figures 6.16, 6.17 and 6.18. Figure 6.16 (for the square tip) also compares the rotor outlet axial velocity to the rotor inlet axial velocity. In all cases the rotor was found to reduce the axial velocity at the tip region. The relationship with tip clearance variation in the tip region was however not monotonic.

Figure 6.19 compares the axial velocity distributions for the real rotor and the linear cascade. The linear cascade data was radically different from the real rotor with the velocity increasing dramatically from approximately 1 at mid span to 4.4 against the endwall while the real distribution followed the normal endwall boundary layer pattern. With the real rotor the tangentially averaged flow near the tip is not a poorly deflected high velocity jet as was found in linear cascades, but a low velocity

rather well deflected flow. It was this discrepancy that also created the unexpected relative flow angles at rotor exit.

As shown in Figure 6.20, the lower axial velocity of the real rotor modifies the velocity diagram to give a relative angle that is greater than was expected from linear cascade data. A possible reason for this is that true relative motion in the small gap reduced the leakage effect to such a degree that normal secondary flow could still flourish. This, however, is probably too simplistic an explanation of this complex periodic tip boundary layer flow in which fluid in the laminar sub-layer may even be exposed to more than one blade passing. The interaction of the tip leakage flow with the mainstream flow in a real rotor with relative flows and centrifugal effects is very complex and cannot be quantified in simple linear cascades.

3 Comparisons between first and second stage nozzles

Thus far, only the flows leaving the rotor have been analysed. The response of the second stage nozzle to the inlet flows that are presented to it may now be discussed and compared to the behaviour of the first stage nozzle. The tangential position of the second nozzle relative to the first was kept constant. Because of the blurring, skewing and twisting of the first nozzle wake, that occurs with axial distance and inside the rotor, the position of the first nozzle wake at the second nozzle inlet was neither exact nor unique. Therefore, somewhat arbitrarily, the mid-span loss peak, which was assumed to be the wake from the first nozzle was found at the traverse

plane ahead of the second nozzle. The second nozzle was positioned such that this first nozzle wake entered the second nozzle at mid-pitch position.

In Figures 6.21, 6.22 and 6.23 the exit flow angle is shown for the two nozzles with the various rotor tip configurations and for design. The first nozzle outlet angle was found to be within one degree of design except for the differing secondary flow effects at hub and tip. At the tip, some under-turning was evident between approximately 8% and 20% of span. At the hub there was very little under-turning while right on the inner casing there was a distinct angle increase.

The angle at second nozzle outlet is shown for the three rotor tip clearances. Since the leakage flow leaving the rotor becomes less deflected with clearance, increasing the rotor tip gap increases the under-turning near the tip. Near the hub, the rotor induces a large zone of under-turning (in the absolute frame of reference), probably due to its own secondary flow.

If a hypothetical second stage rotor, identical to the first, were assumed to be downstream of the second stage nozzle, the two stages can be compared in terms of the relative inlet angles they induce in their respective rotors. The results appear in Figure 6.24 (square tip rotor blade with 1% clearance). Here the two curves are very similar with a slightly better angle near the tip of the second rotor due to tip clearance. Rotors in multistage machines will therefore experience slightly less flow angle distortion when compared to the first rotor.

In the Chapter 5 it was shown that the losses generated within the second nozzle were in the region of 30% below those produced by the first nozzle. To explain this, the radial variation of loss generated across the second nozzle is plotted in Figures 6.25, 6.26 and 6.27 (on a stream-surface basis as done for efficiency in Chapter 5). The radial loss distribution in the second nozzle appears to be fairly evenly spread with no obvious pattern for clearance or tip geometry variation. An interesting point is that for both the radiused and contoured tips, there is almost no loss at about 8% of span at the 2% and 3% clearances. The region of negative loss shown on the 3% case means that there is a higher total pressure at the outlet than at the inlet for that particular radial point.

Figure 6.28 compares the loss generation of the first nozzle with the second nozzle (for clarity the square tip rotor at 2% clearance only). The second nozzle can be seen to have reduced losses in the hub and tip regions which tends to confirm the reasons advanced that the improvements are due to reductions in secondary flow loss. The factors which generate secondary flows in the second nozzle are radically different.

The unexpected relative rotor flow angles discussed in the previous section were deduced from the absolute frame measurements of angle and velocity. Figures 6.29, 6.30 and 6.31 give the tangentially averaged radial distribution of the axial velocity coefficient at the second nozzle outlet for the three rotor tips. Considering Figure 6.29 for square tip blade, a surprising result can be seen in that the smallest rotor clearance of 1% chord generates the highest velocities in the tip clearance

region up to approximately 25% of span. In the region adjacent to this (25% to 50%) the 3% clearance has the highest velocity whereas the 2% clearance stays the same as the 1%. This result was similar for the radiused and contoured tip except that the differences are not as marked. The mainstream flow was probably displaced by the leakage flows. This displaced fluid would then likely cause an increase in velocity in the area adjacent to the area directly affected by the tip.

The radial distribution of the tangentially averaged axial velocity coefficient at inlet and outlet of the first nozzle is presented in Figure 6.32. At the tip the outlet has a slightly thinner boundary layer whereas at the hub the outlet boundary layer is slightly thicker than at inlet. The largest effect appears to be between about 8% and 25% of span where the axial velocity increases at the outlet. This radial distribution of the tangentially averaged axial velocity at inlet and outlet is also presented for the second nozzle (Figure 6.33) for the square tip, 2% clearance rotor. At the tip, the axial velocity does not appear to change much from inlet to outlet. At the hub, however, the outlet flow has a much thinner boundary layer than the inlet flow. This reduction took place despite the fact that the second nozzle was presented with a secondary flow from the rotor. Thus the rotor secondary flows fed to the second stage nozzle at the hub, appear to benefit the axial velocity distribution considerably and tip leakage flows do not have a detrimental effect.

Figure 6.34 compares the radial variation in absolute outlet velocity between the two nozzles. Except for the area near the tip between 10% and 25% of span and a constant offset, the velocity distribution for both nozzles is remarkably similar. This

offset is due to compressibility effects for a constant area annulus. At the tip, however, the second nozzle demonstrates a higher velocity that must be caused by leakage flow energizing this region. The outlet velocity coefficient distribution of the second nozzle appeared to be independent of tip clearance size and geometry. This is important in that it again confirms that tip clearance flows do not adversely effect the performance of the second nozzle.

4 Radial flow angles

Radial flows are thought to be an important part of second nozzle flow phenomena as shown by the most significant study of the second nozzle to date (Boletis & Sieverding (1991)). As was mentioned in the literature review, large radially inward (negative) flow angles as high as -32 degrees were reported.

The blades used had a lower aspect ratio than the present work and would thus create more secondary flows. In addition, the untwisted rotor produces a radial variation in work extraction and hence total pressure that is known to enhance radial flow.

Figure 6.35 shows the maximum radial angle variation that was found at the second nozzle inlet and outlet and compares them to the first nozzle outlet. Note that a positive angle is a radially inward flow. The radiused tip rotor with the 3% clearance produced the maximum radial angles of between -5 and -6 degrees only and all occurred at a distance of 27% of span from the tip at both rotor exit and

second nozzle exit. Unlike to what was found by Boletis & Sieverding (1991), there was very little increase in radial flow in either of the nozzles and the largest increase took place as the first nozzle wake moved through the rotor.

5 Nozzle exit plane loss contours

To qualitatively examine the loss development that takes place within the first and second nozzles, exit plane loss contours were plotted by subtracting the tangentially averaged total pressure coefficient at inlet from the total pressure coefficient at outlet for each point on the two dimensional grid. This is not a true loss contour since the inlet distribution for the second nozzle was time averaged as a result of the rotor outlet flow. In addition it does not allow for radial migration and thus does not follow a certain piece of fluid from inlet to outlet of the nozzle.

The loss contours for the first nozzle are presented in Figure 6.36. Loss contours for the second nozzle were plotted for each of the three blade tip geometries and for all three blade tip clearances. These second nozzle contours are presented in Figures 6.37, 6.38 and 6.39 for the square tip rotor, Figures 6.40, 6.41 and 6.42 for the radiused tip and Figures 6.43, 6.44 and 6.45 for the contoured tip. Contours below 0.2 were spread out in the area between the blade wakes with no clear pattern and were omitted for clarity but obviously contribute to the overall loss.

In Chapter 5, the significant reduction in overall loss coefficient found in the second stage nozzle when compared to the first, was attributed to differences in secondary flow loss. As seen in the radial loss variation, the differences lie within 20% of span at hub and tip. The familiar loss areas associated with the corner vortices can be seen in the first nozzle (Figure 6.36) and are almost absent in the second stage nozzles (Figures 6.37 to 6.45). The second nozzle contours also appear to have a thicker wake than the first nozzle that imply that there is more profile loss. This, obviously, is not a dominant effect since the overall loss is less.

The different rotor tip geometries did not produce significantly differing contour patterns. Although the overall loss in the second stage was not found to be significantly influenced by increasing rotor tip clearance, the tip region contours, particularly for the radiused tip with 1% clearance (Figure 6.40) do reflect some significant changes.

An unusual loss pattern was seen on suction side of the second nozzle blade wakes at a distance of about 30% of span from the tip and is possibly a separation induced by the tip leakage flow. It increased in size and prominence with increasing tip clearance and is present on all three blade tip geometries. It was slightly more distinct with the two streamlined tip geometries and thus appeared to be related to the amount of leakage fluid that is generated. This flow phenomena could possibly be linked to the negative incidence of tip leakage flow as shown in Figure 6.1 and illustrated in Figure 6.46. It could have been formed by separated leakage flow that flows along the suction surface of the blade towards the trailing edge as a high loss

zone. Alternatively it could be a peculiarity of the second nozzle secondary flow pattern, and, like classical cascade results, depends on the nature and magnitude of the inlet vorticity. Its nature and importance were however not studied and adaptations to the rig are required to provide data within these stator blades. Further work should be done to examine its origin, effect on performance and possible elimination.

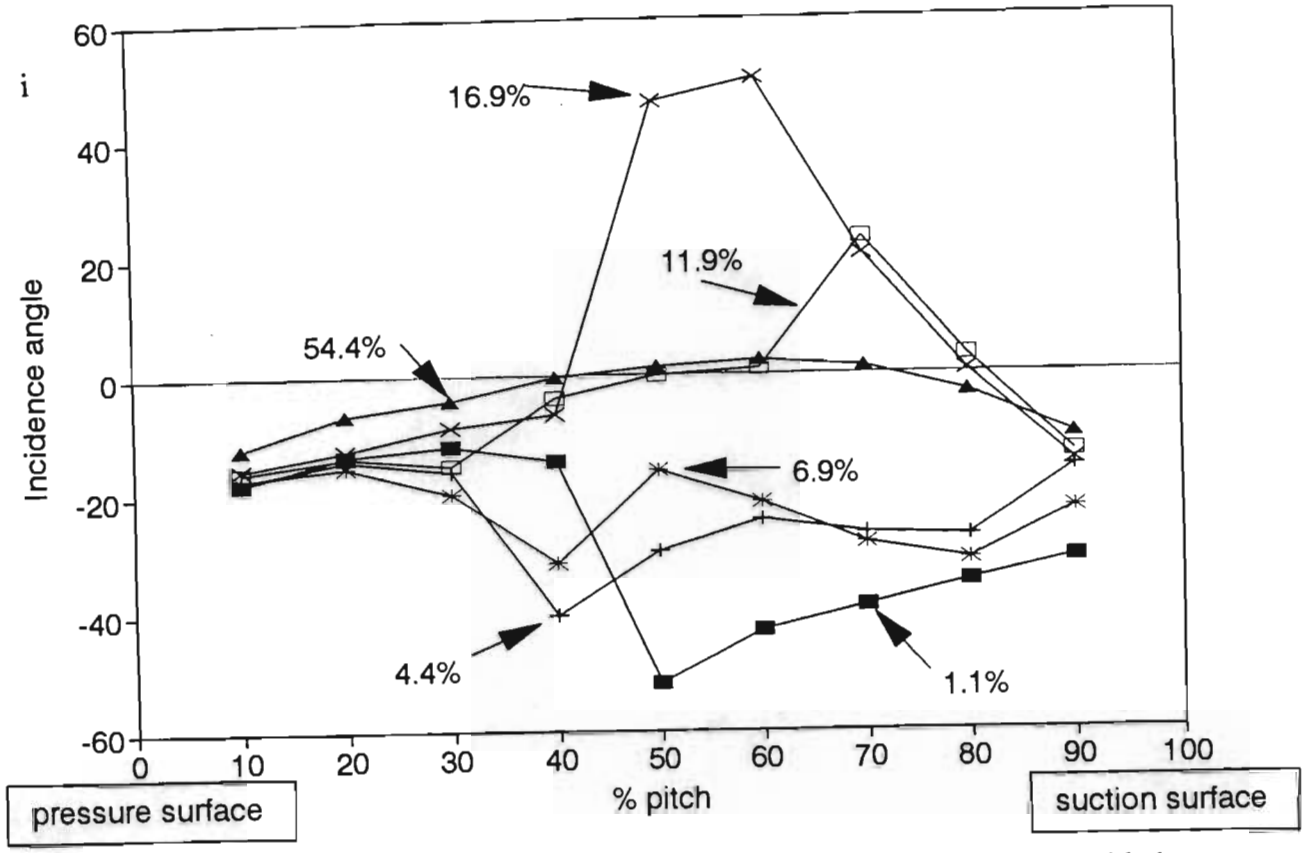

Figure 6.1 Second stage nozzle incidence angle at various distances from the blade tip simulated from linear cascade data with 2% of chord clearance.

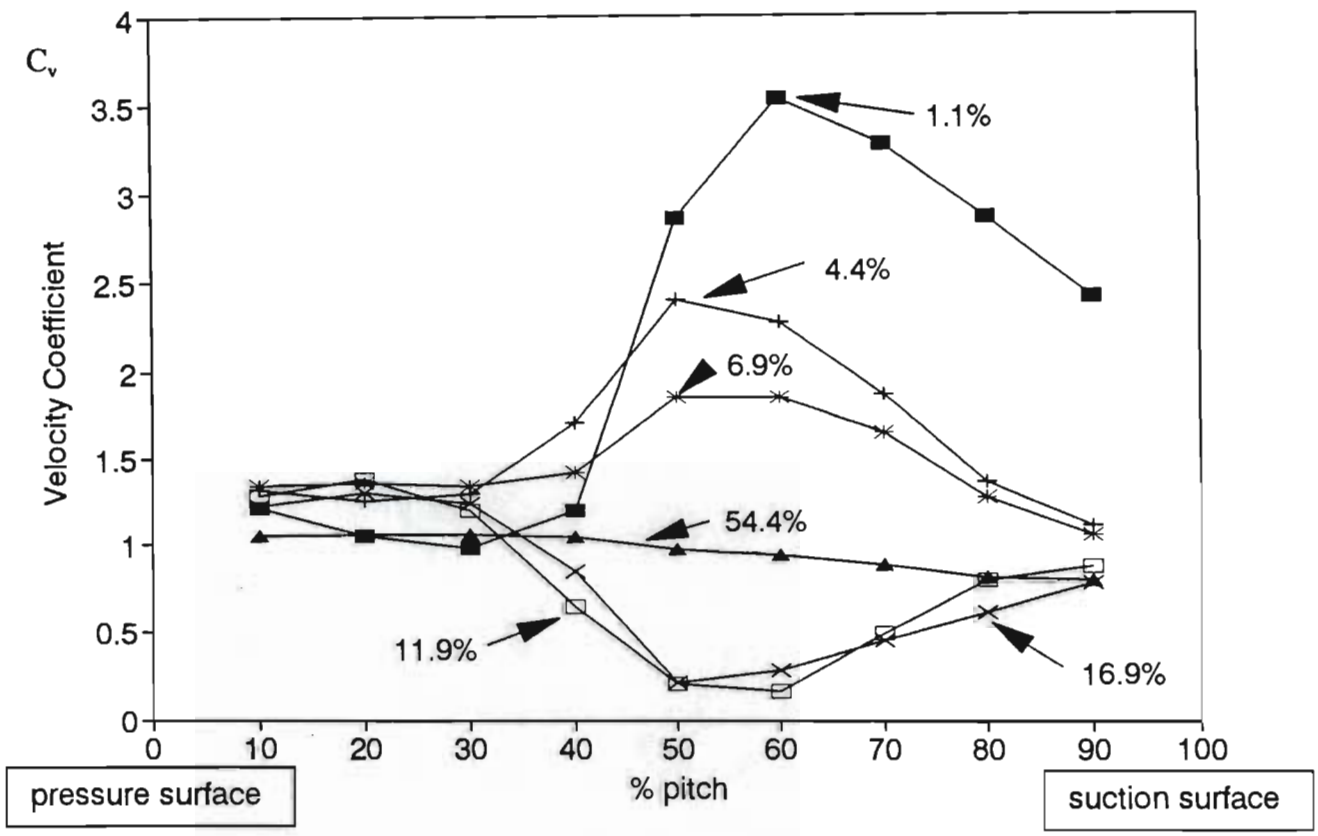

Figure 6.2 Second stage nozzle inlet velocity at varying distances from blade tip simulated from linear cascade data with 2% of chord clearance.

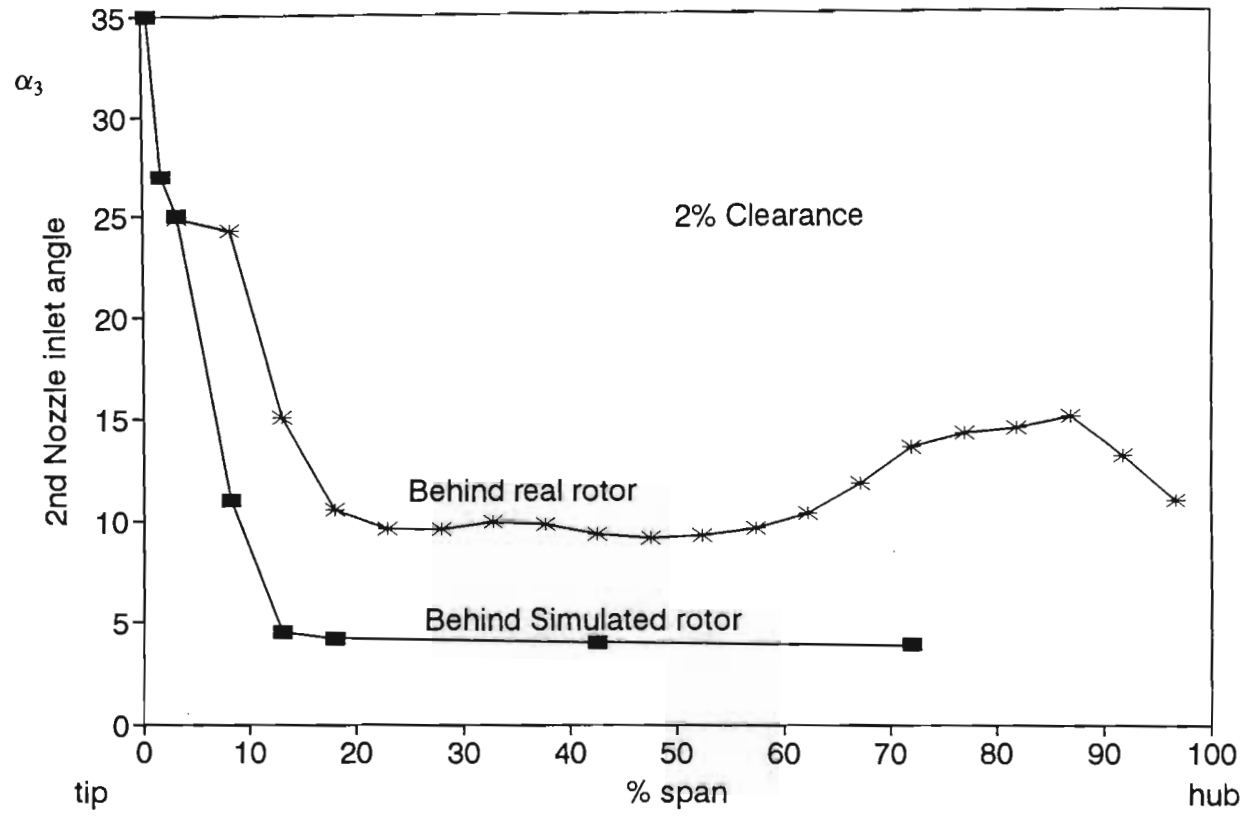

Figure 6.3 Radial variation of tangentially averaged second nozzle inlet angle for real rotor and for nozzle behind the simulated rotor of Morphis (1989)

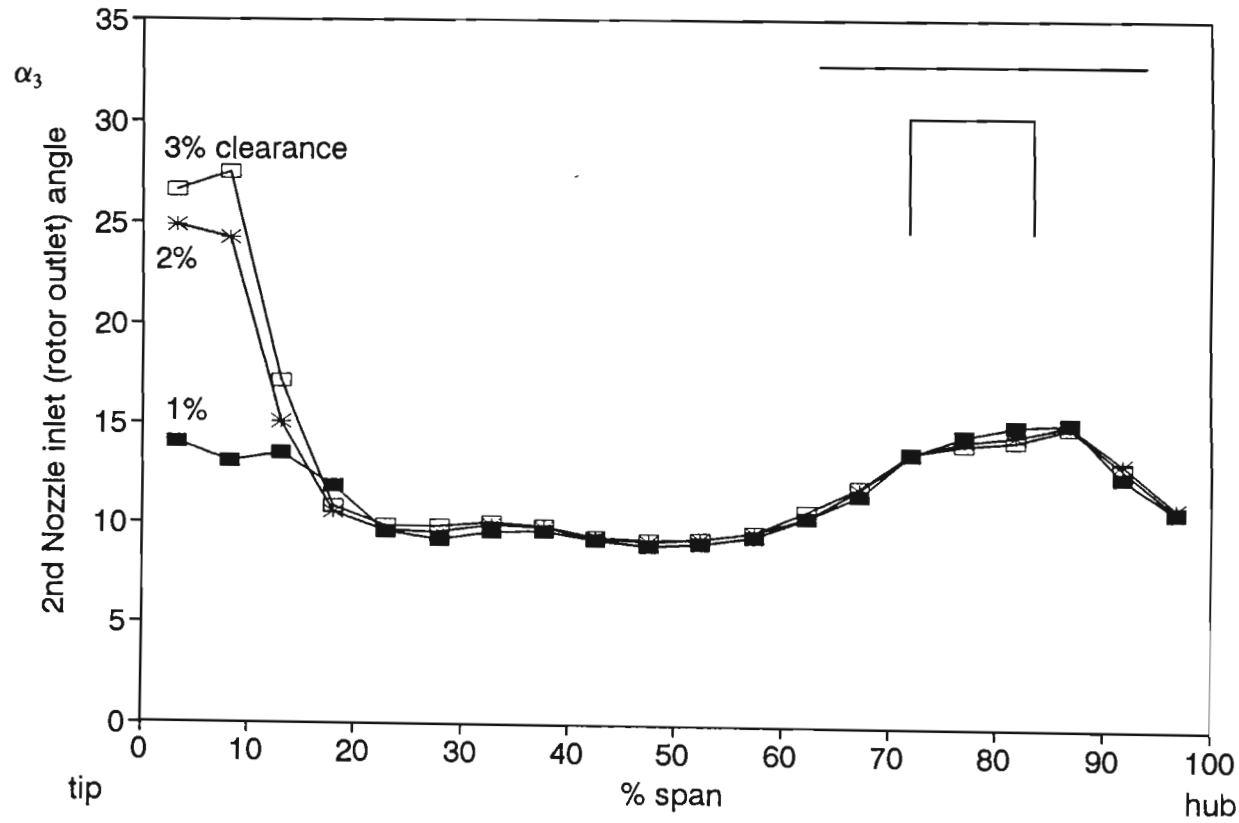

Figure 6.4 Radial variation of tangentially averaged absolute outlet angle for the square tip rotor.

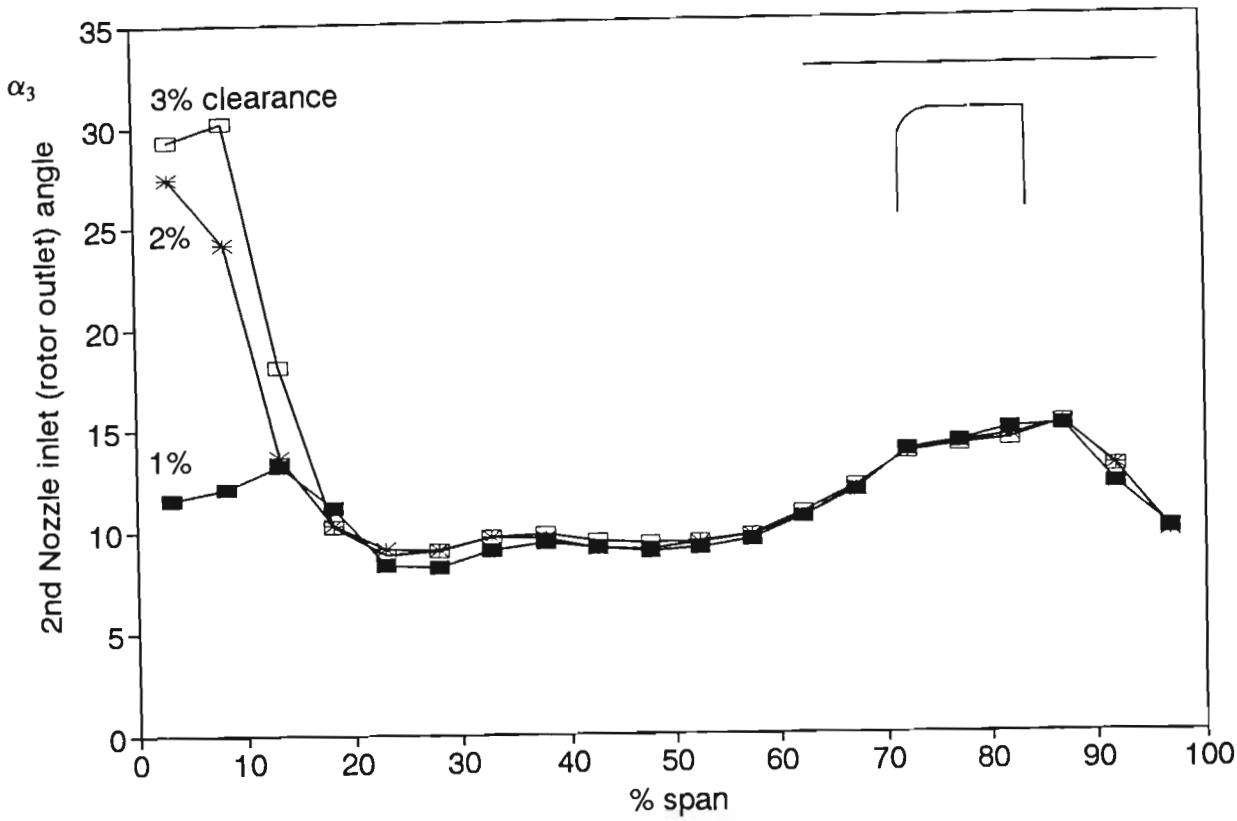

Figure 6.5 Radial variation of tangentially averaged absolute outlet angle for the radiused tip rotor.

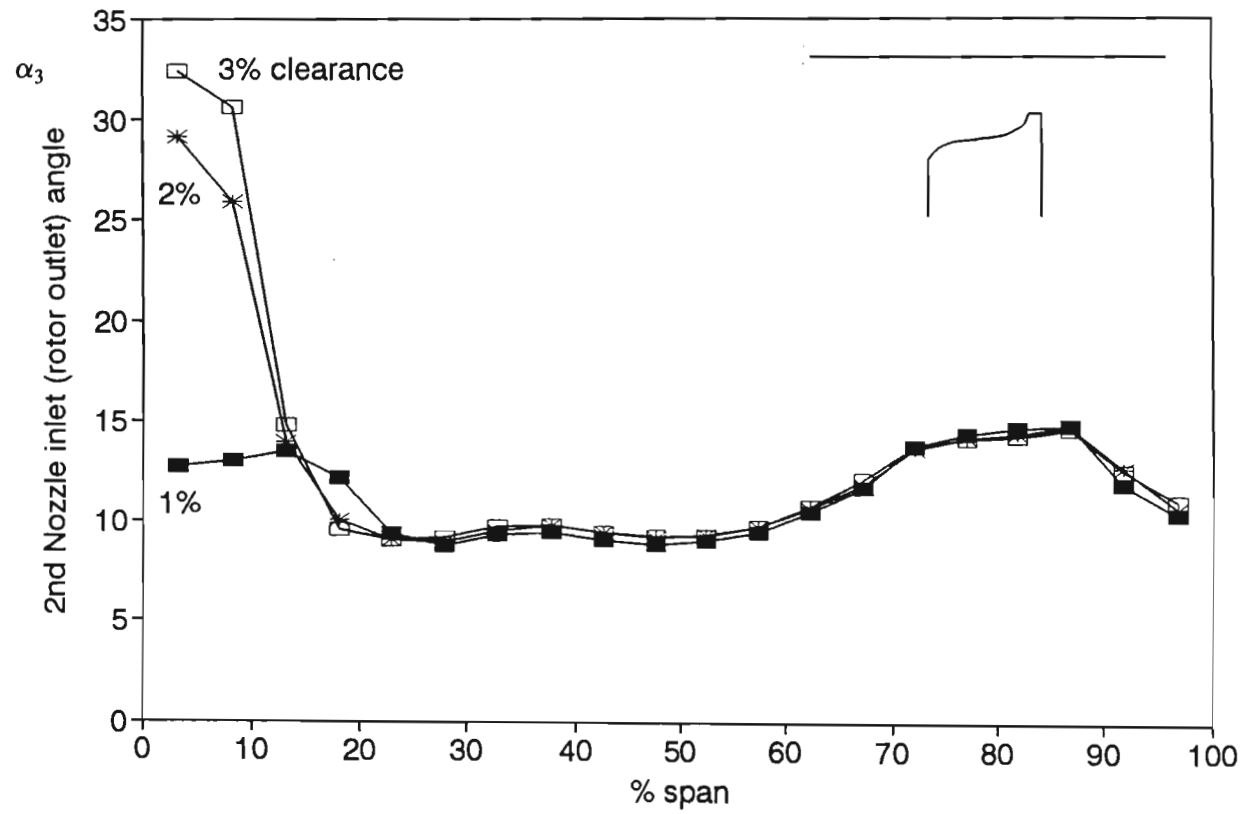

Figure 6.6 Radial variation of tangentially averaged absolute outlet angle for the contoured tip rotor.

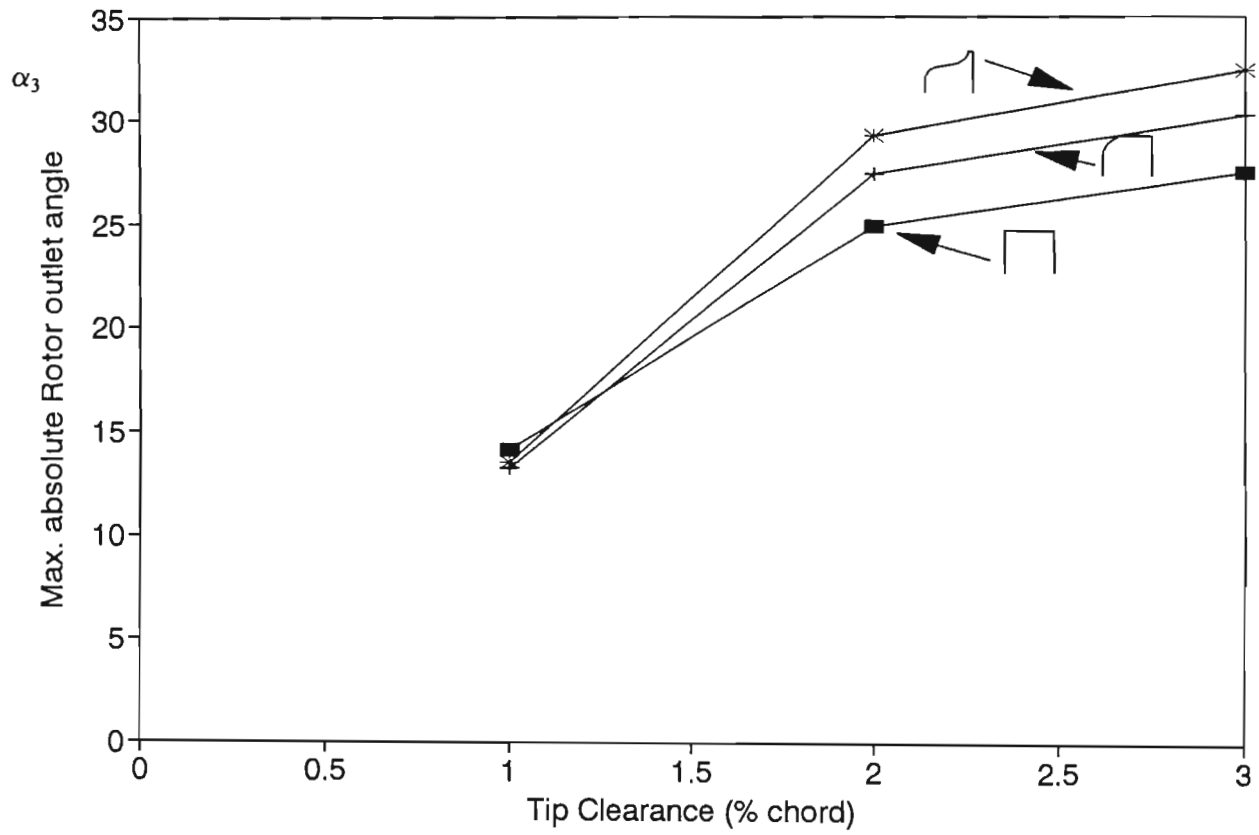

Figure 6.7 Maximum absolute rotor outlet angles for three blade tip geometries.

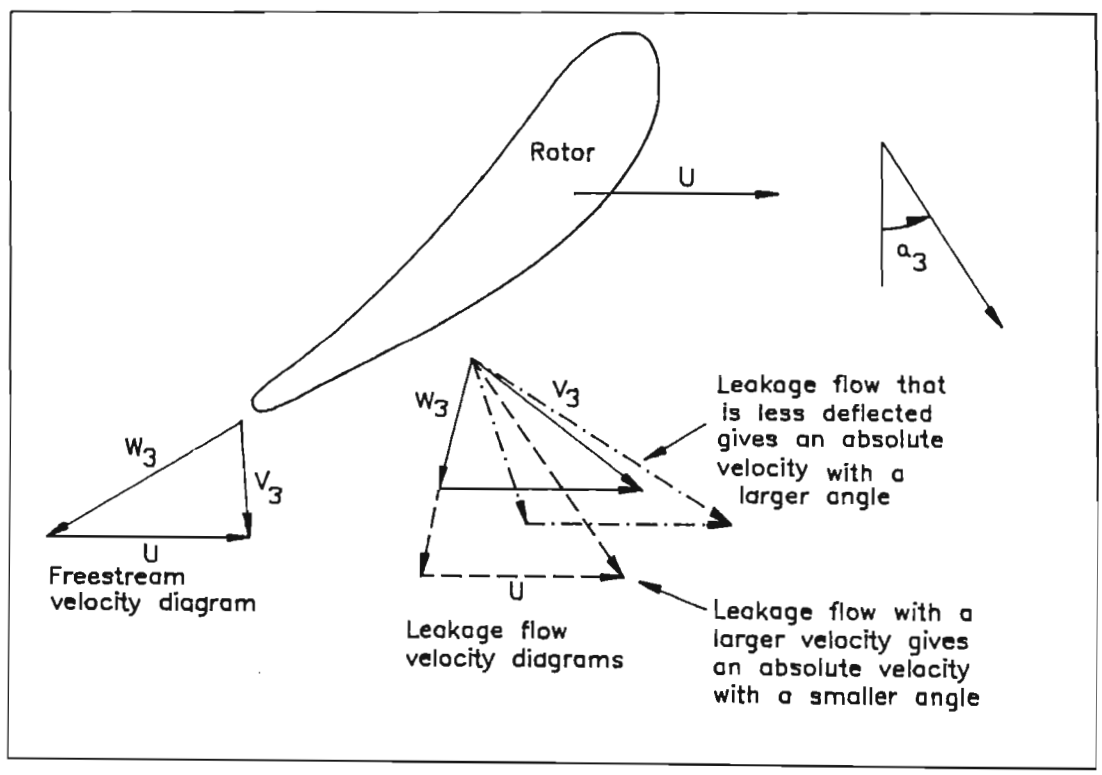

Figure 6.8 Leakage flow velocity diagrams.

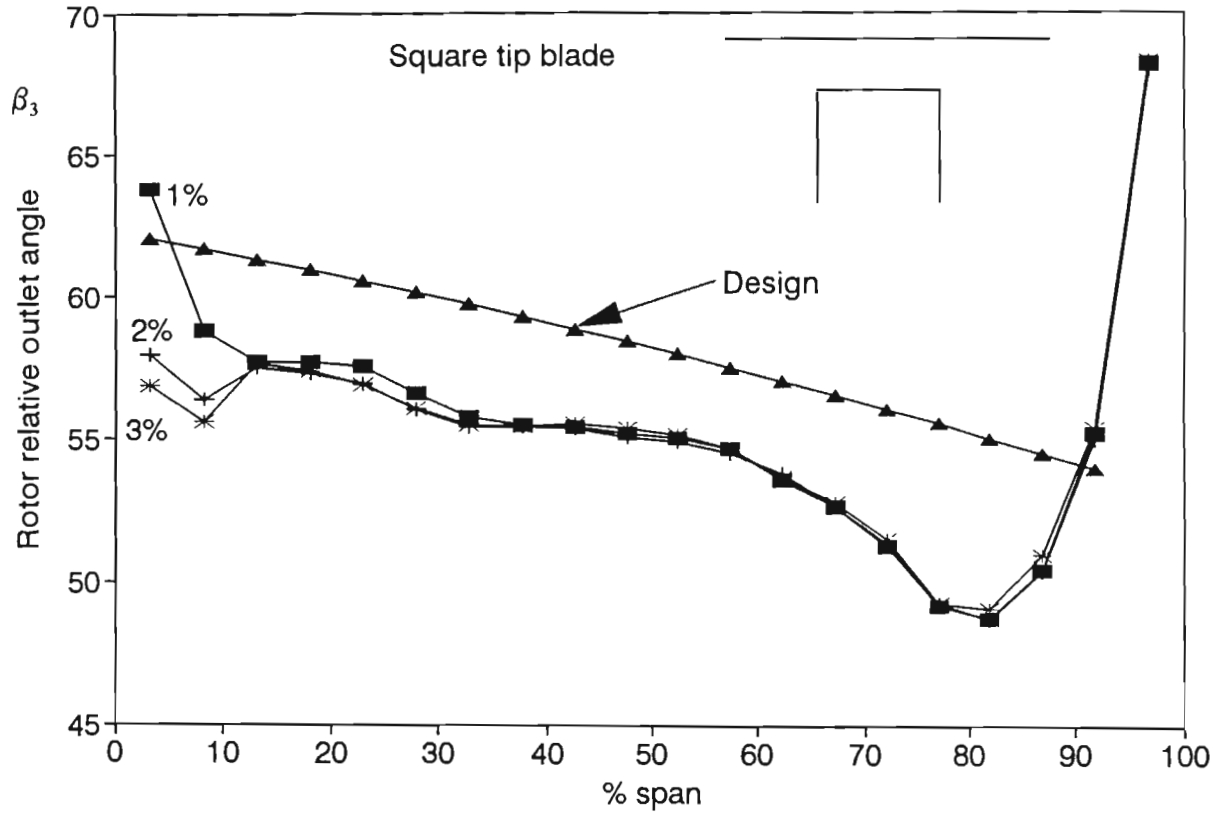

Figure 6.9 Radial variation of tangentially averaged relative outlet angle for the square tip rotor.

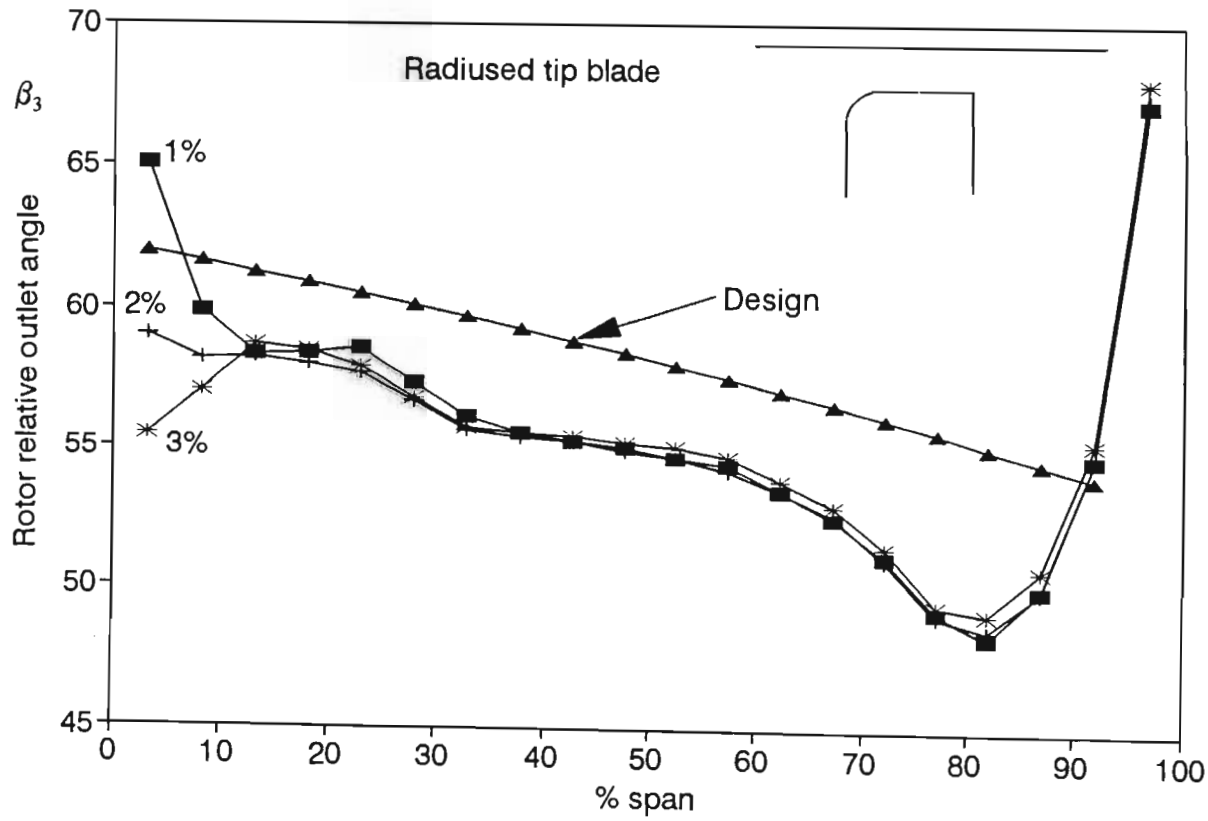

Figure 6.10 Radial variation of tangentially averaged relative outlet angle for the radiused tip rotor.

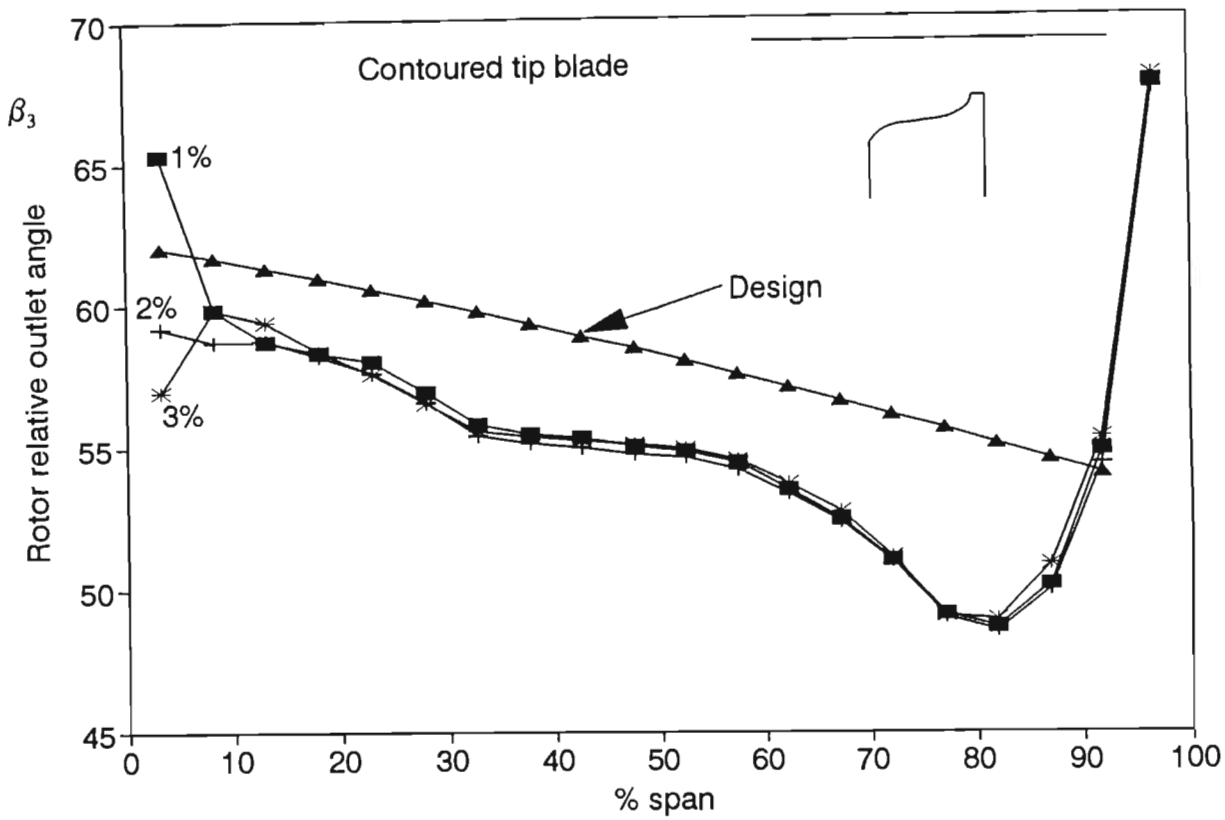

Figure 6.11 Radial variation of tangentially averaged relative outlet angle for the contoured tip rotor.

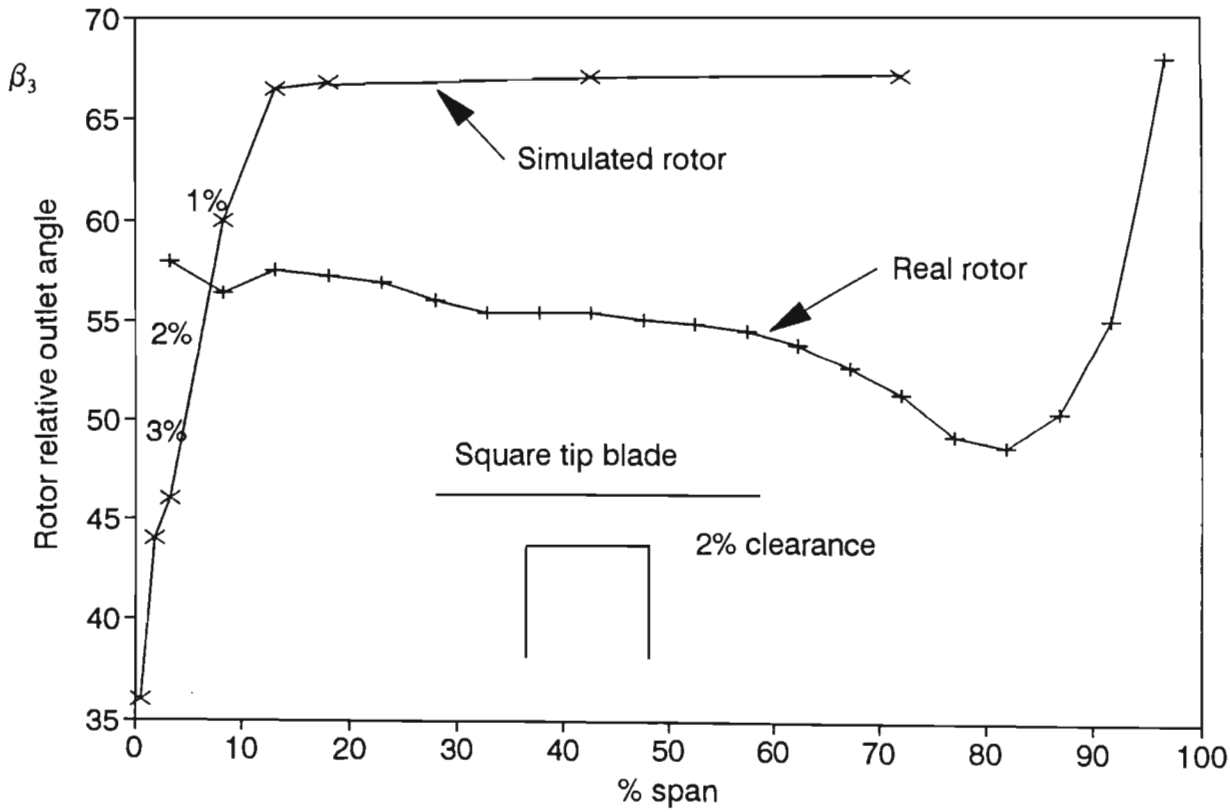

Figure 6.12 Rotor outlet relative angle for real rotor and linear cascade simulated rotor of Morphis (1989).

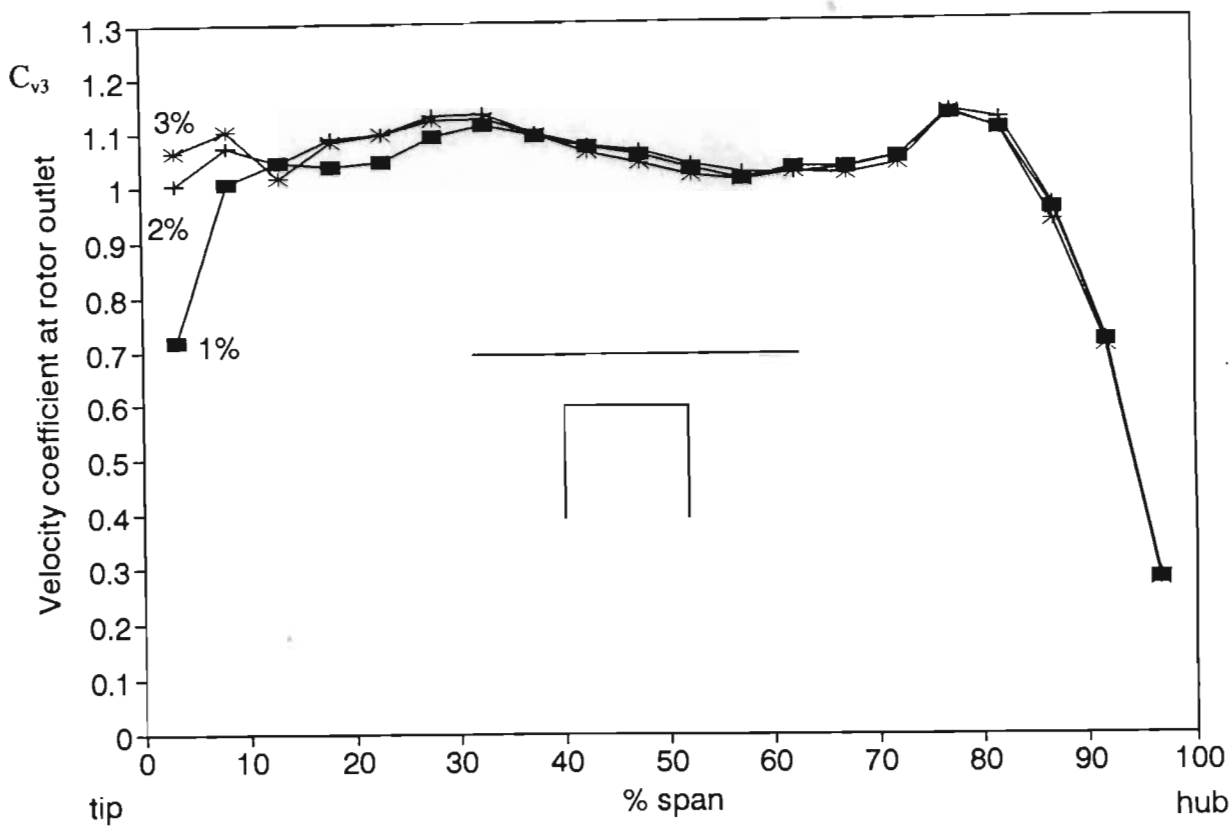

Figure 6.13 Radial variation of tangentially averaged outlet velocity coefficient for square tip rotor.

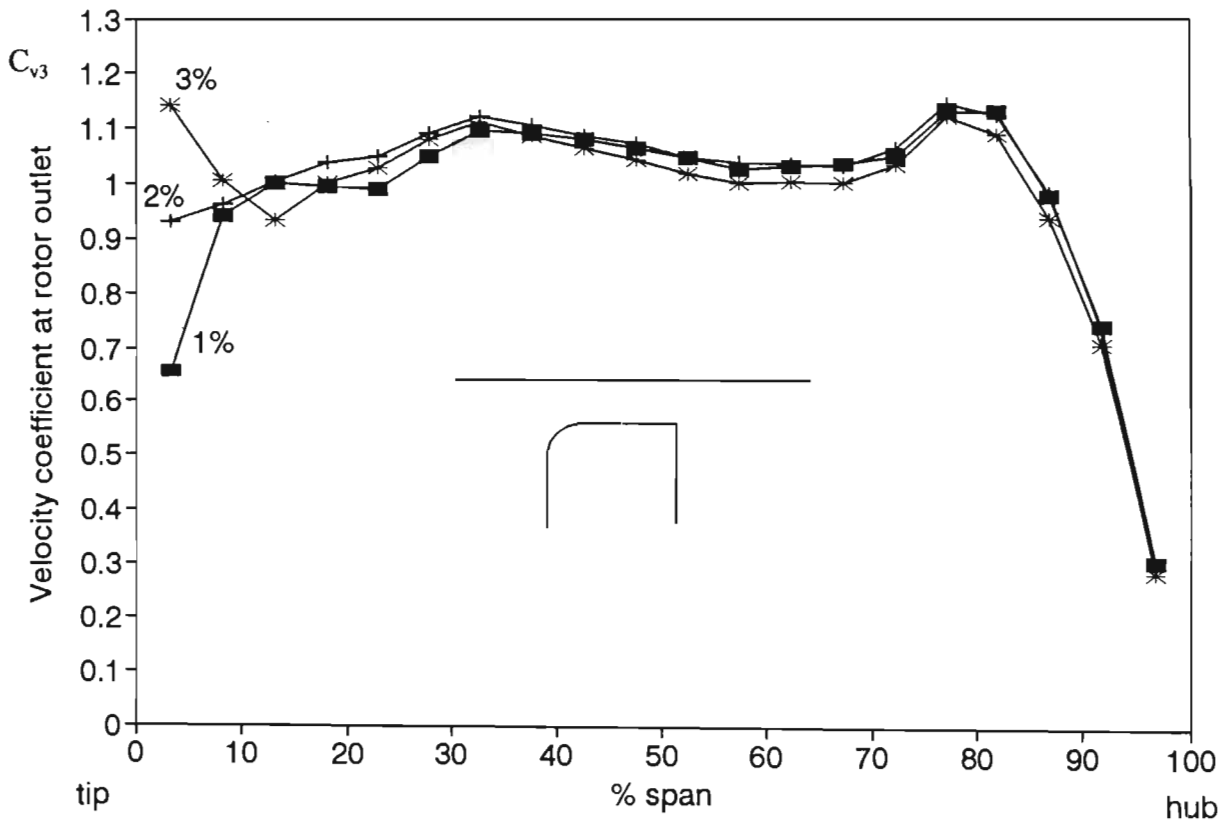

Figure 6.14 Radial variation of tangentially averaged outlet velocity coefficient for radiused tip rotor.

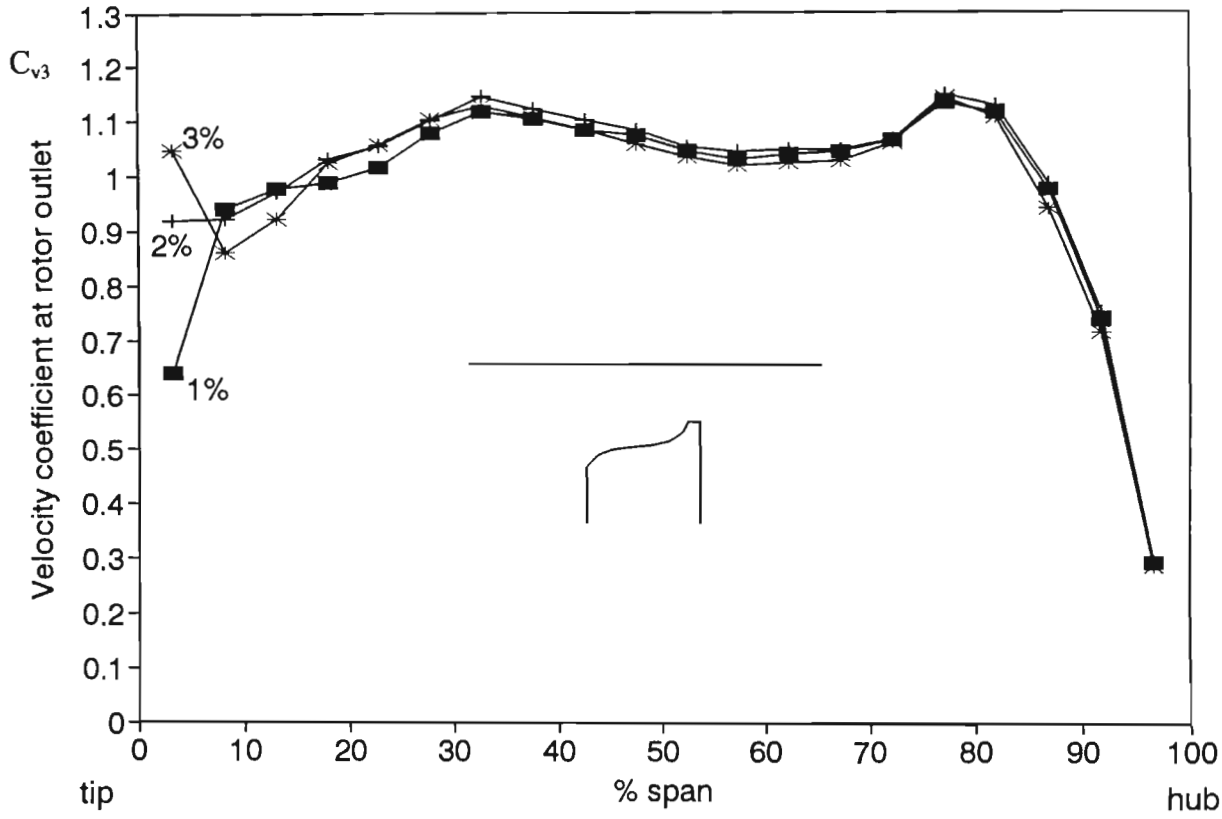

Figure 6.15 Radial variation of tangentially averaged outlet velocity coefficient for contoured tip rotor.

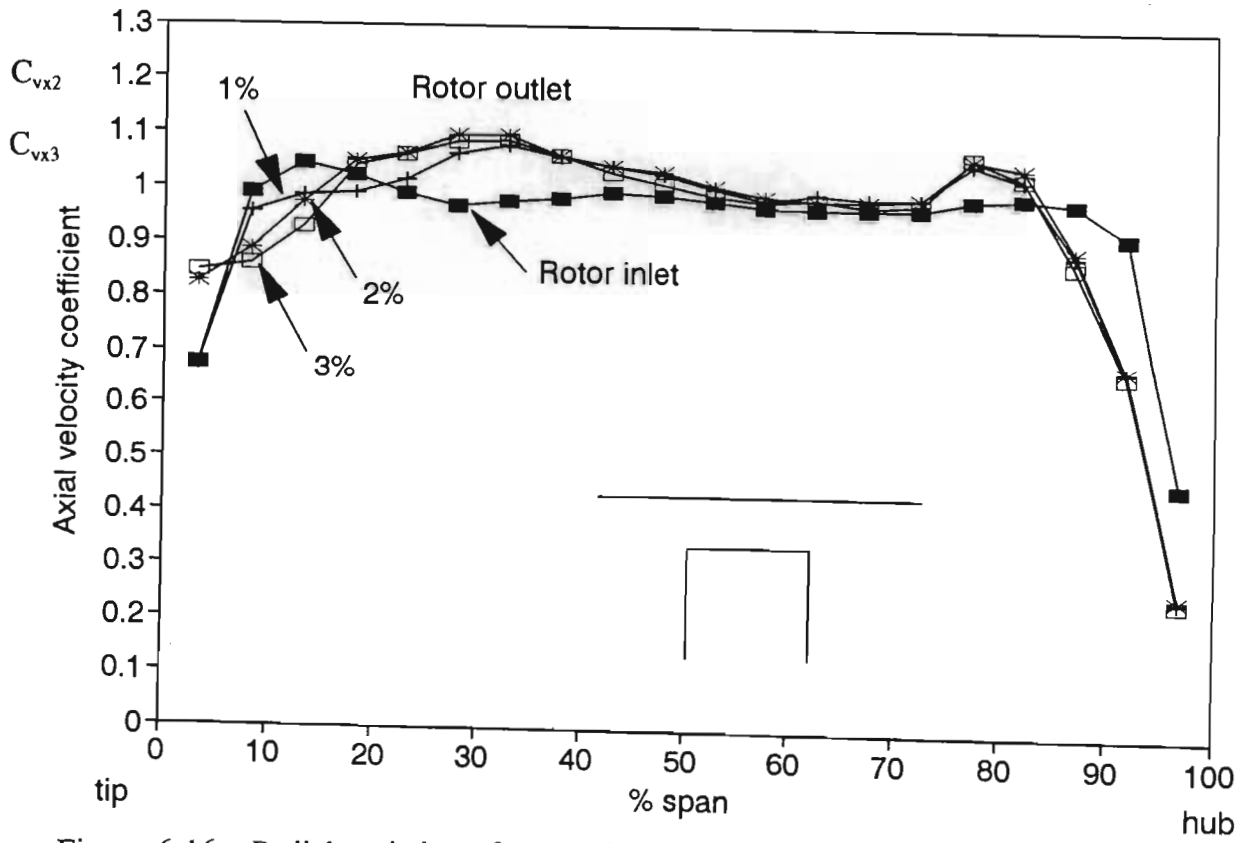

Figure 6.16 Radial variation of tangentially averaged axial velocity coefficient for square tip rotor.

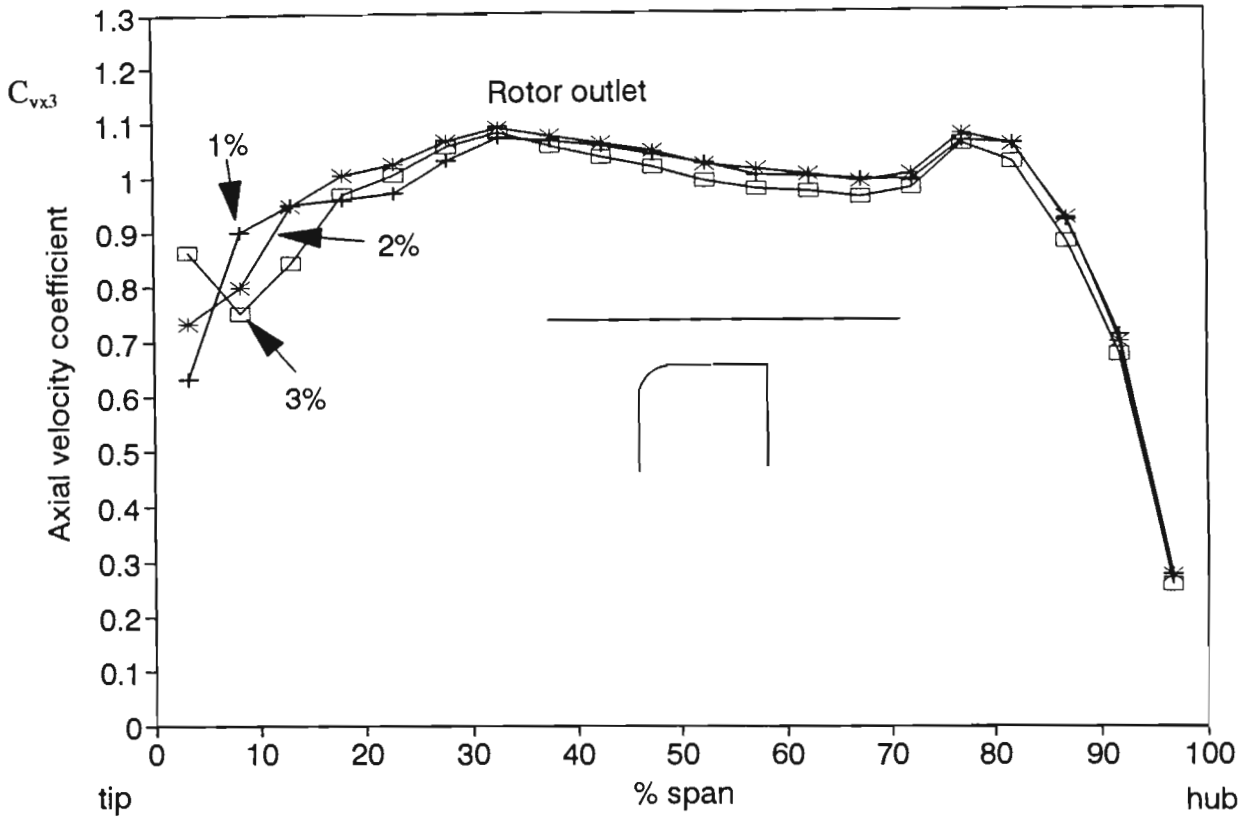

Figure 6.17 Radial variation of tangentially averaged axial velocity coefficient for radiused tip rotor.

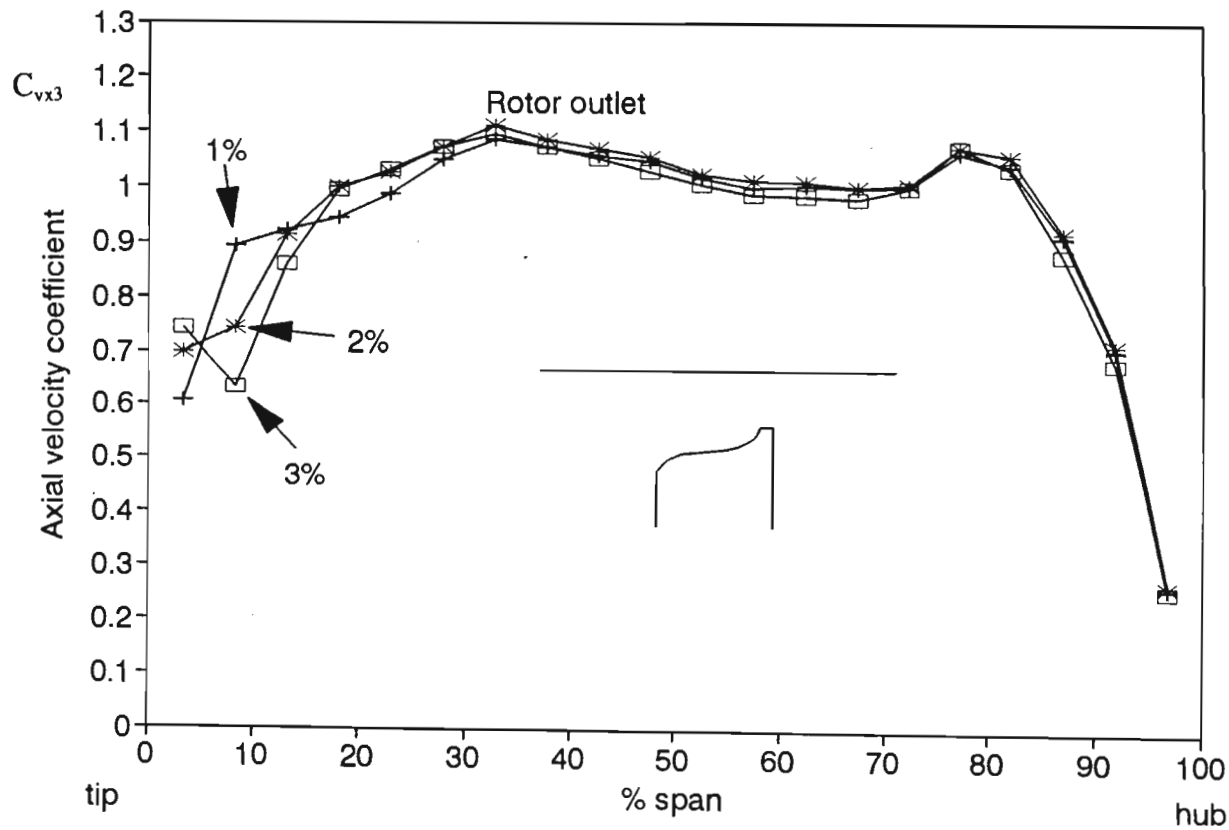

Figure 6.18 Radial variation of tangentially averaged axial velocity coefficient for contoured tip rotor.

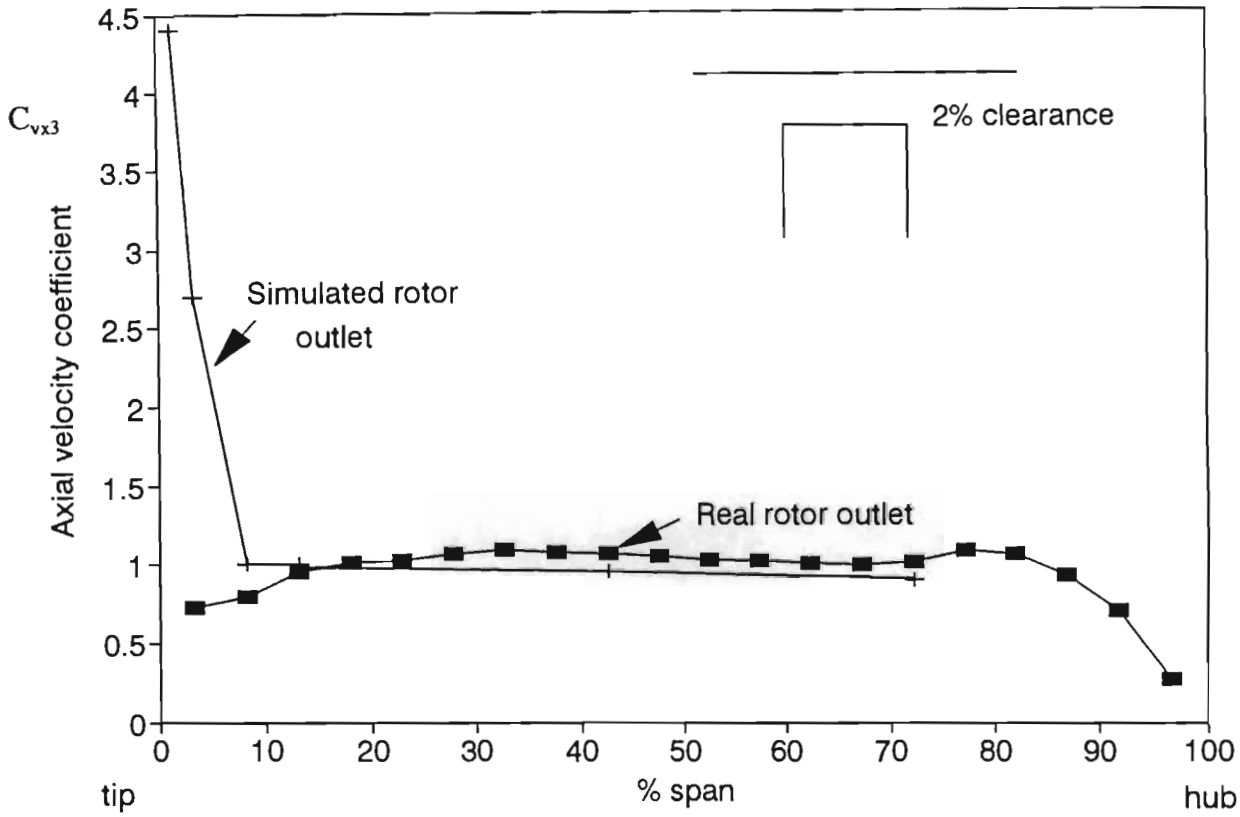

Figure 6.19 Rotor outlet axial velocity coefficient for real rotor and linear cascade simulated rotor of Morphis (1989).

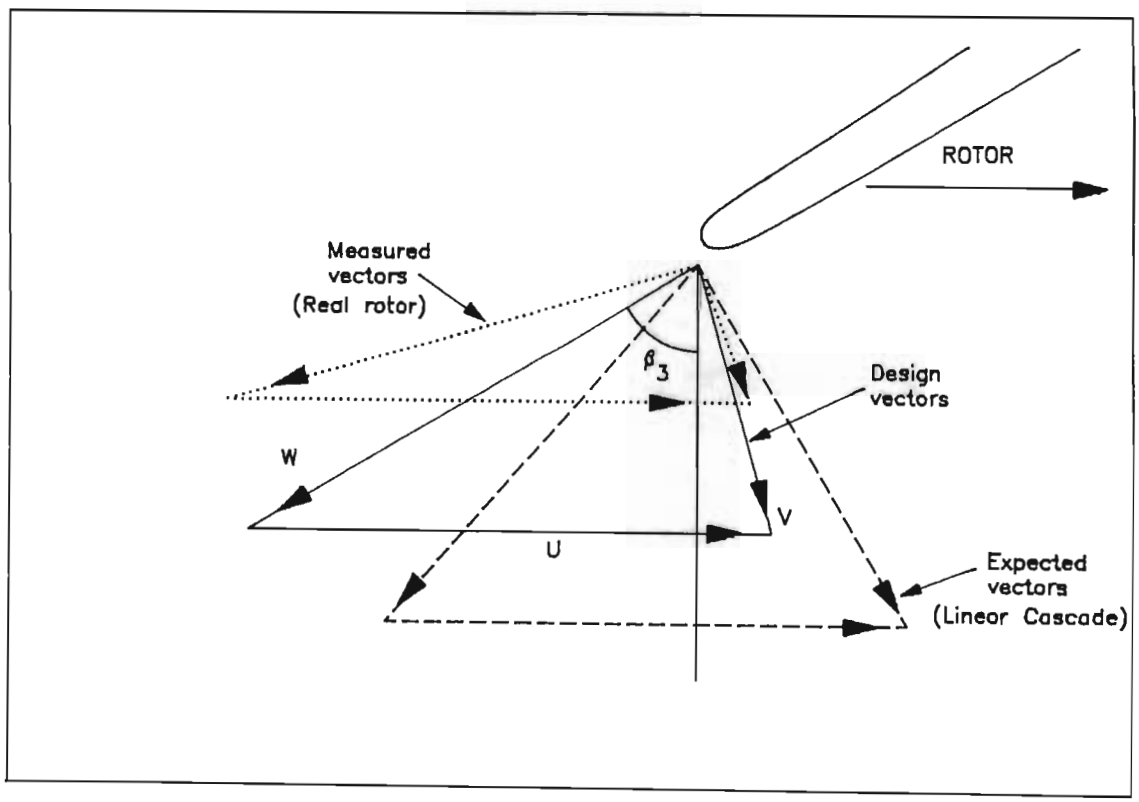

Figure 6.20 Velocity triangles at rotor outlet.

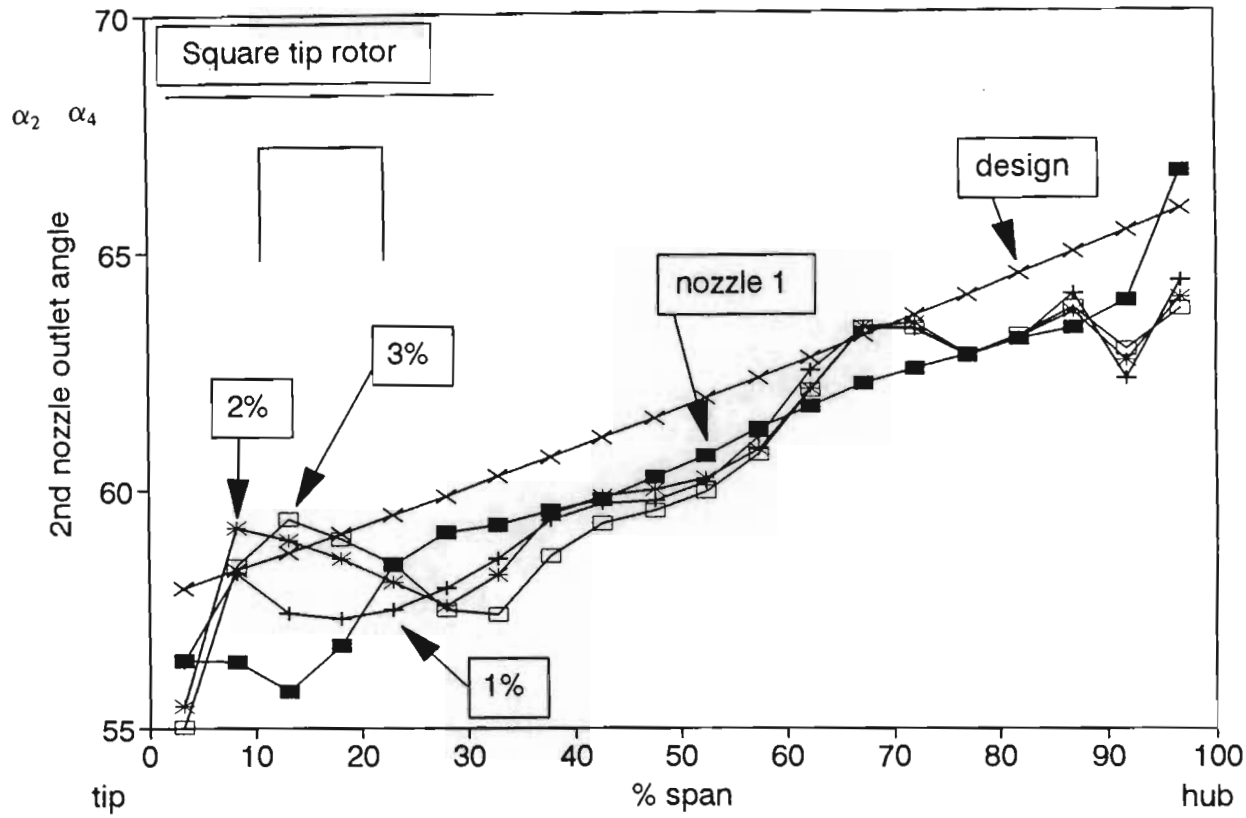

Figure 6.21 Radial variation of tangentially averaged nozzle outlet angle for square tip rotor.

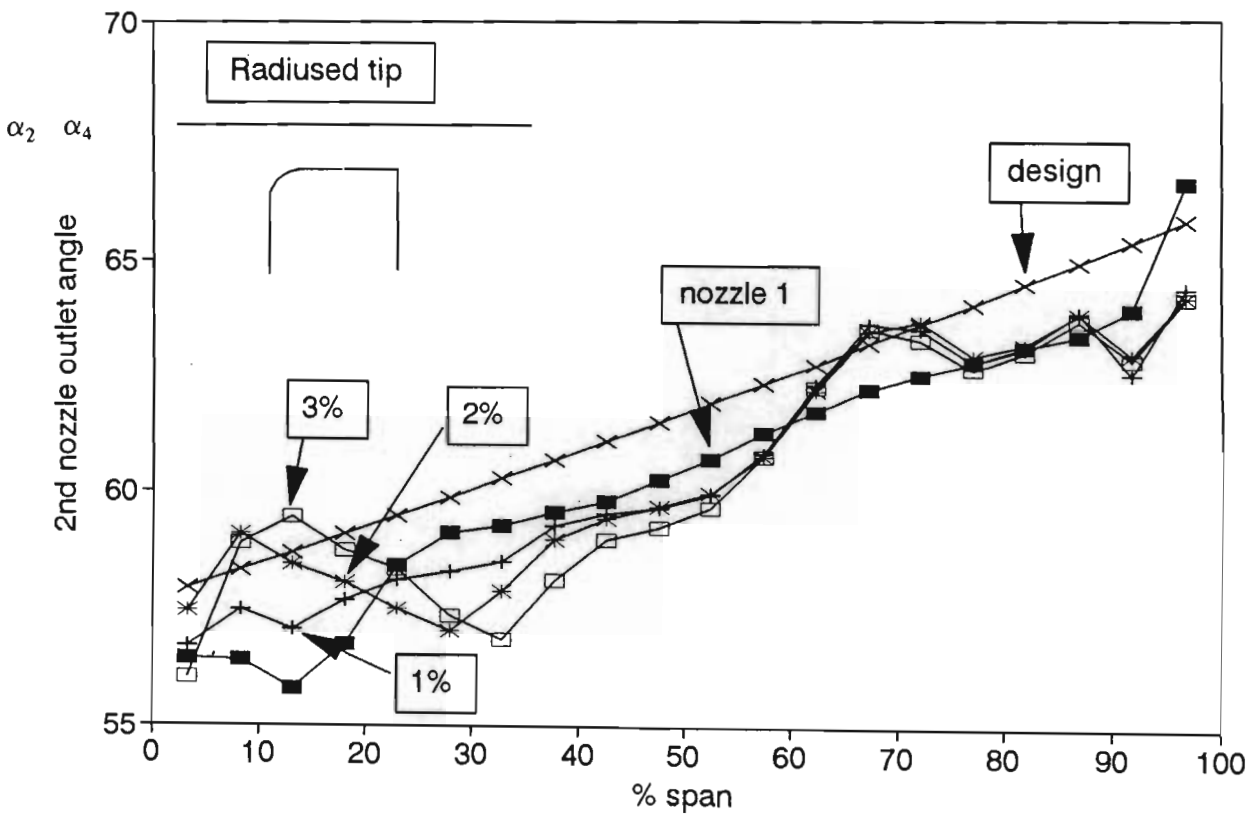

Figure 6.22 Radial variation of tangentially averaged nozzle outlet angle for radiused tip rotor.

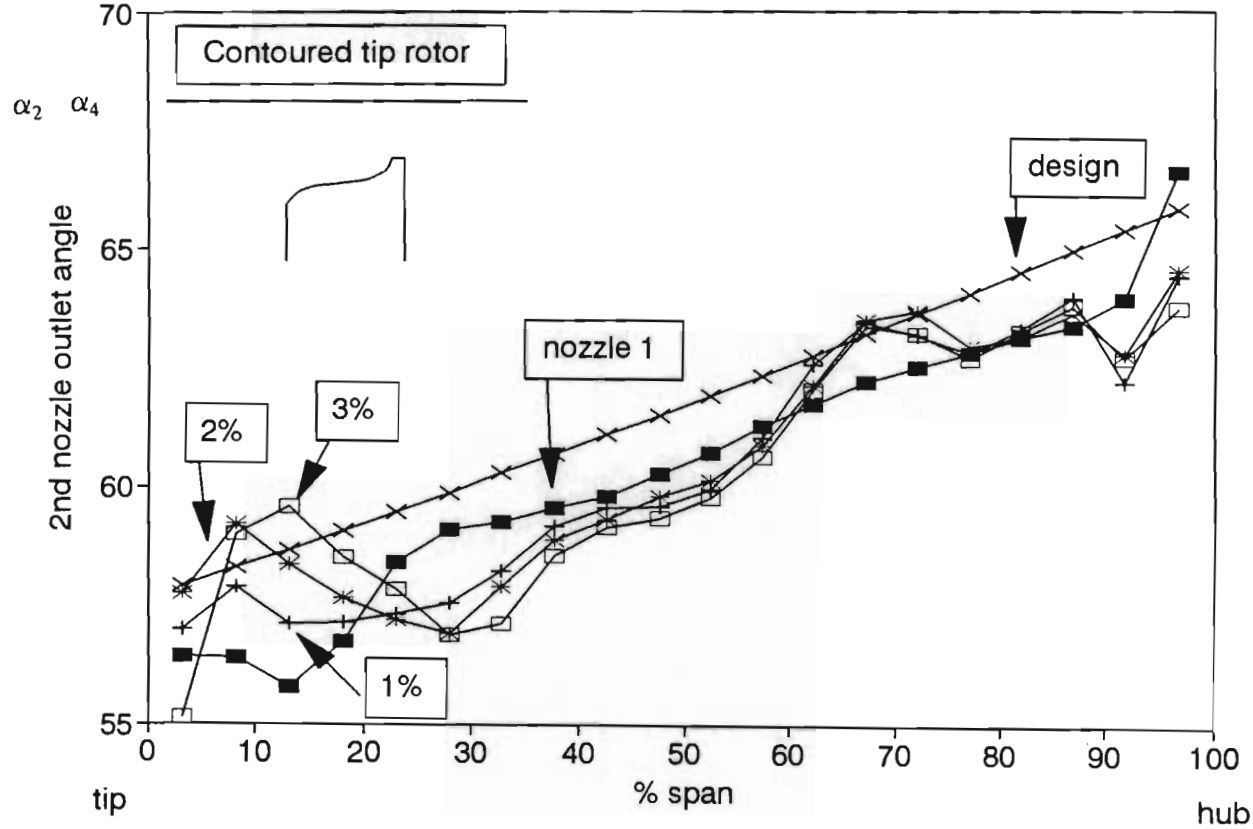

Figure 6.23 Radial variation of tangentially averaged nozzle outlet angle for contoured tip rotor.

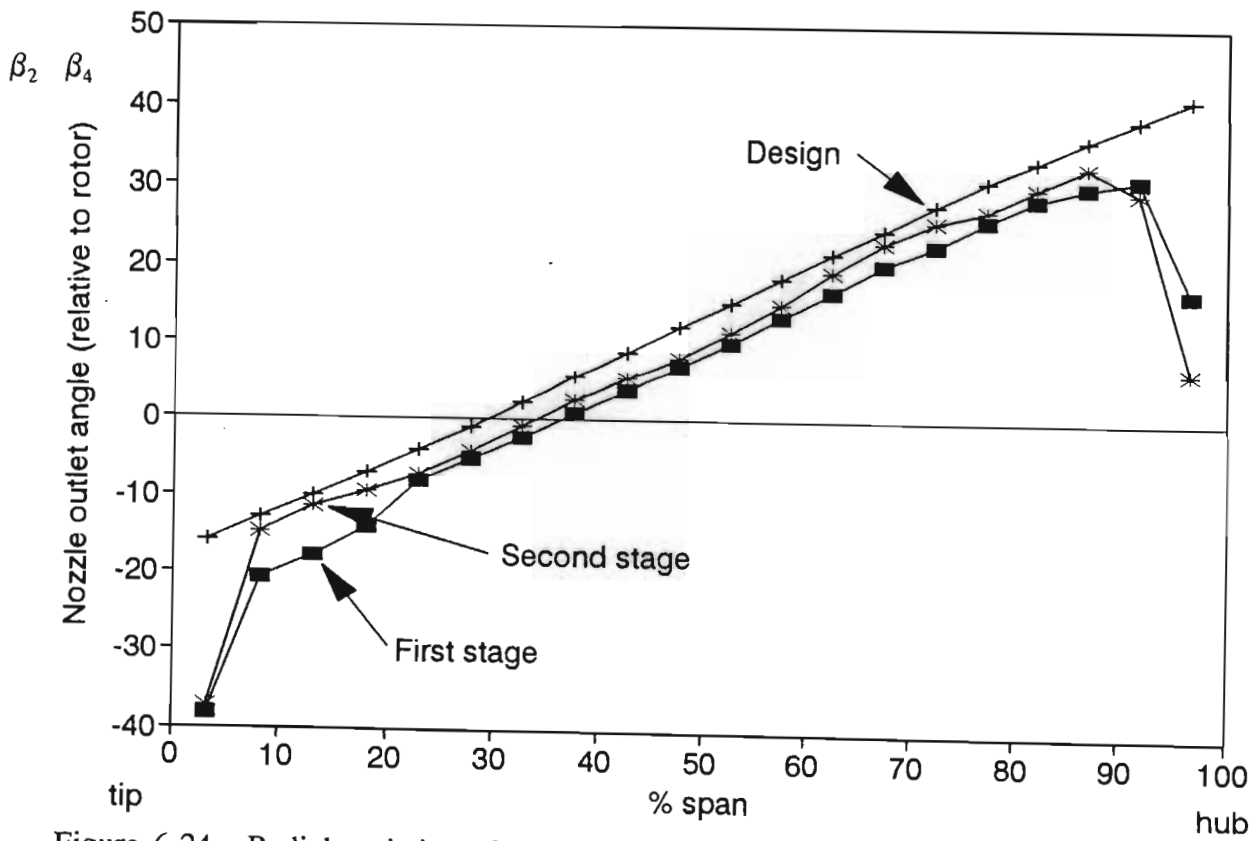

Figure 6.24 Radial variation of tangentially averaged nozzle outlet angle relative to rotor.

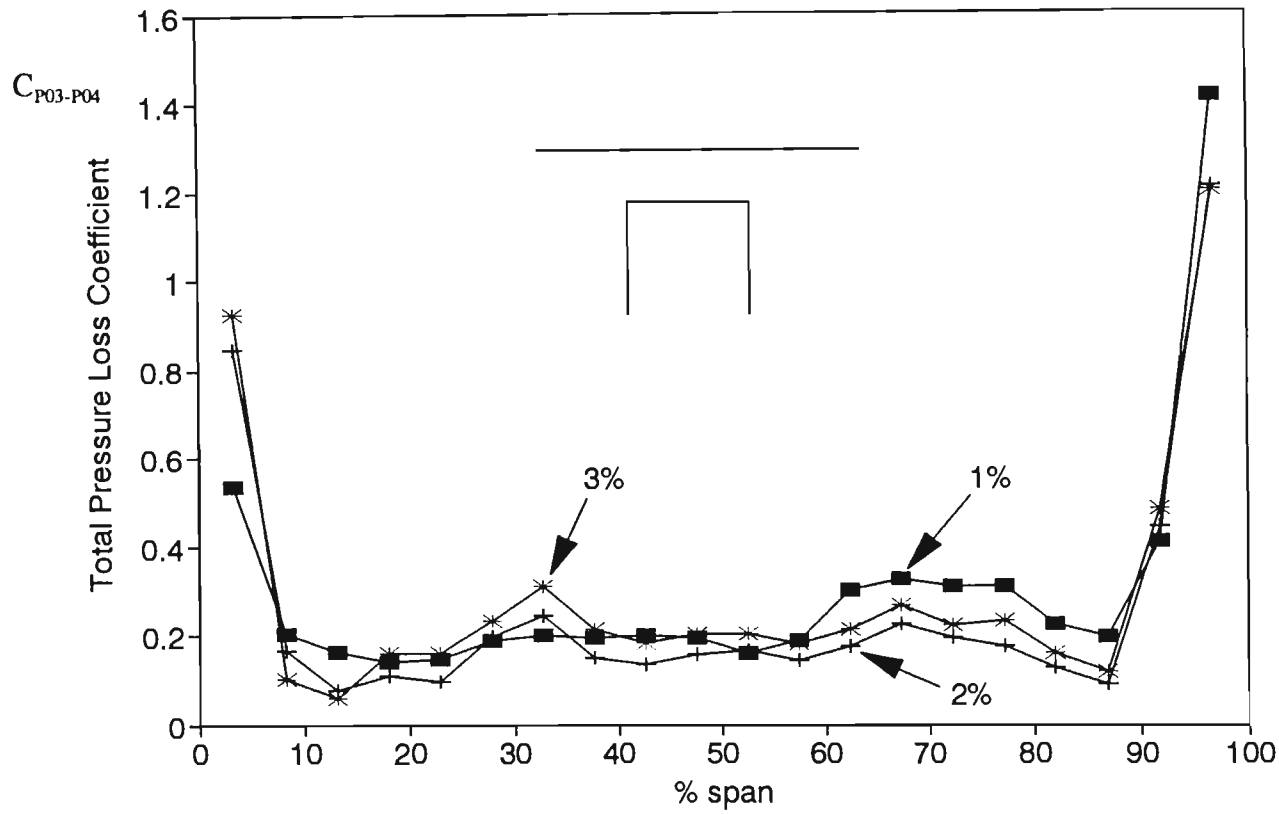

Figure 6.25 Radial variation of tangentially averaged total pressure loss coefficient for second nozzle with square tip first stage rotor.

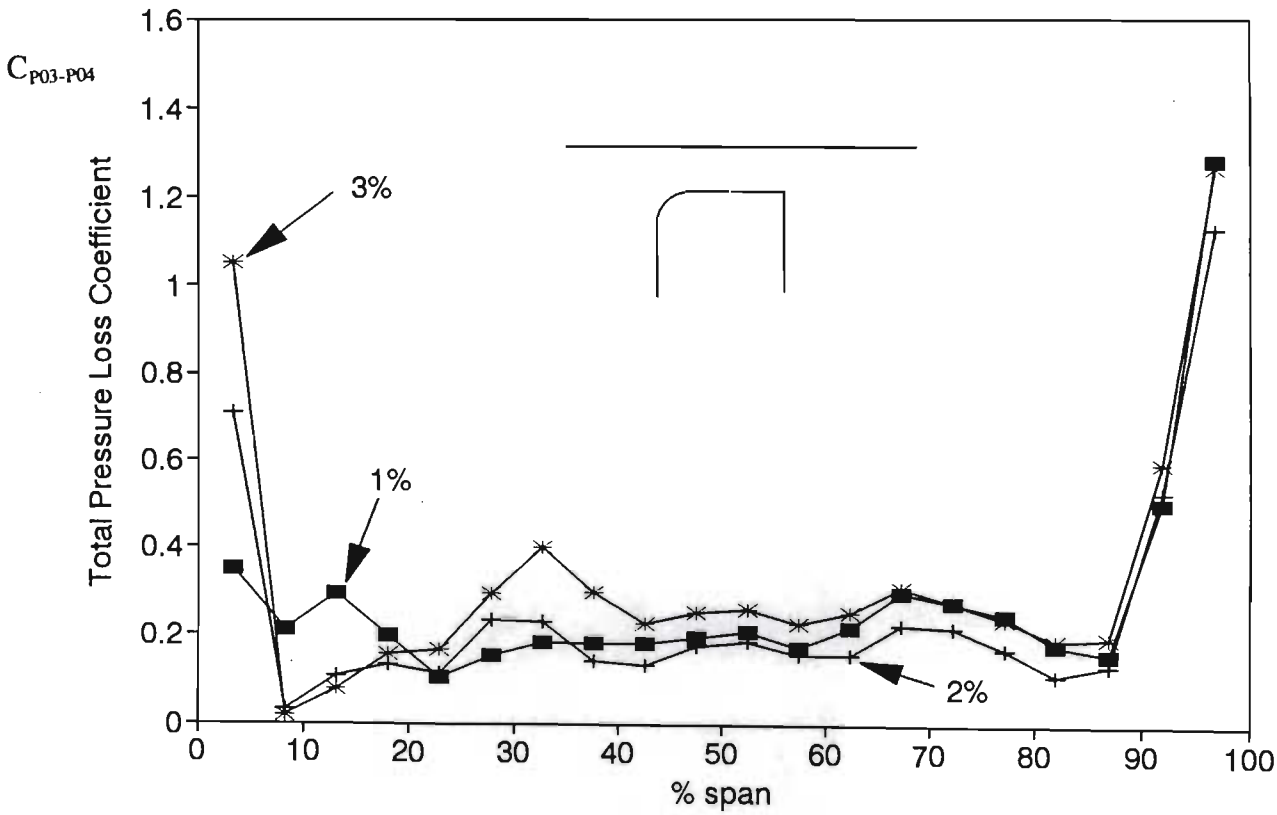

Figure 6.26 Radial variation of tangentially averaged total pressure loss coefficient for second nozzle with radiused tip first stage rotor.

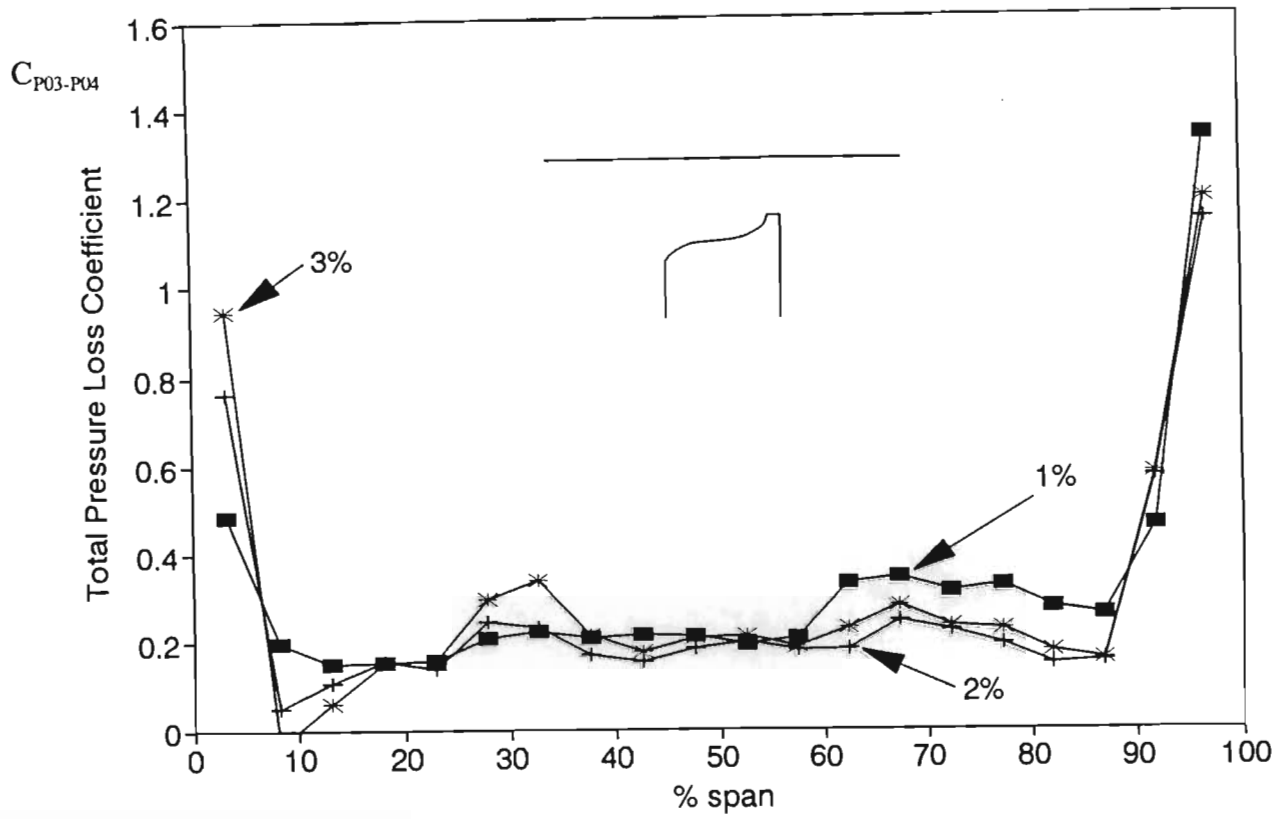

Figure 6.27 Radial variation of tangentially averaged total pressure loss coefficient for second nozzle with contoured tip first stage rotor.

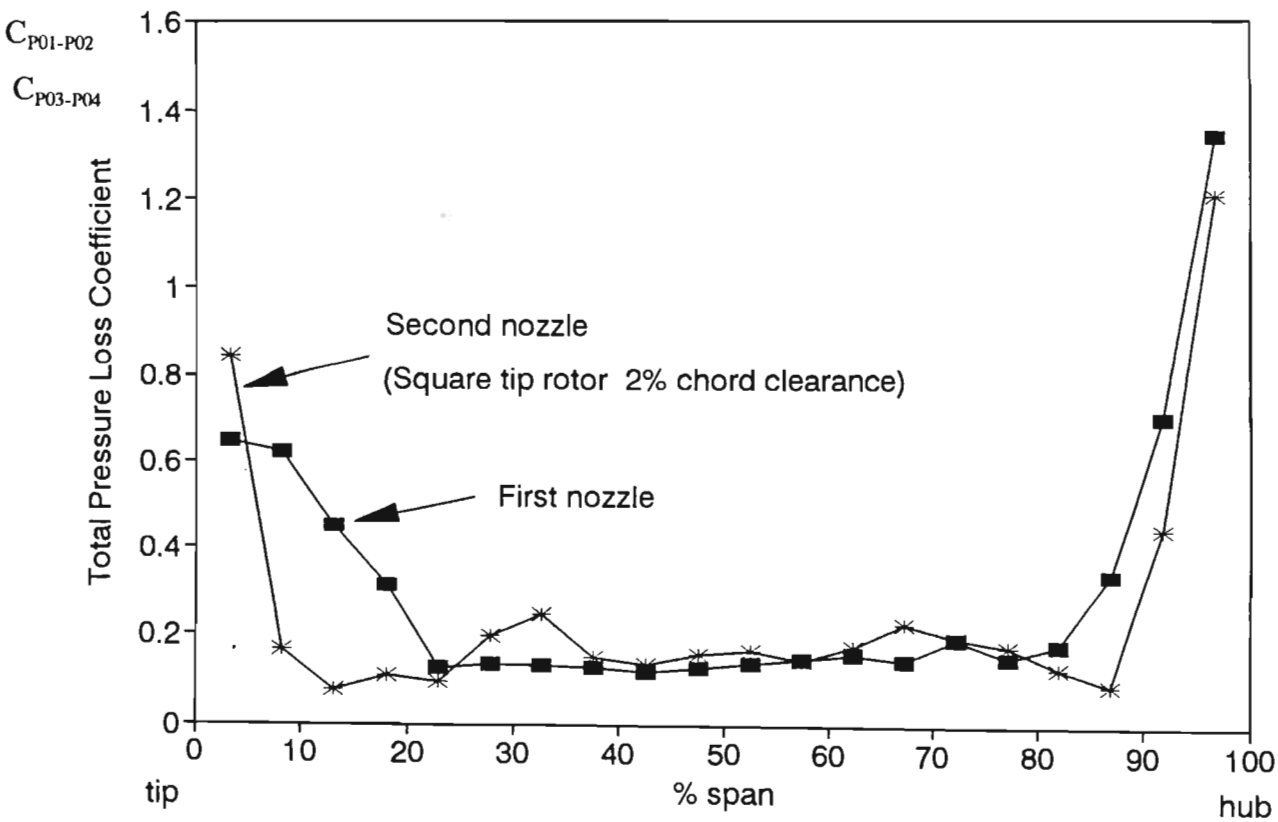

Figure 6.28 Radial variation of tangentially averaged total pressure loss coefficient for first and second nozzles.

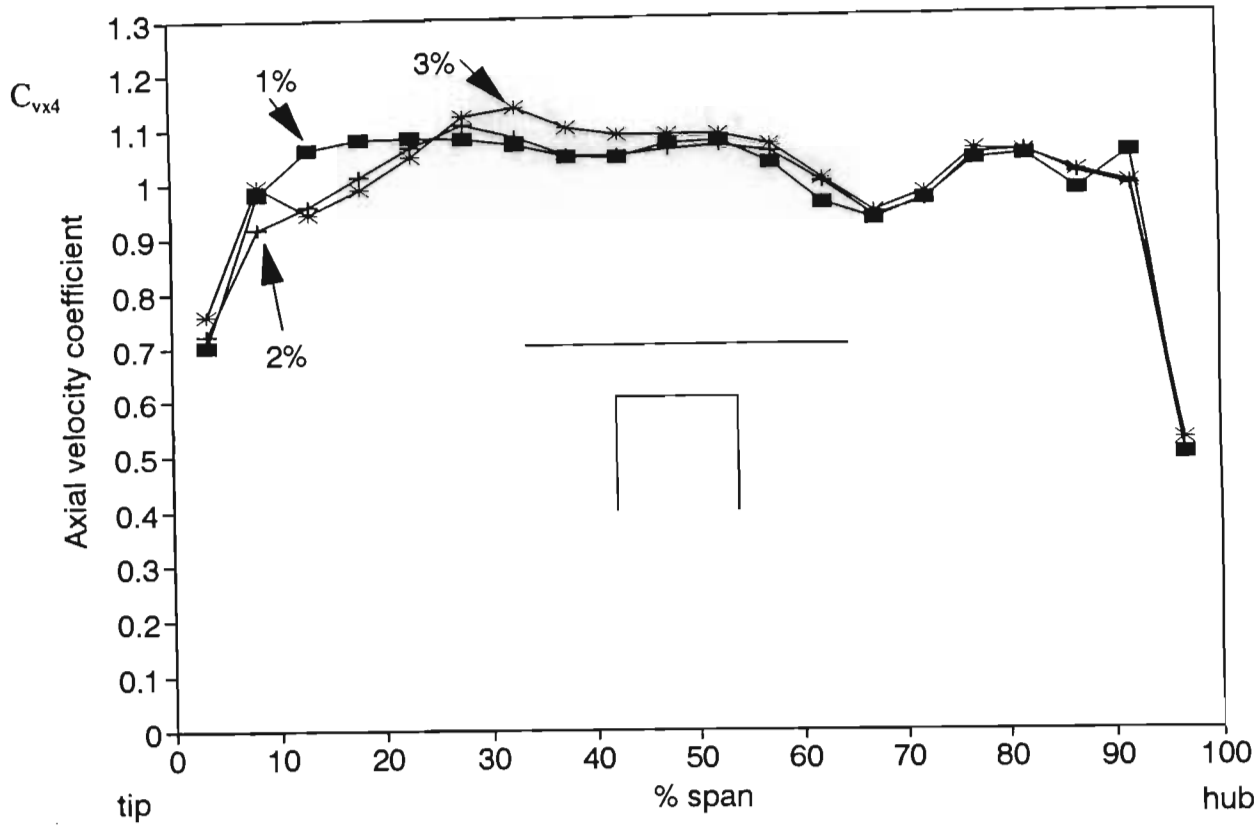

Figure 6.29 Radial variation of tangentially averaged outlet axial velocity coefficient for second nozzle with square tip first stage rotor.

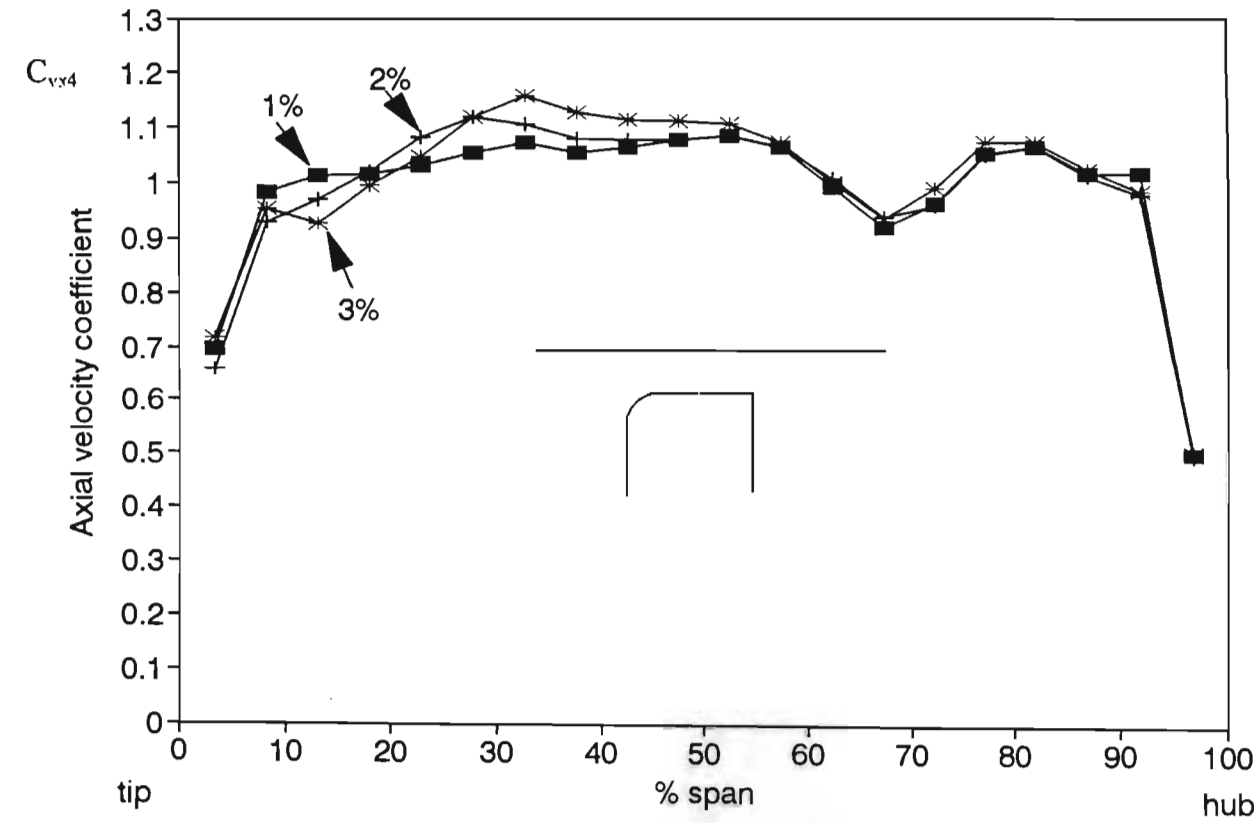

Figure 6.30 Radial variation of tangentially averaged outlet axial velocity coefficient for second nozzle with radiused tip first stage rotor.

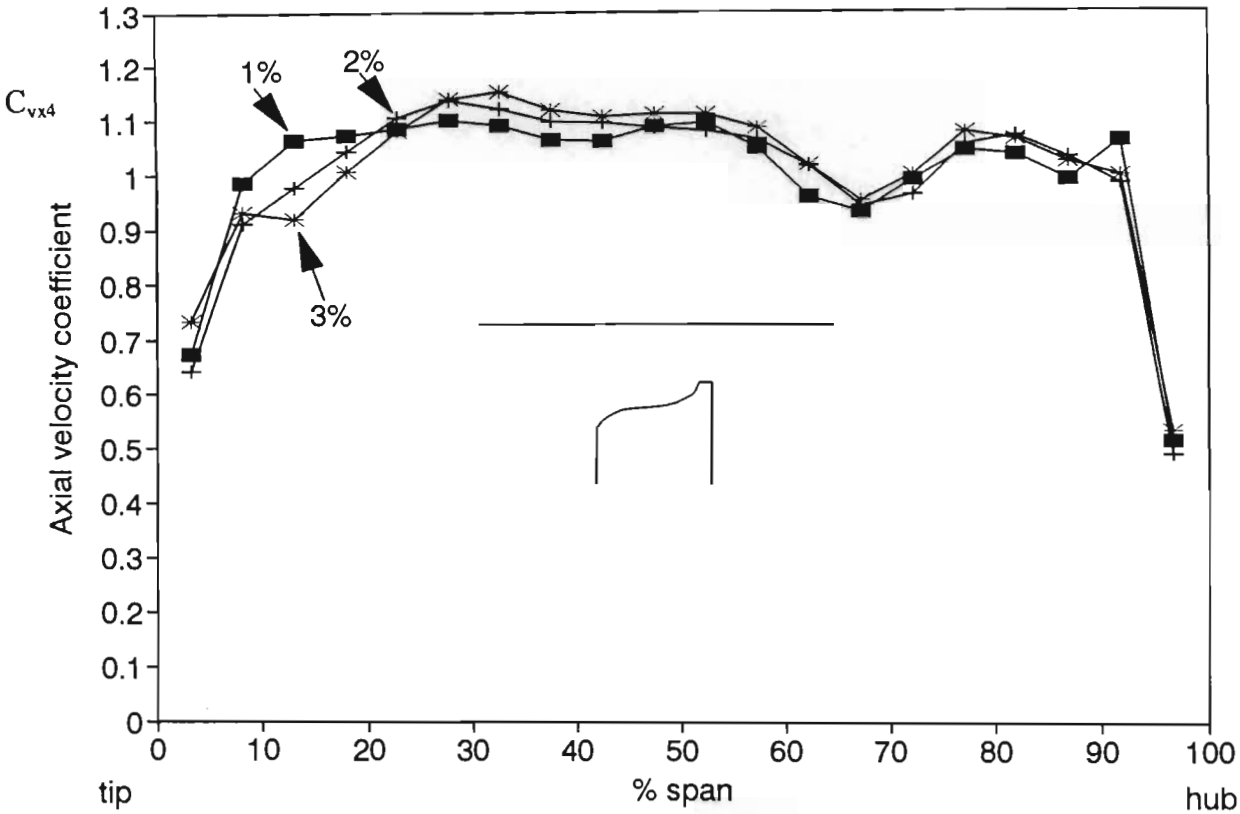

Figure 6.31 Radial variation of tangentially averaged outlet axial velocity coefficient for second nozzle with contoured tip first stage rotor.

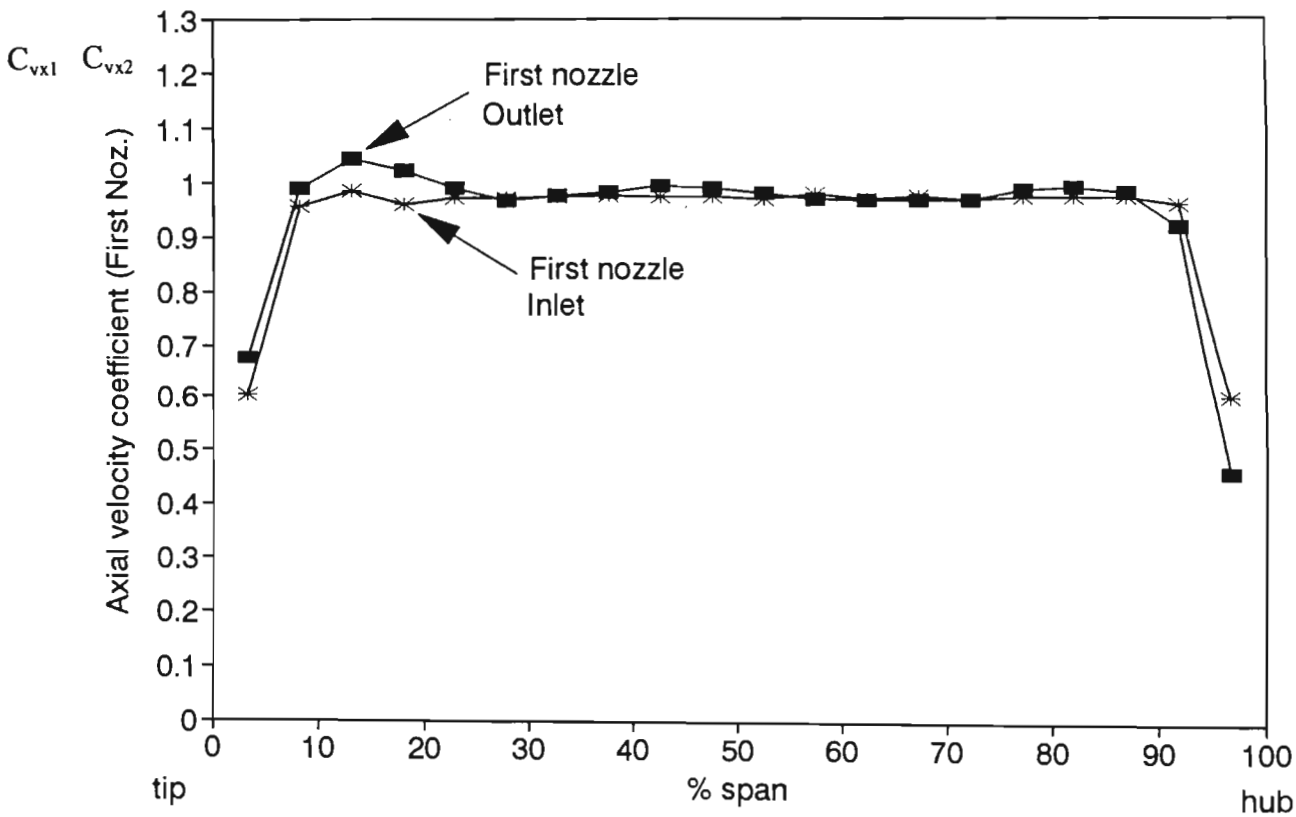

Figure 6.32 Radial variation of tangentially averaged inlet and outlet axial velocity coefficient for first stage nozzle.

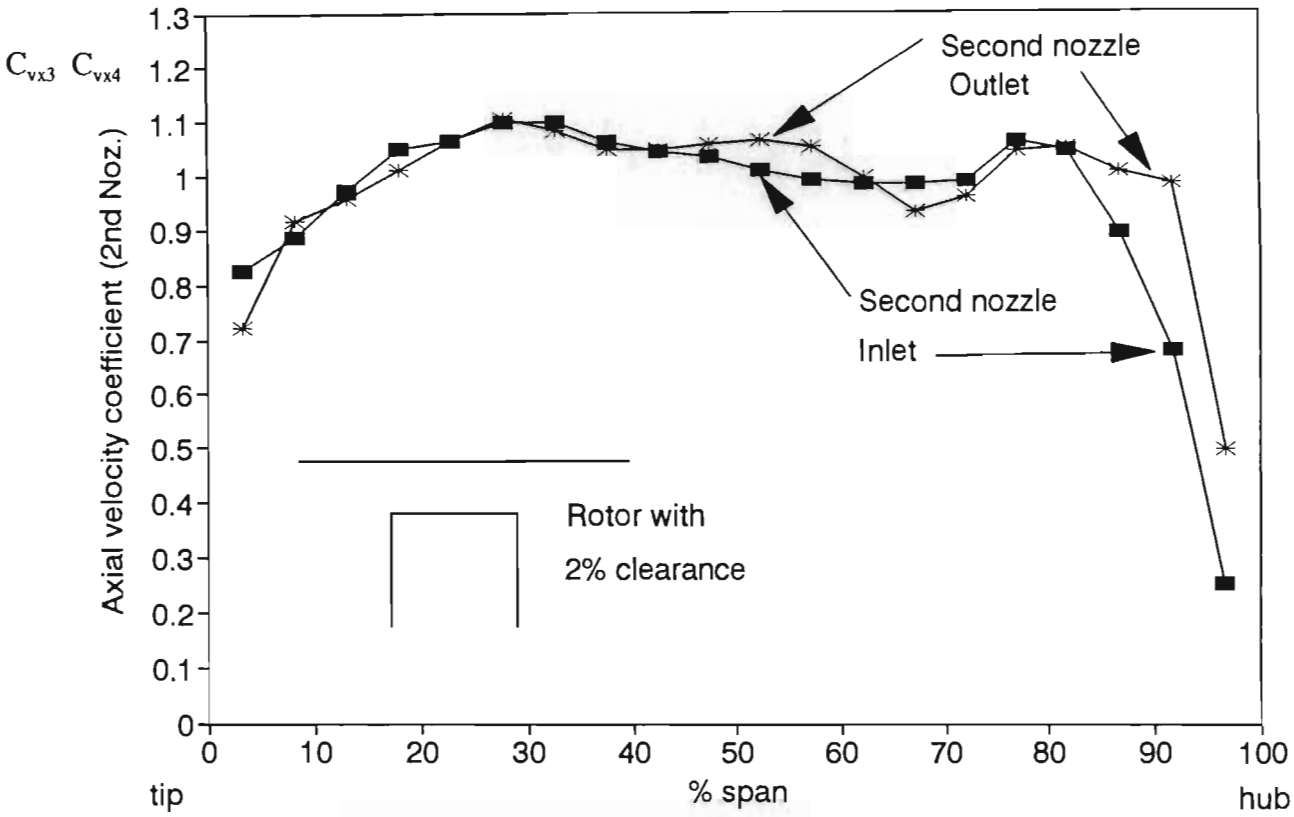

Figure 6.33 Radial variation of tangentially averaged inlet and outlet axial velocity coefficient for second stage nozzle.

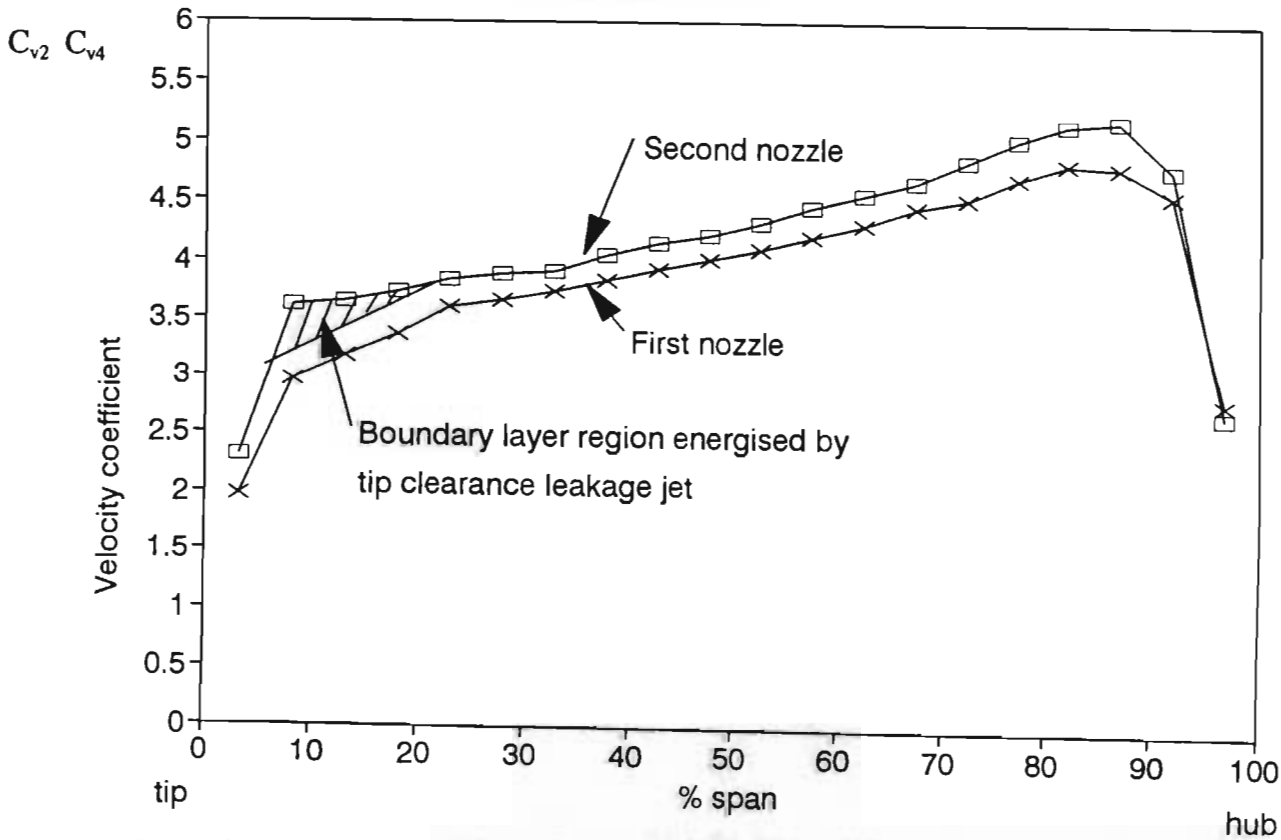

Figure 6.34 Radial variation of tangentially averaged first and second stage nozzle outlet velocity coefficient (curves similar for all clearances).

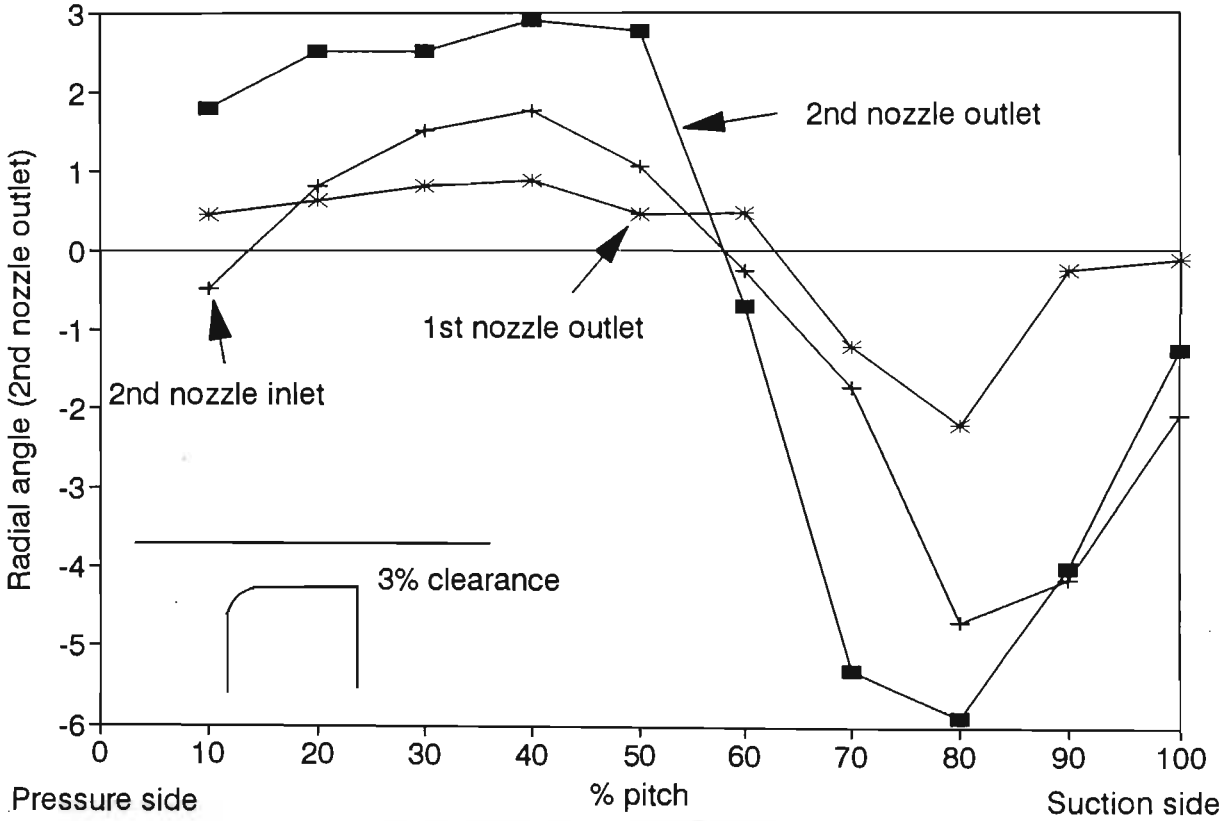

Figure 6.35 Tangential variation of second stage nozzle radial flow angle at 27% of span from tip where angles were maximum.

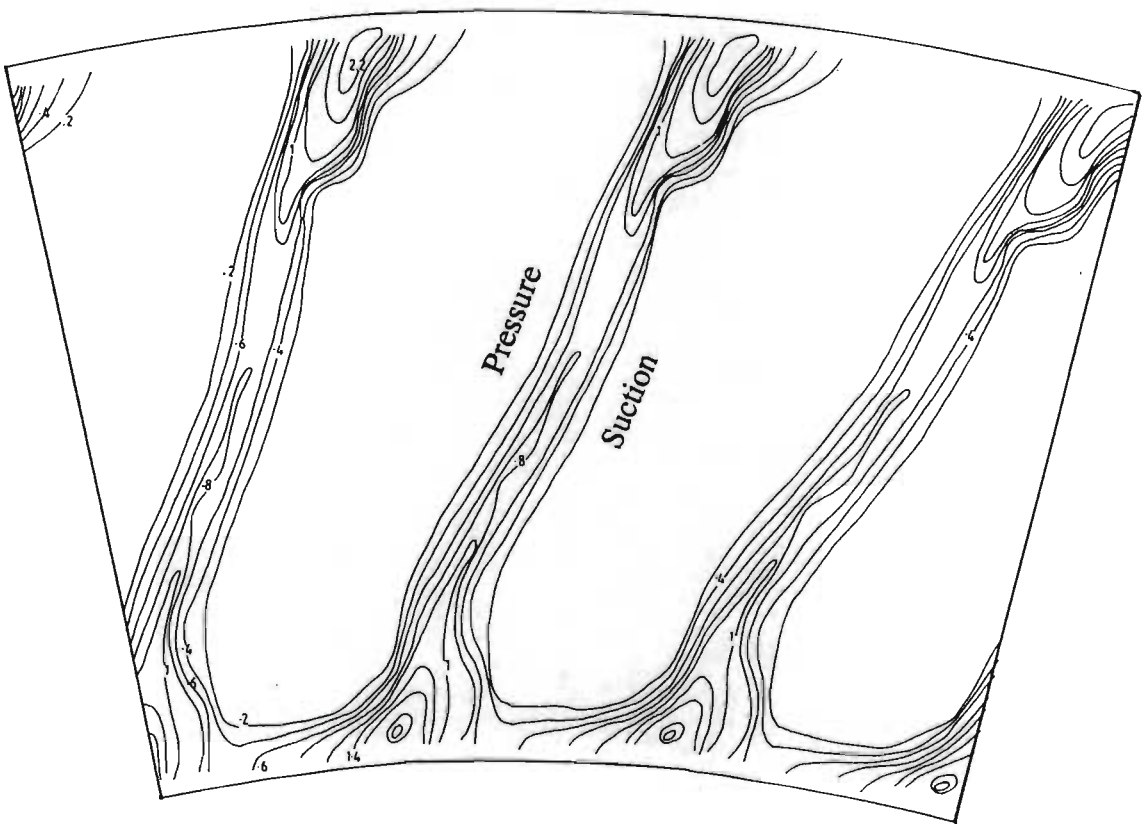

Figure 6.36 Total pressure loss contours for first stage nozzle.

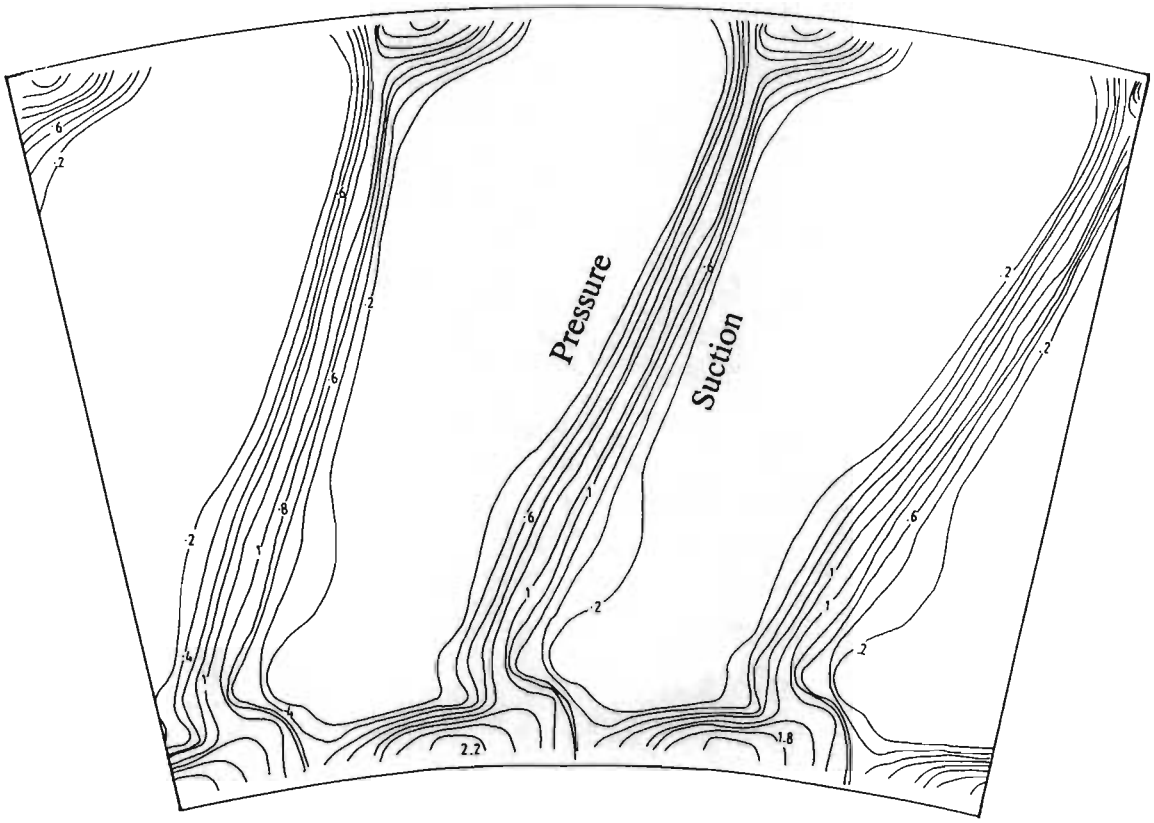

Figure 6.37 Total pressure loss contours for second stage nozzle with square tip first stage rotor at 1% clearances.

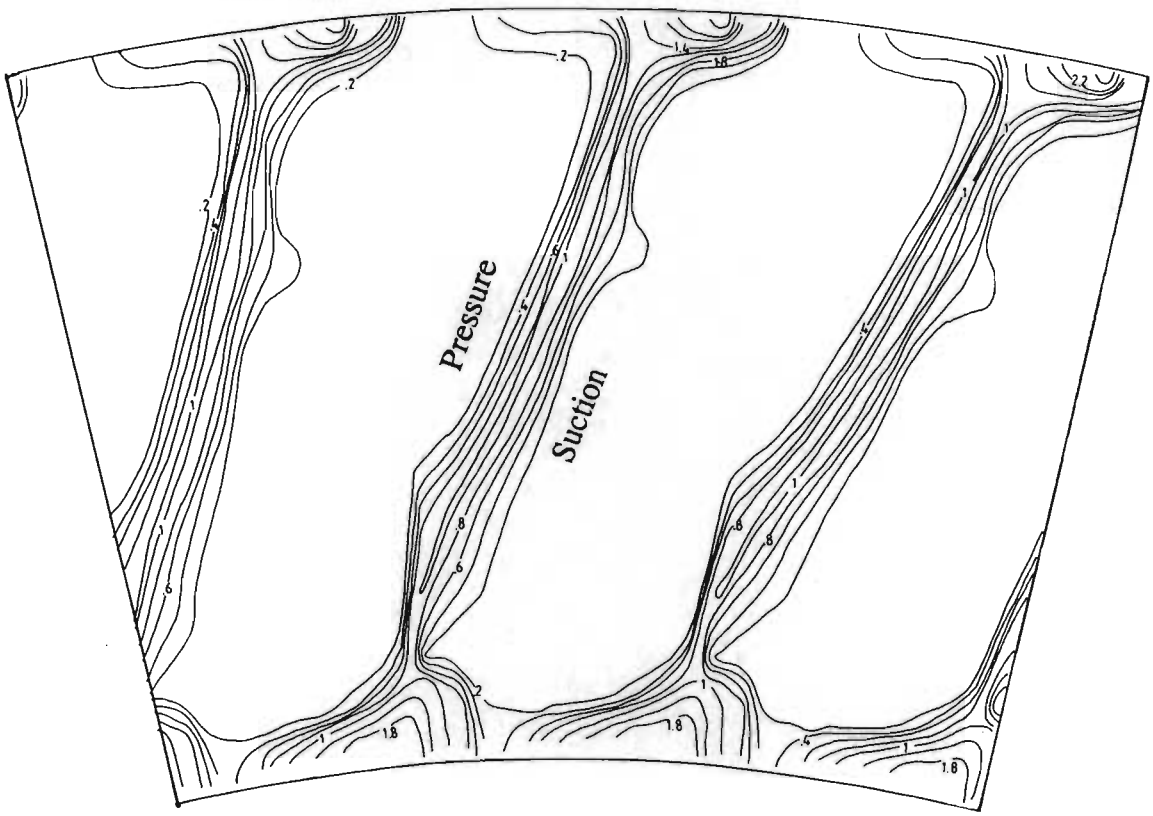

Figure 6.38 Total pressure loss contours for second stage nozzle with square tip first stage rotor at 2% clearances.

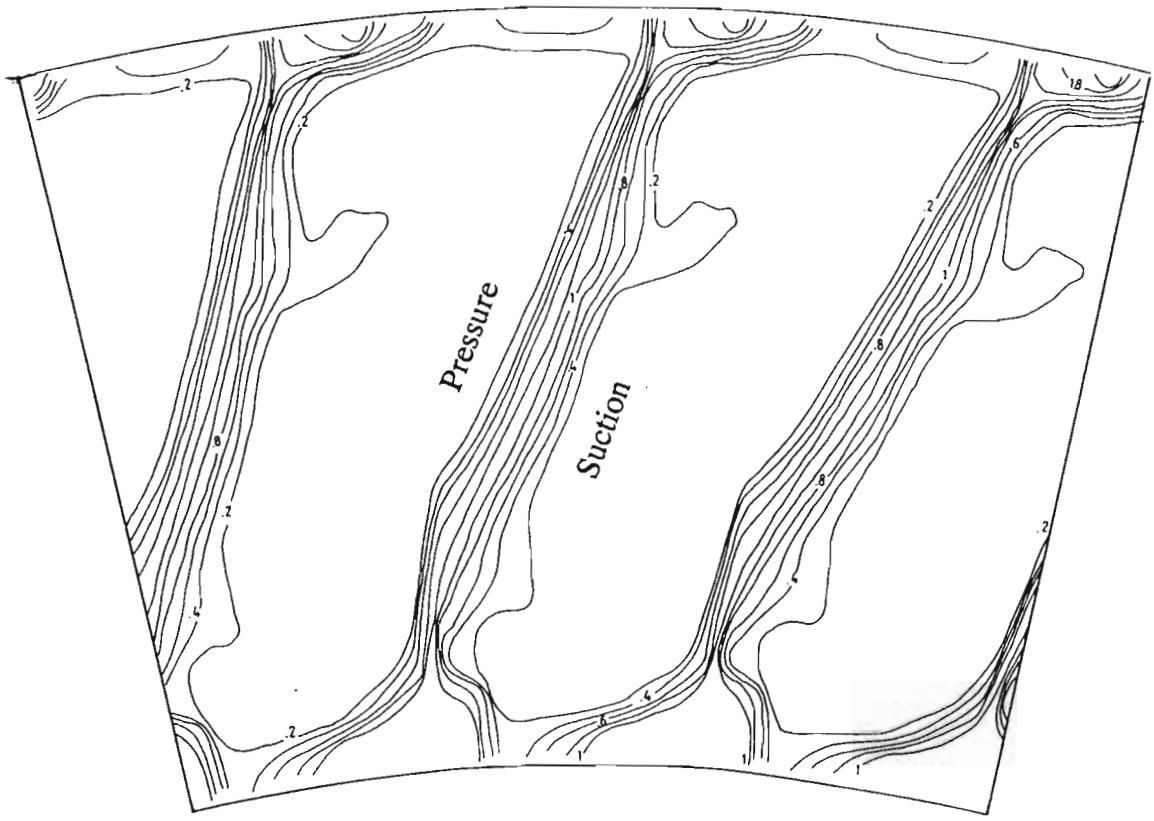

Figure 6.39 Total pressure loss contours for second stage nozzle with square tip first stage rotor at 3% clearances.

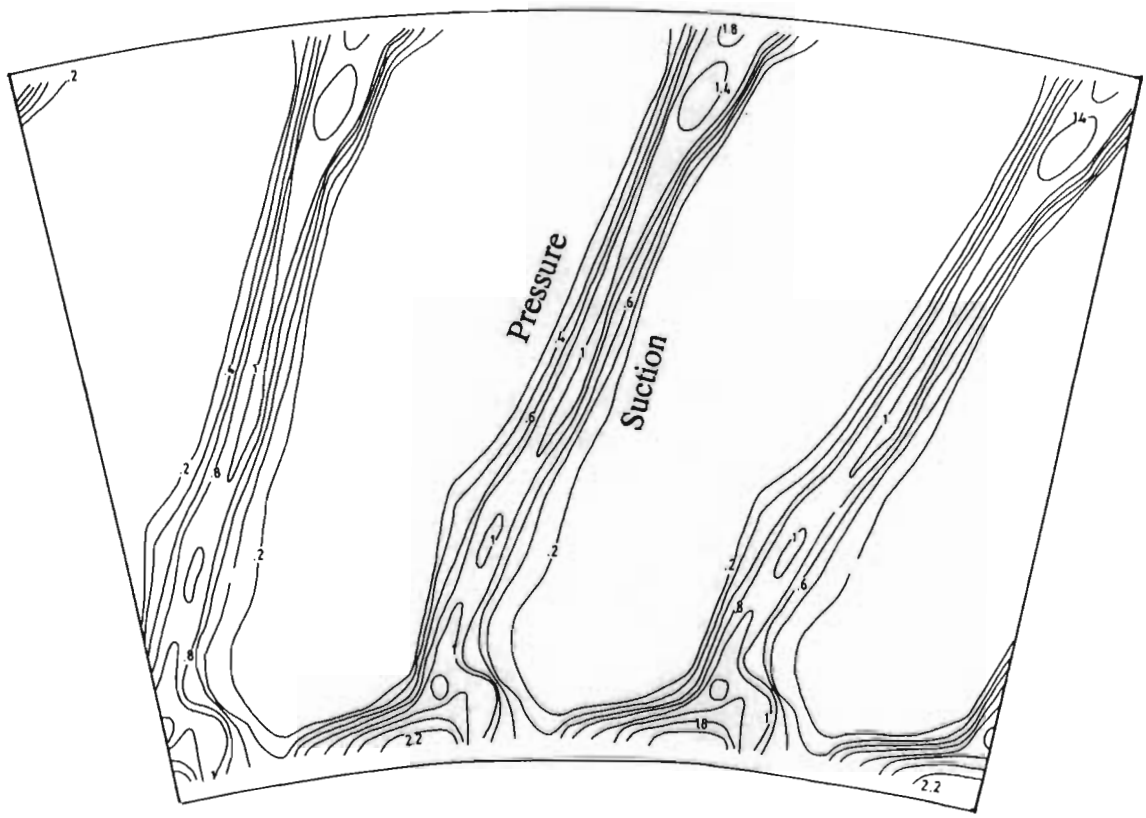

Figure 6.40 Total pressure loss contours for second stage nozzle with radiused tip first stage rotor at 1% clearances.

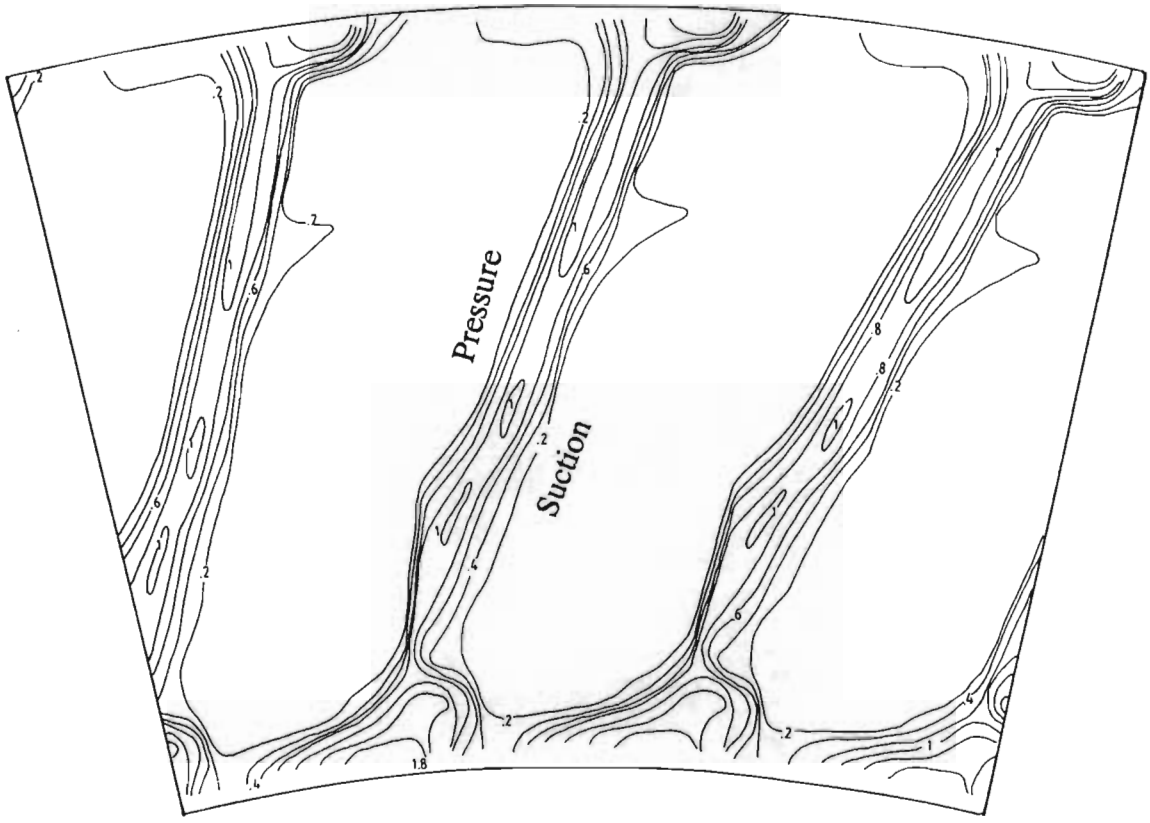

Figure 6.41 Total pressure loss contours for second stage nozzle with radiused tip first stage rotor at 2% clearances.

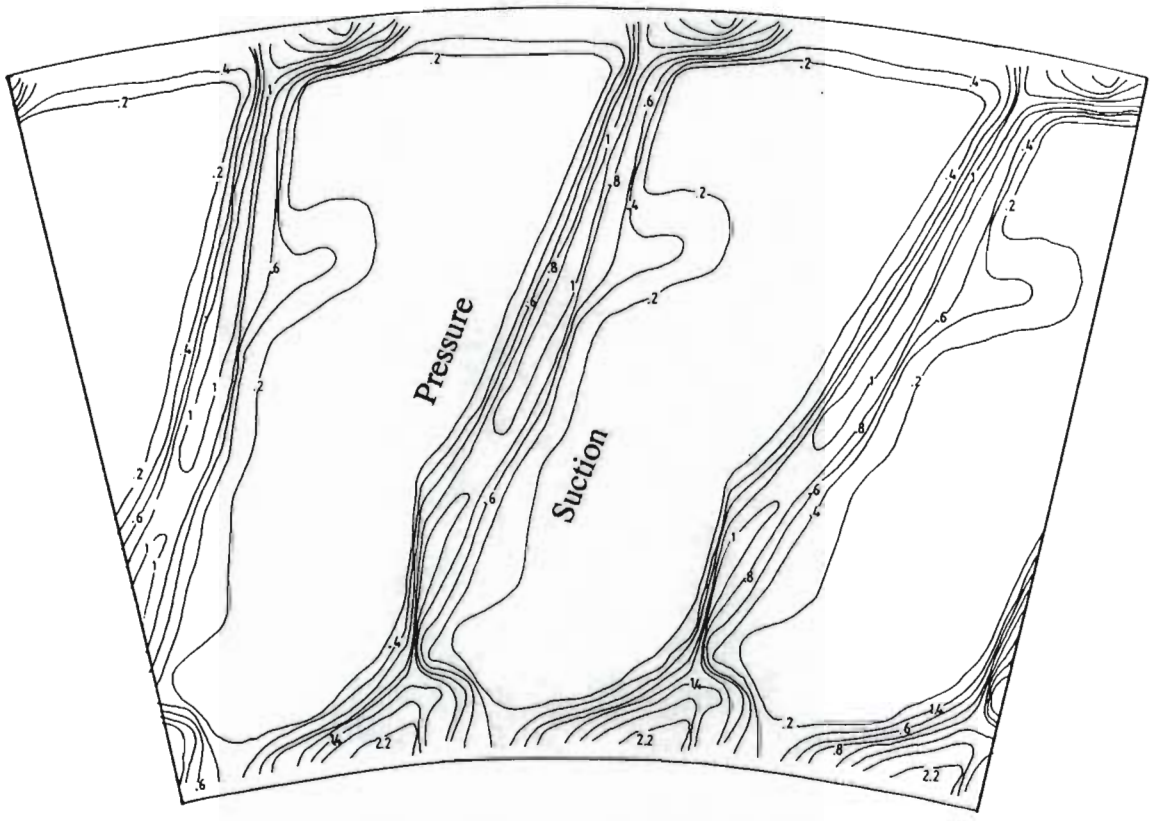

Figure 6.42 Total pressure loss contours for second stage nozzle with radiused tip first stage rotor at 3% clearances.

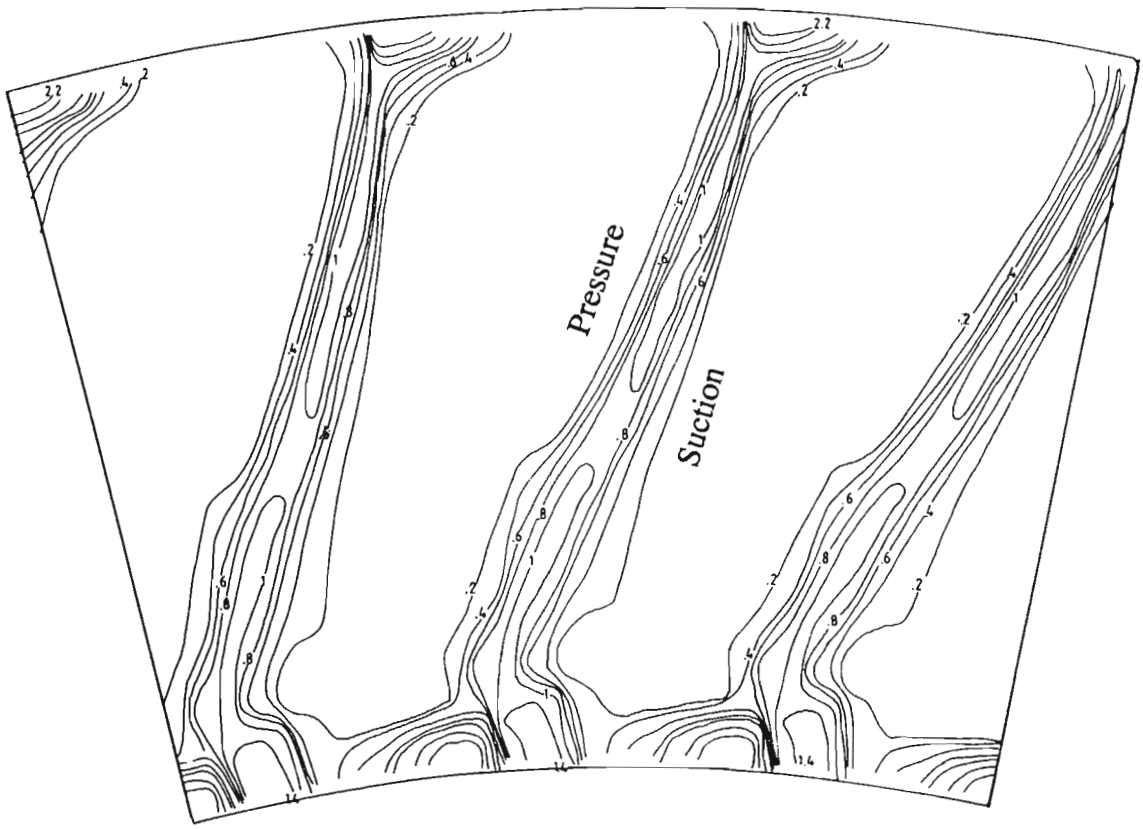

Figure 6.43 Total pressure loss contours for second stage nozzle with contoured tip first stage rotor at 1% clearances.

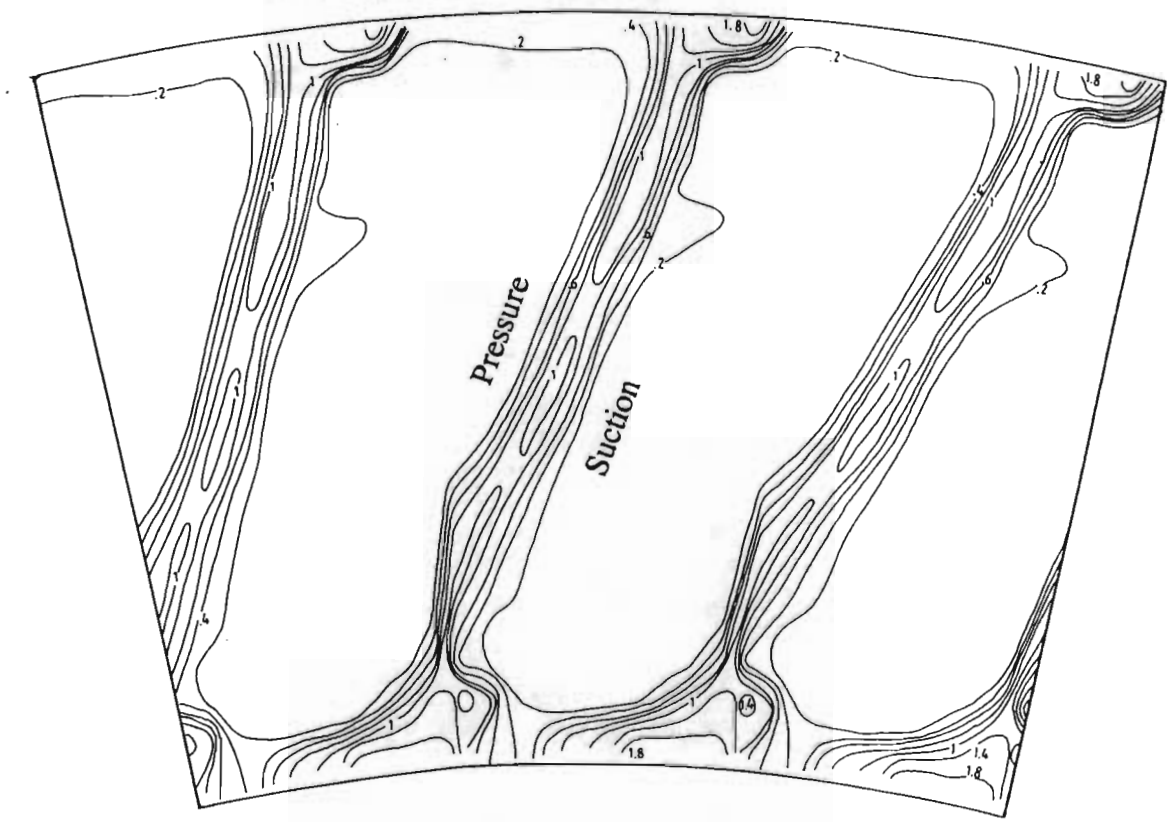

Figure 6.44 Total pressure loss contours for second stage nozzle with contoured tip first stage rotor at 2% clearances.

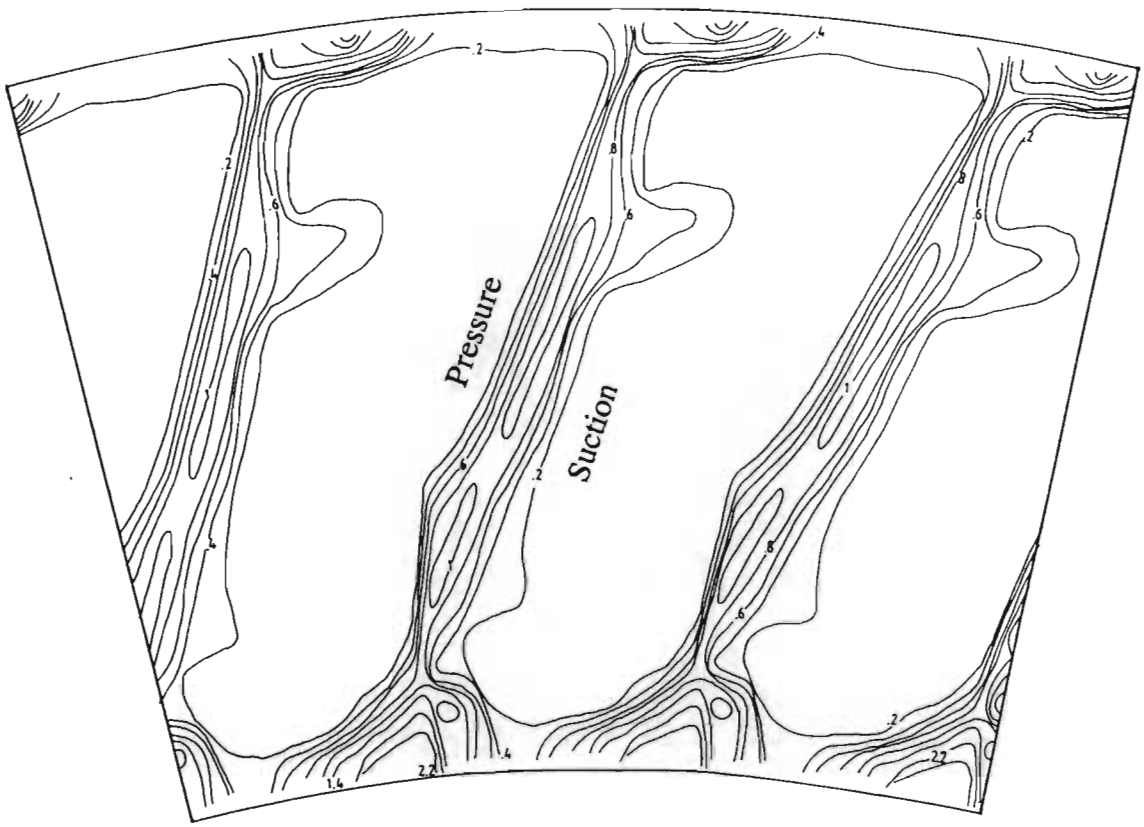

Figure 6.45 Total pressure loss contours for second stage nozzle with contoured tip first stage rotor at 3% clearances.

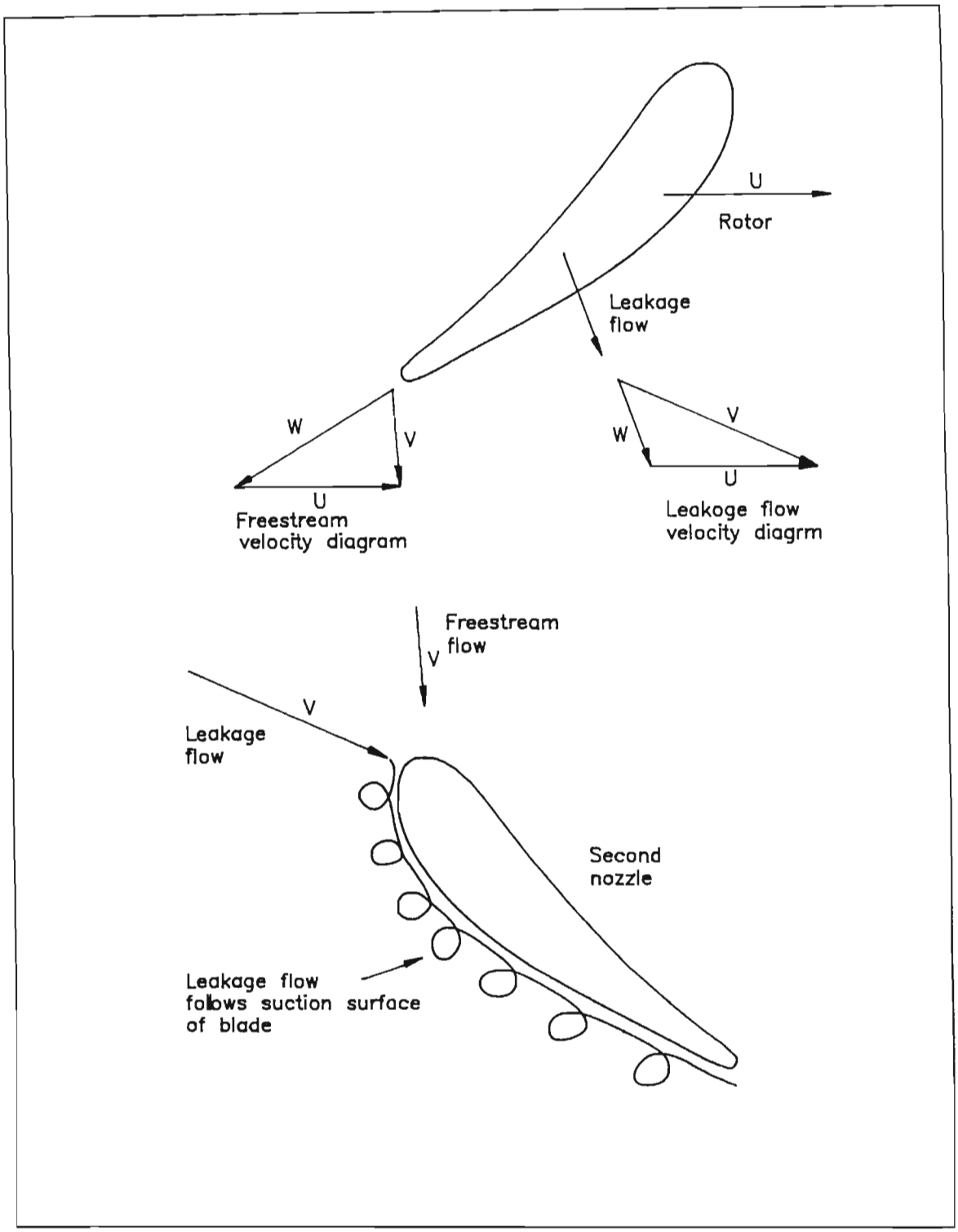

Figure 6.46 Possible explanation of unusual loss pattern found on the suction side of the second nozzle outlet.

CHAPTER 7

CONCLUSIONS

The one and a half stage research turbine and the associated instrumentation and data analysis are believed to be sufficiently reliable and accurate to resolve the minute performance differences resulting from variations in tip clearance flow. Studies of the flow field with varying levels of tip clearance and for different rotor blade tips has revealed a number of interesting aspects of tip clearance flow and of flow in a multistage machine. The effect of tip clearance flow and loss phenomena identified in cascades have been explored with a real rotor and a downstream second stage nozzle. Receiving particular attention was the complex interrelationship between gap mass flow, leakage mixing loss and the possible benefits of low loss rotor tips without the entropy generating flow separations normally used to inhibit leakage.

The rotor blade tip with a simple radiused pressure edge to suppress the internal gap separation bubble and hence the internal gap loss was found to improve the efficiency of a single stage rotor and of a one and a half stage turbine at the small tip clearance levels for which the tip radius was selected. This is in contrast to what was found in a linear cascade and the result leads to some important conclusions. Tip clearance flows, like other flows in turbomachines, need to avoid the entropy generating mechanisms of flow separation. Mixing loss, and indeed all flows in the rotor and

downstream of it, are complex and do not readily respond to the simple rules that have been used to design for minimum overall tip clearance loss.

With respect to the rotor alone, mixing loss appears to be less dominant than was previously deduced in a cascade, as a result of all low speed aspects of the flow being correctly modeled. Even in a cascade, the most likely form of the tip leakage jet was seen to be a flat, high energy wall jet containing most of the leakage fluid rather than a tip leakage vortex. However, the true nature of the tip flow leaving the rotor tip, was found to differ radically from that seen in cascades where a region of underturned flow with a high axial velocity was found. Instead, the real rotor shows a region of overturned flow with a traditional endwall boundary layer pattern. Cascade models of tip clearance cannot therefore accurately represent the real flow.

Tip leakage flows appear to be readily accepted by the second stage and expanded with not only no additional loss formation, but the efficiency of the second stage nozzle was found to be significantly higher than that of the first stage nozzle. This is a surprising result since it was expected that incidence and secondary and tip leakage mixing effects would be evident. An increased clearance actually decreases the second nozzle loss. Thus the manner in which unmixed rotor flow is processed by a second stage nozzle needs a better explanation. The higher efficiencies appear to be due to a reduction in secondary flow loss at both hub and tip which is caused by a combination of the lower blade loading (resulting from the pre-deflected flow i.e. poorly deflected by the rotor) and of the low momentum fluid being remote from the endwall.

The superiority of the low loss rotor blade tips was not maintained at large clearances and while details such as using the correct blade tip radii for the increased gap size may need to be corrected, the increased loss was seen primarily in the second stage nozzle and this complex flow requires a great deal of investigation.

The nozzle exit loss-contours showed that tip leakage suppressed the formation of the classical secondary flow pattern in the second nozzle. Also seen in the contours at the second nozzle exit was a new tip clearance related loss phenomena on the suction surface that appears to be connected to the leakage mass flow rate and requires further study.

The second stage nozzle also showed that the hub endwall boundary layer was reduced below that of both the first nozzle and that behind the rotor. Secondary and tip clearance flows were rectified to such a degree that a second stage rotor would experience no greater flow distortion than the first stage rotor. The small amounts of leakage related overturning that persist right through the second stage nozzle near the tip thus have very little effect on the downstream rotor inlet angle.

Radial flow angles were much smaller (-6 degrees as compared to -32 degrees) than previously found by Boletis & Sieverding (1991). The difference was thought to be due to the present use of lower aspect ratio, twisted nozzle and rotor blades.

Future work should establish the applicability of the results to machines with real engine Reynold's Numbers and Mach Numbers. The two low loss tips studied were

adaptations to an existing blade tip and perhaps advanced design techniques are required that involve not only the whole tip region geometry but also the complex downstream flows that stream periodically from a rotor and ultimately interact with the downstream nozzle. Finally, the detailed flow within a second stage nozzle needs an extensive analysis where not only are new phenomena thought to be present, but the manner in which the secondary flow and loss develop is quite different from that in classical cascades.

REFERENCES

Adams P C (1988) "Assessment of the performance of axial slot casing treatments in a low speed axial flow compressor" Masters Thesis, University of Natal, Durban, South Africa, May 1988.

Basson A, Lakshminarayana B (1993) "Numerical simulation of tip clearance effects in turbomachinery" Paper 93-GT-316, ASME Gas Turbine Congress, Cincinnati, May 1993.

Bindon J P (1979) "The effect of hub inlet boundary layer skewing on the endwall shear flow in an annular turbine cascade". ASME International Gas Turbine Conference, San Diego, March 1979, paper 79-GT-13.

Bindon J P (1986a) "Pressure and flow field measurements of axial turbine tip clearance flow using a linear cascade" Cambridge University, Whittle Laboratory Report CUED/A-Turbo TR123

Bindon J P (1986b) "Visualization of axial turbine tip clearance flow using a linear cascade" Cambridge University, Whittle Laboratory Report CUED/A-Turbo TR123

Bindon J P (1987a) "The measurement of tip clearance flow structure on the endwall and within the clearance gap of an axial turbine cascade",Proceedings of the I Mech E International Conference on Turbomachinery Efficiency, Prediction and Improvement, Cambridge, September 1987, page 43-52, No C273/87.

Bindon J P (1987b) "Pressure Distributions in the tip clearance region of an unshrouded axial turbine as affecting the problem of tip burnout", ASME Paper no. 87-GT-230 presented at the Gas Turbine Conference and Exhibition , Anaheim, California, 31 May - 4 June.

Bindon J P (1987c) "Visualisation of axial turbine tip clearance flow using a linear cascade", Published by the the American institute of Aeronautics and Astronautics, ISABE 87-7032

Bindon J P (1989) "The measurement and formation of tip clearance loss" Transactions of ASME, Journal of Engineering for Power, V 111, N 3, July 1989. Also Paper 88-GT-203 presented at the Gas Turbine and Aeroengine Congress and Exposition, 5-9 June 1988, Amsterdam, The Netherlands.

Bindon J P & Morphis G (1992) "The development of axial turbine leakage loss for two profiled tip geometries using linear cascade data", Trans. of the ASME, Journal of Turbomachinery, Vol 114, p198 - 203, Jan 1992. Also Paper 90-GT-152,

Blair M F, Dring R P, Joslyn H D (1989) "The effects of turbulence and stator/rotor interactions on turbine heat transfer: Part 1 - Design operating conditions" ASME J of Turbomachinery, Vol 111, January 1989 (88-GT-125)

Boletis E, Sieverding C H, Van Hove W (1983) "Effects of a skewed inlet endwall boundary layer on the three dimensional flow field in an annular turbine cascade" AGARD CP 351, Paper 16

Boletis E, Sieverding C H (1991) "Experimental study of the three dimensional flow field in turbine stator preceded by a full stage" ASME Journal of Turbomachinery, Vol 113, January 1991

Booth T C, Dodge P R and Hepworth H K (1982) "Rotor tip leakage: Part 1 -Basic methodology" Transactions of the ASME, volume 104, page 154, January 1982.

Booth T C (1985) "Tip Clearance Effects in Axial Turbomachines", von Karman Institute for Fluid Dynamics, Lecture Series 1985-05, 15-18 April, 1985.

Denton J D (1993) "Loss mechanisms in turbomachines", Scholars Paper, ASME Gas Turbine Congress, Cincinnati, May 1993

Dishart P T & Moore J (1989) "Tip leakage losses in a linear turbine cascade", Paper 89-GT-56, ASME Gas Turbine Congress, June 1989, Toronto

Graham J A H (1986) "Investigation of a tip clearance cascade in a water anology rig" Transactions of ASME, Journal of engineering for gas turbines and power, Vol. 108, January 1986.

Gregory-Smith D G, Graves C P & Walsh J A (1987) "Growth of secondary losses and vorticity in an axial tubine cascade" ASME Paper 87-GT-114, Presented at the gas turbine conference and exhibition, Anaheim, California, May 31-June 4, 1987

Heyes F J G & Hodson H P (1992) "The measurement and prediction of the tip clearance flow in linear turbine cascades" ASME Paper No. 92-GT-214, Presented at the International Gas Turbine and Aeroengine Congress and Exposition, Cologne, Germany, June 1-4, 1992

Heyes F J G, Hodson H P & Dailey G M (1991) "The effect of Blade Tip Geometry on the Tip Leakage Flow in Axial Turbine Cascades", Whittle Laboratory , Cambridge University, Madingley Rd, Cambridge CB3 ODY, England. ASME paper 91-GT-135 presented at the International Gas Turbine and Aeroengine Congress and Exposition, Orlando, FL 3-6 June, 1991

Horlock J H (1966) "Axial flow turbines, Fluid mechanics and thermodynamics", Published by Butterworth & Co Ltd, 1966

Joslyn H D, Dring R P and Sharma O P (1983) "Unsteady three-dimensional turbine aerodynamics" Transactions of ASME Pg 322, Vol. 105, April 1983

Kaiser I (1992) "Tip clearance gap flow measurements in an annular cascade with a rotating endwall" Masters Thesis, University of Natal, Durban, RSA, 1992.

Lakshminarayana (1985) "Tip clearance effects in axial turbomachines",(Experimental investigation on the effects of tip clearance in turbomachinery), von Karman Institute for Fluid Dynamics, Lecture series 1985-05, April 15-19, 1985

Mc Donald (1993) Private communication and Msc thesis (1994) to be completed, Department of Mechanical Engineering, University of Natal, Durban, RSA.

Moore J & Tilton J S (1987) "Tip Leakage Flow in a Linear Turbine Cascade", ASME Paper 87-GT-222 presented at the Gas Turbine Conference and Exhibition, Anaheim, California, 31 May - 4 June, 1987.

Malan P (1986) "PC-NREC softwear system - User's manual" National Institute for Scientific and Systems Technology, Report NIAST 86/133, Council for Scientific and Industrial Research (CSIR), Pretoria, Republic of South Africa, November 1986

Morphis G & Bindon J P (1988) "The effects of relative motion, blade edge radius and gap size on the blade tip pressure distribution in an annular turbine cascade", Paper 88-GT-256 33rd ASME International Gas Turbine Congress, Amsterdam, June 1988

Morphis G & Bindon J P (1988) "Tip Engineering Understanding, Effect of rotor tip flow on second stage nozzle" Project Izmar 1991/92, activity code 15221-03, University of Natal, Durban, South Africa

Morphis G (1989), "The measurement of axial turbine tip clearance flow phenomena in a moving wall annular cascade and in a linear cascade", Masters Thesis, University of Natal, Durban, October 1989.

Northern Research and Engineering Corporation (1972) "The Design and performance analysis of axial flow turbines, Volume 1 & Volume 2" Software & Manuals, 219 Vassar street, Cambridge, Massachusetts, 02139

Offenburg L S, Fisher J D, Vander Hoek T J (1987) "An experimental investigation of turbine casing treatment" AIAA/SAE/ASME/ASEE 23rd Joint Propulsion Conference, Paper No AIAA-87-1919

Rains D A, 1954 "Tip clearance flows in axial flow compressors and pumps" California Institude of Technology, Hydrodynamics Laboratory Report No. 5 1954.

Sieverding C H (1985) "Recent Progress in the understanding of the basic aspects of secondary flows in turbine blade passages" Presented at the 29th IGTI Conference and Exhibit, Amsterdam, The Netherlands, June 4-7 1984. Paper no. 84-GT-78. Also Transactions of ASME Journal, Vol.107, April 1985, Pg 248.

Sjolander A S, Amrud K K (1986) "Effects of tip clearance on blade loading in a planar cascade of turbine blaades" ASME Paper no. 86-GT-245, Presented at the IGTI Conference and Exhibit, Dusseldorf, West Germany, June 8-12, 1986

Storer J A (1989) "The intereaction between tip clearance flow and the passage flowfield in an axial compressor cascade", ISABE Paper no. 89-7024, Ninth International Symposium on Air Breathing Engines, Athens, Greece, September 1989.

Walsh J A, Gregory-Smith D G (1987) "The effect of inlet skew on the secondary flow and losses in a turbine cascade" Proc.I Mech E, Int. Conf. - Turbomachinery Efficiency Prediction and Improvement, Cambridge, September 1987.

Yamamoto A, Mimura F, Tominaga J, Tomihisha S, Outa E & Matsuki M (1993) "Unsteady three-dimensional flow behaviour due to rotor-stator interaction in an axial-flow turbine" ASME Paper No. 93-Gt-404, Presented at the International Gas Turbine and Aeroengine Congress and Exposition, Cincinati, Ohio, May 24-27, 1983

Yaras M, Yingkang Z & Sjolander S A (1988) "Flow field in the tip gap of a planar cascade of turbine blades", Paper 88-GT-29, Asme Gas Turbine Congress, Amsterdam, June 1988

Yaras M, Sjolander S A (1989) " Losses in the tip-leakage flow of a planar cascade of turbine blades", Paper #20, Agard-CP-469, "Secondary flows in turbomachines", Luxembourg, Sept. 1989.

Yaras M , Sjolander S (1991) "Effects of simulated rotation on tip leakage in a planar cascade of turbine blades" Part 1 :Tip gap flow, Paper 91-GT-127, ASME International Gas Turbine Congress, Orlando, June 1991.

Appendix 3.1

Nozzle and Rotor blade coordinates

NOZZLE SECTION 1 (HUB SECTION) 41 BLADES

RADIUS = 142 MM

SUCTION SURFACE COORDINATES

X	Y
-0.01424	0.00511
-0.01284	0.00583
-0.01104	0.00710
-0.00911	0.00810
-0.00701	0.00863
-0.00484	0.00855
-0.00282	0.00779
-0.00100	0.00661
0.00064	0.00518
0.00210	0.00357
0.00344	0.00186
0.00467	0.00007
0.00583	-0.00177
0.00693	-0.00364
0.00799	-0.00554
0.00901	-0.00746
0.01000	-0.00939
0.01095	-0.01135
0.01185	-0.01332
0.01273	-0.01531
0.01359	-0.01731
0.01446	-0.01930

PRESSURE SURFACE COORDINATES

X	Y
-0.01424	0.00511
-0.01265	0.00463
-0.01089	0.00400
-0.00917	0.00333
-0.00748	0.00259
-0.00581	0.00179
-0.00418	0.00092
-0.00258	0.00000
-0.00102	-0.00100
0.00047	-0.00208
0.00190	-0.00327
0.00325	-0.00452
0.00455	-0.00584
0.00579	-0.00721
0.00696	-0.00864
0.00807	-0.01012
0.00912	-0.01164
0.01012	-0.01320
0.01106	-0.01479
0.01197	-0.01640
0.01285	-0.01802
0.01372	-0.01966

NOZZLE SECTION 2 41 BLADES

RADIUS = 157.25 MM

SUCTION SURFACE COORDINATES

X	Y
-0.01553	0.00542
-0.01416	0.00610
-0.01223	0.00739
-0.01018	0.00843
-0.00796	0.00899
-0.00568	0.00888
-0.00352	0.00809
-0.00156	0.00691
0.00023	0.00548
0.00186	0.00386
0.00336	0.00212
0.00475	0.00029
0.00607	-0.00159
0.00732	-0.00351
0.00852	-0.00547
0.00968	-0.00745
0.01080	-0.00946
0.01186	-0.01150
0.01288	-0.01355
0.01388	-0.01562
0.01487	-0.01769
0.01586	-0.01976

PRESSURE SURFACE COORDINATES

X	Y
-0.01553	0.00542
-0.01397	0.00500
-0.01206	0.00442
-0.01018	0.00378
-0.00834	0.00305
-0.00653	0.00224
-0.00475	0.00136
-0.00301	0.00041
-0.00131	-0.00062
0.00033	-0.00172
0.00191	-0.00292
0.00340	-0.00423
0.00481	-0.00563
0.00615	-0.00709
0.00743	-0.00860
0.00865	-0.01017
0.00982	-0.01177
0.01093	-0.01341
0.01200	-0.01508
0.01303	-0.01678
0.01403	-0.01849
0.01503	-0.02021

NOZZLE SECTION 3 (MID SPAN SECTION) 41 BLADES

RADIUS = 172.5 MM

SUCTION SURFACE COORDINATES

X	Y
-0.01675	0.00568
-0.01539	0.00633
-0.01336	0.00766
-0.01121	0.00874
-0.00888	0.00931
-0.00649	0.00914
-0.00423	0.00834
-0.00213	0.00717
-0.00020	0.00574
0.00159	0.00413
0.00324	0.00239
0.00479	0.00055
0.00626	-0.00136
0.00765	-0.00332
0.00900	-0.00531
0.01028	-0.00734
0.01151	-0.00941
0.01269	-0.01151
0.01383	-0.01362
0.01495	-0.01575
0.01606	-0.01789
0.01717	-0.02002

PRESSURE SURFACE COORDINATES

X	Y
-0.01675	0.00568
-0.01520	0.00531
-0.01316	0.00477
-0.01115	0.00415
-0.00918	0.00342
-0.00724	0.00262
-0.00533	0.00173
-0.00346	0.00076
-0.00164	-0.00029
0.00013	-0.00142
0.00185	-0.00263
0.00349	-0.00395
0.00503	-0.00537
0.00648	-0.00690
0.00786	-0.00848
0.00918	-0.01011
0.01045	-0.01179
0.01168	-0.01350
0.01286	-0.01524
0.01400	-0.01700
0.01512	-0.01878
0.01625	-0.02056

NOZZLE SECTION 4 41 BLADES

RADIUS = 187.75 MM

SUCTION SURFACE COORDINATES

X	Y
-0.01843	0.00598
-0.01708	0.00657
-0.01488	0.00791
-0.01259	0.00904
-0.01012	0.00965
-0.00757	0.00949
-0.00514	0.00872
-0.00286	0.00757
-0.00074	0.00615
0.00124	0.00453
0.00309	0.00277
0.00483	0.00090
0.00647	-0.00106
0.00805	-0.00307
0.00955	-0.00513
0.01099	-0.00725
0.01236	-0.00940
0.01369	-0.01159
0.01497	-0.01380
0.01623	-0.01602
0.01748	-0.01825
0.01874	-0.02047

PRESSURE SURFACE COORDINATES

X	Y
-0.01843	0.00598
-0.01689	0.00569
-0.01467	0.00521
-0.01249	0.00460
-0.01035	0.00388
-0.00825	0.00306
-0.00618	0.00214
-0.00415	0.00114
-0.00217	0.00006
-0.00024	-0.00111
0.00164	-0.00237
0.00345	-0.00372
0.00518	-0.00517
0.00679	-0.00675
0.00833	-0.00841
0.00980	-0.01012
0.01122	-0.01188
0.01259	-0.01368
0.01391	-0.01551
0.01521	-0.01736
0.01648	-0.01923
0.01775	-0.02110

NOZZLE SECTION 5 (TIP SECTION) 41 BLADES

RADIUS = 203 MM

SUCTION SURFACE COORDINATES

X	Y
-0.01930	0.00601
-0.01797	0.00666
-0.01573	0.00807
-0.01337	0.00924
-0.01080	0.00982
-0.00819	0.00959
-0.00567	0.00883
-0.00328	0.00772
-0.00104	0.00633
0.00107	0.00475
0.00305	0.00302
0.00492	0.00116
0.00670	-0.00078
0.00840	-0.00280
0.01002	-0.00487
0.01156	-0.00702
0.01303	-0.00920
0.01446	-0.01141
0.01585	-0.01365
0.01722	-0.01590
0.01858	-0.01816
0.01995	-0.02041

PRESSURE SURFACE COORDINATES

X	Y
-0.01930	0.00601
-0.01775	0.00568
-0.01546	0.00518
-0.01320	0.00457
-0.01097	0.00385
-0.00878	0.00303
-0.00663	0.00213
-0.00451	0.00114
-0.00243	0.00006
-0.00040	-0.00110
0.00158	-0.00234
0.00350	-0.00367
0.00535	-0.00510
0.00711	-0.00663
0.00877	-0.00828
0.01034	-0.01001
0.01185	-0.01180
0.01331	-0.01362
0.01473	-0.01548
0.01612	-0.01736
0.01750	-0.01925
0.01887	-0.02114

ROTOR SECTION 1 (HUB SECTION) 43 BLADES

RADIUS = 142 MM

SUCTION SURFACE COORDINATES

X	Y
-0.01984	-0.00310
-0.01930	-0.00201
-0.01807	0.00066
-0.01646	0.00310
-0.01420	0.00494
-0.01158	0.00625
-0.00877	0.00703
-0.00586	0.00730
-0.00295	0.00709
-0.00010	0.00644
0.00263	0.00538
0.00520	0.00399
0.00762	0.00235
0.00989	0.00050
0.01203	-0.00149
0.01405	-0.00361
0.01597	-0.00581
0.01782	-0.00808
0.01960	-0.01040
0.02134	-0.01275
0.02306	-0.01511
0.02478	-0.01748

PRESSURE SURFACE COORDINATES

X	Y
-0.01984	-0.00310
-0.01862	-0.00267
-0.01629	-0.00188
-0.01394	-0.00124
-0.01154	-0.00081
-0.00911	-0.00057
-0.00667	-0.00053
-0.00424	-0.00068
-0.00182	-0.00102
0.00056	-0.00153
0.00290	-0.00222
0.00519	-0.00307
0.00741	-0.00406
0.00957	-0.00520
0.01166	-0.00647
0.01367	-0.00785
0.01560	-0.00933
0.01747	-0.01090
0.01926	-0.01256
0.02099	-0.01428
0.02266	-0.01605
0.02430	-0.01786

ROTOR SECTION 2 43 BLADES

RADIUS = 157.25 MM

SUCTION SURFACE COORDINATES

X	Y
-0.01907	0.00057
-0.01826	0.00180
-0.01683	0.00427
-0.01490	0.00632
-0.01236	0.00752
-0.00959	0.00804
-0.00678	0.00802
-0.00400	0.00754
-0.00132	0.00667
0.00124	0.00548
0.00366	0.00402
0.00592	0.00235
0.00805	0.00049
0.01002	-0.00152
0.01189	-0.00364
0.01366	-0.00584
0.01536	-0.00809
0.01700	-0.01038
0.01860	-0.01271
0.02017	-0.01505
0.02172	-0.01741
0.02328	-0.01976

PRESSURE SURFACE COORDINATES

X	Y
-0.01907	0.00057
-0.01750	0.00070
-0.01510	0.00084
-0.01273	0.00090
-0.01035	0.00079
-0.00799	0.00052
-0.00566	0.00010
-0.00335	-0.00048
-0.00109	-0.00119
0.00113	-0.00205
0.00329	-0.00304
0.00539	-0.00415
0.00742	-0.00538
0.00939	-0.00671
0.01128	-0.00815
0.01310	-0.00967
0.01486	-0.01127
0.01654	-0.01295
0.01816	-0.01468
0.01973	-0.01647
0.02124	-0.01830
0.02273	-0.02016

ROTOR SECTION 3 (MID SECTION) 43 BLADES

RADIUS = 172.25 MM

SUCTION SURFACE COORDINATES

X	Y
-0.01785	0.00378
-0.01673	0.00496
-0.01499	0.00705
-0.01276	0.00855
-0.01012	0.00902
-0.00744	0.00882
-0.00484	0.00814
-0.00237	0.00709
-0.00003	0.00575
0.00215	0.00418
0.00420	0.00244
0.00613	0.00056
0.00795	-0.00142
0.00968	-0.00349
0.01132	-0.00562
0.01289	-0.00781
0.01439	-0.01005
0.01584	-0.01231
0.01727	-0.01460
0.01866	-0.01690
0.02005	-0.01921
0.02145	-0.02151

PRESSURE SURFACE COORDINATES

X	Y
-0.01785	0.00378
-0.01615	0.00348
-0.01384	0.00305
-0.01156	0.00262
-0.00930	0.00208
-0.00708	0.00143
-0.00488	0.00066
-0.00273	-0.00021
-0.00063	-0.00119
0.00141	-0.00229
0.00340	-0.00349
0.00531	-0.00480
0.00715	-0.00622
0.00891	-0.00773
0.01060	-0.00932
0.01222	-0.01098
0.01378	-0.01270
0.01527	-0.01448
0.01672	-0.01629
0.01812	-0.01814
0.01948	-0.02002
0.02083	-0.02191

ROTOR SECTION 4 43 BLADES

RADIUS = 187.75 MM

SUCTION SURFACE COORDINATES

X	Y
-0.01671	0.00685
-0.01542	0.00770
-0.01334	0.00935
-0.01092	0.01027
-0.00832	0.01011
-0.00584	0.00932
-0.00351	0.00814
-0.00134	0.00668
0.00067	0.00502
0.00255	0.00320
0.00431	0.00127
0.00597	-0.00074
0.00754	-0.00283
0.00903	-0.00498
0.01045	-0.00716
0.01183	-0.00938
0.01318	-0.01162
0.01449	-0.01388
0.01578	-0.01615
0.01705	-0.01843
0.01832	-0.02071
0.01960	-0.02299

PRESSURE SURFACE COORDINATES

X	Y
-0.01671	0.00685
-0.01520	0.00621
-0.01306	0.00528
-0.01095	0.00436
-0.00887	0.00337
-0.00682	0.00231
-0.00481	0.00119
-0.00283	0.00000
-0.00090	-0.00126
0.00098	-0.00259
0.00281	-0.00399
0.00458	-0.00547
0.00628	-0.00703
0.00791	-0.00866
0.00947	-0.01035
0.01098	-0.01209
0.01242	-0.01389
0.01381	-0.01573
0.01515	-0.01761
0.01644	-0.01951
0.01771	-0.02144
0.01896	-0.02338

ROTOR SECTION 5 (TIP SECTION) 43 BLADES

RADIUS = 203 MM

SUCTION SURFACE COORDINATES

X	Y
-0.01579	0.00939
-0.01415	0.00981
-0.01182	0.01085
-0.00934	0.01119
-0.00692	0.01053
-0.00471	0.00935
-0.00268	0.00787
-0.00081	0.00619
0.00091	0.00437
0.00252	0.00244
0.00404	0.00043
0.00547	-0.00163
0.00683	-0.00375
0.00813	-0.00589
0.00940	-0.00806
0.01063	-0.01025
0.01183	-0.01246
0.01302	-0.01468
0.01418	-0.01690
0.01534	-0.01913
0.01649	-0.02137
0.01764	-0.02360

PRESSURE SURFACE COORDINATES

X	Y
-0.01579	0.00939
-0.01425	0.00849
-0.01231	0.00724
-0.01040	0.00600
-0.00851	0.00471
-0.00666	0.00339
-0.00483	0.00202
-0.00303	0.00062
-0.00127	-0.00082
0.00046	-0.00231
0.00215	-0.00384
0.00377	-0.00544
0.00532	-0.00712
0.00681	-0.00885
0.00823	-0.01062
0.00961	-0.01245
0.01093	-0.01431
0.01220	-0.01620
0.01342	-0.01812
0.01461	-0.02007
0.01578	-0.02203
0.01694	-0.02399

Appendix 4.1

Compressible to Incompressible Flow

The one and a half stage efficiency was defined in Chapter 4 as

$$\eta_{1.5} = \frac{\omega + \frac{1}{2}V_4^2}{h_{o1} - h_{4is}} \tag{1}$$

Expressing enthalpy in terms of specific quantities,

$$h_{o1} = u_1 + \frac{P_{o1}}{\rho_1} \tag{2}$$

and

$$h_{4is} = u_{4is} + \frac{P_{4is}}{\rho_{4is}} \tag{3}$$

where

$$u_1 = c_v T_1 \quad \& \quad u_{4is} = c_v T_{4is} \tag{4}$$

Now assuming that the flow is incompressible, then

$$\rho_1 = \rho_{4is} = \rho \quad \& \quad T_1 = T_{4is} \tag{5}$$

Therefore

$$u_1 = u_{4is} \tag{6}$$

Subtracting equation (3) from (2) gives

$$h_{o1} - h_{4is} = \frac{P_{o1}}{\rho} - \frac{P_{4is}}{\rho} \qquad (7)$$

Therefore equation (1) becomes

$$\eta_{1.5} = \frac{\rho\omega + \frac{1}{2}\rho V_4^2}{P_{o1} - P_{s4}} \qquad (8)$$

(note: $P_{s4} = P_{4is}$)

Appendix 4.2

Derivation of coefficients from five hole probe data

The method used to calibrate the five hole probe and to calculate the velocity, total pressure and static pressure coefficients is presented here. In this appendix the subscripts 1,2,3,4 and 5 refer to the various holes of the five hole probe. Subscript 1 refers to the centre hole, 2 and 3 are yaw angle (tangential direction) holes, and 4 and 5 are the pitch angle (radial direction) holes.

Calibration

The following calibration coefficients were defined as

$$K_\theta = \frac{P_4 - P_5}{P_1 - P_2} \tag{1}$$

$$F(\theta) = \frac{P_o - P_s}{P_1 - P_2} \tag{2}$$

$$G(\theta) = \frac{P_1 - P_o}{P_o - P_s} \tag{3}$$

To calibrate the probe, K_θ, $F(\theta)$ and $G(\theta)$ were calculated and plotted for various θ.

Measurements

From the measurements taken with the probe K_θ was calculated using equation (1)

and then θ was found from the K_θ verses θ curve that was generated during calibration. $F(\theta)$ and $G(\theta)$ were then found from the curves of $F(\theta)$ and $G(\theta)$ verses θ.

From equations (2) and (3)

$$F(\theta)(P_1 - P_2) = \frac{P_1 - P_o}{G(\theta)} \tag{4}$$

Therefore

$$P_o = P_1 - F(\theta)\, G(\theta)\, (P_1 - P_2) \tag{5}$$

rearranging equation (2)

$$P_s = P_o - F(\theta)\, (P_1 - P_2) \tag{6}$$

Substituting equation (5) into (6) gives

$$\begin{aligned} P_s &= P_1 - F(\theta)\, G(\theta)\, (P_1 - P_2) - F(\theta)\, (P_1 - P_2) \\ &= P_1 - F(\theta)\, (P_1 - P_2)\, (1 + G(\theta)) \end{aligned} \tag{7}$$

Velocity coefficient

The velocity coefficient was defined as

$$C_{v_{ij}} = \frac{(P_o - P_s)_{ij}}{(P_o - P_s)_{ref_{ij}}} \tag{8}$$

Substituting equations (5) and (7) into (8) gives

$$C_{V_{ij}} = \frac{\left(P_1 - F(\theta)\, G(\theta)\, (P_1 - P_2) - P_1 + F(\theta)\, (P_1 - P_2)\, (1 + G(\theta)) \right)_{ij}}{(P_o - P_s)_{ref_{ij}}}$$

$$= \frac{\left(F(\theta)\, (P_1 - P_2) \right)_{ij}}{(P_o - P_s)_{ref_{ij}}} \qquad (9)$$

Static pressure coefficient

The static pressure coefficient was defined as

$$C_{(P_{o\,ref} - P_s)_{ij}} = \frac{(P_{o\,ref} - P_s)_{ij}}{(P_o - P_s)_{ref_{ij}}} \qquad (10)$$

Substituting equation (7) into (10) gives

$$C_{(P_{o\,ref} - P_s)_{ij}} = \frac{\left((P_{o\,ref} - P_1) + F(\theta)\, (P_1 - P_2)\, (1 + G(\theta)) \right)_{ij}}{(P_o - P_s)_{ref_{ij}}} \qquad (11)$$

Total pressure coefficient

The total pressure coefficient was defined as

$$C_{(P_{o\,ref} - P_o)_{ij}} = \frac{(P_{o\,ref} - P_o)_{ij}}{(P_o - P_s)_{ref_{ij}}} \qquad (12)$$

Substituting equation (5) into (12) gives

$$C_{(P_{o\,ref} - P_o)_{ij}} = \frac{\left((P_{o\,ref} - P_1) - F(\theta)\, G(\theta)\, (P_1 - P_2) \right)_{ij}}{(P_o - P_s)_{ref_{ij}}} \qquad \textbf{(13)}$$

And substituting equations (2) and(3) into (13) gives

$$C_{(P_{o\,ref} - P_o)_{ij}} = \frac{\left((P_{o\,ref} - P_1) + (P_o - P_1) \right)_{ij}}{(P_o - P_s)_{ref_{ij}}} \qquad \textbf{(14)}$$